Numerical Analysis on Quantitative Influence of Initial Deflections on Load-bearing Capacity and Its Formulation for Welded Box Section Columns under Axial Compression

December 2019

Graduate School of Engineering
Nagasaki University

Xiang CHEN

Acknowledgement

Throughout the research works when I study in Structural engineering laboratory of department of civil and environmental engineering in Nagasaki University, I have received a great deal of support and assistance so that I could successfully complete my dissertation. I would like to take this opportunity to express my sincere gratitude to all people for their contribution.

Foremost, I would like to express my special appreciation and thanks to my supervisor, Prof. Shozo Nakamura, for the continuous guidance to my Ph.D study and research, for very useful advice to the writing of this dissertation, for his warm encouragement. His immense knowledge and earnest for research work gave me a deep impression and will encourage me to study and work hard on the research work. My sincere thanks also go to my supervisor in master study, Prof. QingXiong Wu for his guidance and encouragement during both master study and doctoral study.

I wish to express my sincere thanks to Associate Prof. Toshihiro Okumatsu and Associate Prof. Takafumi Nishikawa for giving kind advice to my research and deepening my understanding on technology through workshop practice. I would like to give thanks to other faculty members for their kind help on various stages of my study and research.

I would like to thank to Prof. Kuniei Nogami and Associate Prof. Yusuke Kishi in Graduate School of Urban Environmental Sciences, Tokyo Metropolitan University, Mr. Ikezue in Yokogawa Bridge Corporation for their valuable comments and helpful suggestions to my research paper.

I would like to give thanks to Dr. Qu Wang, Dr. Jian Zheng, Miss YaJing Ge, Mr. SuCheng Rui and Mr. Muraoka Toshihiko for their kind supports and helps on my daily life when I first came to Nagasaki. I am also very grateful to all my friends in China and Japan for their supports and encouragements. I deeply thanks to the scholarship support of China Scholarship Council.

I would also like to say a heartfelt thank you to my parents for their eternal love and for always believing in me and encouraging me to follow my dreams.

Abstract

Steel structures are famous for its lightweight, high strength, good ductility, easy construction and aesthetics, therefore, widely used in actual engineering. Steel compression members made from thin plates accounts for a larger proportion of these kind of structures. For a wish of full utilization of the cross section and strength, they are usually made into thin-walled structures. However, such kind of structure are susceptible to loss of load-bearing capacity at the point far away lower than the yield resistance due to buckling. After buckling phenomenon occurs, load-bearing capacity of the structures significantly decreases and the deformation intensely increases, which will result in disaster in practical engineering.

Since the post-buckling strength behavior of the plate is stable, high width-thickness ratios exceeding the limit value are usually used in medium or long columns for a wish of economic benefit. It should be mentioned that although the structures satisfy with the requirement of local and overall buckling individually, the triggering of both local and overall buckling simultaneously will result in severe instability behavior. Aiming at stability design, many researches were conducted, and various countries have drawn up their own codes for design of this kind of structures. However, the stability design methods differ greatly among different codes.

On the other hand, initial deflections, which are unavoidable during the manufacturing and assembling procedure, will result in significant decrease on the load-bearing capacity of steel compression members. So far, many experiments and numerical analysis on load-bearing capacity of steel columns with both welded unstiffened and stiffened box cross section under axial compression have been conducted. And it is revealed that the local and overall initial deflections will significantly deteriorate the load-bearing capacity of the structures. However, the quantitative influence caused by initial deflections on load-bearing capacity for such structure is still not clear.

In this dissertation, in order to provide a reference to the revision of the specification and improve the stability design of steel compression members with welded box cross section, the author carried out the comparison on the stability design among various codes and developed formulae for the quantitative influence of initial deflections on the load-bearing capacity. The dissertation consists of six chapters as follows:

In Chapter 1, it gives the background and objectives of the research together with the overview of the previous researches carried out in the related field. In addition, the layout was given.

In Chapter 2, provisions concerning about stability design of steel compression member for steel bridge in those codes adopting the Partial Factor Design Method including Chinese code *Specification for Design of Highway Steel Bridge*, Japanese code *Specification for Highway Bridges*, American code *AASHTO LRFD Bridge Design Specification*, European code *Eurocode 3*: *Design of Steel Structures - Part 2: Steel Bridges*, are outlined first. Nominal strengths related to the buckling parameters slenderness and width-thickness ratios following these codes are calculated and compared with each other. Safety factor performed as a function of ratio of live load to dead load is developed. In addition, design strength defined as nominal strength divided by resistance factor and allowable strength defined as nominal strength divided by safety factor are also discussed. The results may offer a reference for the revision of the design criteria for steel compression member in steel bridges.

In Chapter 3, previous experiments relating to the load-bearing capacity of steel columns with welded box cross section under compression were collected. The FE models to analyze the load-bearing capacity of this kind of columns with residual stress as well as local and overall initial deflections into consideration were developed. Evaluation on accuracy of the developed FE models are carried out by comparing with the experimental results. The FEA results show good agreement with experimental results. Therefore, the developed FE models can be used for further parametrical analysis.

In Chapter 4, it concentrated on the quantitative influence caused by local and overall initial deflections on the load-bearing capacity of steel columns with welded unstiffened box cross section under compression. A variety of the normalized width-thickness and slenderness ratios were considered to cover the possible diverse range of columns. Various combinations of amplitude of the local and overall initial deflections were prepared for FE models. Based on the results of parametric analyses, initial deflection influence coefficient is proposed as a function of the initial deflections and the normalized width-thickness and slenderness ratios to describe the quantitative influence caused by the difference in amplitude of the local and overall initial deflections on the load-bearing

capacity. The accuracy of proposed formulae was verified by comparing with the experimental and FEA results.

In Chapter 5, it focused on the quantitative influence caused by local and overall initial deflections on the load-bearing capacity of steel columns with welded stiffened box cross section under compression. Stiffened box section columns under axial compression were chosen as a target for FE analysis with a wide range of the normalized width-thickness and slenderness ratios into consideration. Furthermore, various combinations of amplitude of the local and the overall initial deflections are analyzed. In addition, applicability of the formulae developed to predict their influence on ultimate strength of unstiffened box section columns to stiffened box section columns was discussed.

In Chapter 6, the main conclusions of this dissertation are summarized. In addition, the points which worth to be studied in the future work are figured out.

Table of Contents

CHAPTER 1

Introduction

1.1 Background

Steel structures are famous for its lightweight, high strength, good ductility, easy construction and aesthetics, therefore, widely used in actual engineering. Steel compression members made from thin plates accounts for a larger proportion of these kind of structures. For example, they are used for bars of truss girder as well as arch ribs or columns in cable bent tower and industrial building as shown in **Fig.1.1**. For a wish of full utilization of the cross section and strength, they are usually made into thin-walled structures.

However, such kind of structure are susceptible to loss of load-bearing capacity at the point far away lower than the yield resistance due to buckling [1,2,3]. After buckling phenomenon occurs, load-bearing capacity of the structures significantly decreases and the deformation intensely increases, which will result in disaster in practical engineering [4]. In general, buckling problem for the steel compression members can be divided into three kinds including overall buckling, local buckling and coupled buckling. For the columns with high slenderness ratio while low width-thickness ratio, the failure mode is mainly controlled by overall buckling. In the condition of short column with high width-thickness ratio, out-of-plane buckling tend to occur on the plate and hence result in local buckling failure. Considering the medium or long columns with high width-thickness ratio, local buckling is likely to occur at the early loading stage and the columns can continue to work due to the existing of the post-buckling strength. With the increasing of the external force, the columns will failed in the interaction of local and overall buckling.

Since the post-buckling strength behavior of the plate is stable [5,6], high width-thickness ratios exceeding the limit value are usually used in medium or long columns for a wish of economic benefit. It should be mentioned that although the structures satisfy with the requirement of local and overall buckling individually, the triggering of both local and overall buckling simultaneously will result in severe instability behavior [7,8,9,10,11]. Aiming at stability design, many researches were conducted, and various countries have drawn up their own codes for design of this kind of structures. However, the stability design methods differ greatly among different codes.

On the other hand, initial deflections, which are unavoidable during the manufacturing and assembling procedure, will result in significant decrease on the load-

bearing capacity of steel compression members. Initial deflections consist of local initial deflection on the plate and overall initial deflection along the member length. So far, many experiments and numerical analysis on load-bearing capacity of steel columns with both welded unstiffened and stiffened box cross section under axial compression have been conducted. And it is revealed that the local and overall initial deflections will significantly deteriorate the load-bearing capacity of the structures [12,13,14,15,16]. However, the quantitative influence caused by initial deflections on load-bearing capacity for such structure is still not clear.

(a) Truss bridge

(b) Arch bridge

(c) Suspension bridge

(d) Industrial building

Fig. 1.1 Structures including steel compression members

1.2 Literature Review

1.2.1 Stability design for steel compression member

1.2.1.1 Development of stability theory for overall stability

For a purpose of full use of strength and improving utilization of cross section, steel structures are always made into thin-walled structures, which make them so competitive in engineering such as long span bridges. However, the stability problems, which is the controlled factor of load-bearing capacity, appears and need to be considered in the steel structure design.

The critical load formula [17] for the elastic buckling of ideal axial compression members without initial imperfections taken into consideration was first proposed by Euler L and performed as follows:

$$P_{cr} = \pi^2 EI / L^2 \tag{1.1}$$

where E is the Young's modulus, I is the moment of inertia, L is the column length.

Based on the yield criterion of cross-sectional edge stress, the Perry-Robertson formula was proposed and used to calculate the stability coefficient for the columns failed in overall buckling. This formula is the basic for the overall buckling formulation adopted in EC3 as well as JTG and can be expressed as follows:

$$\sigma_{cr} / \sigma_y = \left[1+(1+\varepsilon_0)/\lambda^2\right]/2 - \sqrt{\left[1+(1+\varepsilon_0)/\lambda^2\right]^2/4 - 1/\lambda^2} \tag{1.2}$$

where λ is the normalized slenderness ratio, ε_0 is a factor relating to overall initial deflection.

Since the residual stress is not considered, the Perry Formula is more suitable to cold-formed thin-walled structures. However, for the welded steel compression columns, not only the initial deflections but also the residual stress need to be considered. Due to the influence of initial deflections and residual stress, the column tend to failed in the elastic-plastic stage and the failure belongs to limit load instability.

European Convention for Constructional Steelwork had carried out experimental study [18,19] on the load-bearing capacity of 1067 columns with different cross section. Finally, with L/1000 considered for the overall initial deflection and five kinds of cross-sectional residual stress distribution taken into consideration, five column curves were summarized. Based on the Perry-Roberson formula combined with experimental study, the formulae for overall buckling reduction adopted in EC3 [20] were proposed.

On the other hand, Li and Xiao et al. [21,22]. used the contrary calculation segment length method calculate ninety-six curves for the columns with overall initial deflection of L/1000 and residual stress distribution relating to several typical cross section considered. Finally, three column curves were summarized and based on Perry-Roberson formula, the design formulae against overall buckling were provided for Chinese design code, GB 50017 [23].

Based on experimental data of 1665 columns from West Europe, North America and

Japan with various cross section taken into consideration, Fukumoto and Itoh [24,25,26] had proposed three column curves. In JRA-2002 [27], only one column curve, which is on the conservative side of the column curves proposed in ECCS and closed to the Curve d, was adopted for the design against overall buckling.

Bjorhovde [28] had conducted research on fifty-six columns with different combinations of shape, steel grade and residual stress. With overall initial deflection of *L*/1000 taken into consideration, 112 maximum strength column curves were generated. In 1976, based on Bjorhovde's research, Structural Stability Research Council proposed three column curves. In AISC-1986 [29], one column curve with overall initial deflection of *L*/1500 taken into consideration was provided for both allowable strength design and load and resistance factor design.

So far, the formulae for the overall buckling design have been revised several times according to feedback in practice and further theoretical research. The formulae in recent codes for design of steel bridge are listed in **Table.1.1**, including Chinese code: *Specification for Design of Highway Steel Bridge* [30], Japanese code *Specification for Highway Bridges* [31], American code: *AASHTO LRFD Bridge Design Specification* [32] and European code: *Eurocode 3*: *Design of Steel Structures - Part 2: Steel Bridges* [33].

Table.1.1 Design formulae for overall buckling

Design code	Non-dimensional nominal strength
Ref [30]	$\sigma_{cr,o}/\sigma_y = \begin{cases} 1 & \lambda \le 0.2 \\ \left[1+(1+\varepsilon_0)/\lambda^2\right]/2 - \sqrt{\left[1+(1+\varepsilon_0)/\lambda^2\right]^2/4 - 1/\lambda^2} & \lambda > 0.2 \end{cases}$
Ref [31]	$\sigma_{cr,o}/\sigma_y = \begin{cases} 1 & \lambda \le 0.2 \\ 1.059 - 0.258\lambda - 0.19\lambda^2 & 0.2 < \lambda \le 1.0 \\ 1.427 - 1.039\lambda + 0.223\lambda^2 & \lambda > 1.0 \end{cases}$
Ref [32]	$\sigma_{cr,o}/\sigma_y = \begin{cases} 0.658^{\lambda^2} & \lambda \le 1.5 \\ 0.877/\lambda^2 & \lambda > 1.5 \end{cases}$
Ref [33]	$\sigma_{cr,o}/\sigma_y = \begin{cases} 1 & \lambda \le 0.2 \\ \dfrac{1}{\Phi + \sqrt{\Phi^2 - \lambda^2}} & \lambda > 0.2 \end{cases}$

1.2.1.2 Development of stability theory for local stability

For a plate simply supported along all edges and subjected to uniform compression, Bryan [34] developed a solution for the elastic critical stress performed as follows:

$$\sigma_{cr,\ el} = k\frac{\pi^2 E}{12(1-\nu^2)}(\frac{t}{b})^2 \tag{1.3}$$

where k is the buckling efficient, ν is the Poisson's ratio, b is the plate width, t is the plate thickness.

In 1932, the concept of effective width was first proposed by von Kármán et al. [35]. It is defined that two strips with total width, b_e, on the both sides of the plate supported along all edges can reach the yield stress. The approximate formula was proposed as follows:

$$b_e = 1.9t\sqrt{\frac{E}{\sigma_y}} \tag{1.4}$$

However, due to the exiting of initial deflection and residual stress in practice, the theoretical formula failed to provide accurate results for actual plate. According to many experimental studies, Winter [36] proposed the modified effective width formula as follows:

$$b_e = 1.9t\sqrt{\frac{E}{\sigma_y}}\left[1-0.574(\frac{t}{b})\sqrt{\frac{E}{\sigma_y}}\right] \tag{1.5}$$

Based on Winter formula, EC3 has developed formula after several times revision. As for design following JTG D64, the concept of effective width was also used. The difference is that the calculation of the local buckling reduction is based on the Perry-Roberson formula with normalized width-thickness ratio as parameter replacing the normalized slenderness ratio.

With respect to design in Japanese code, the design formula for local buckling reduction factor was proposed according to Euler critical stress formula. In JRA-2002, the design formula was performed as half of the Euler critical stress. In recent version of code, JRA-2017, the design formula was revised on the basis of Euler critical stress combined with experimental data and located at the conservative side of the experimental data.

In the 2012 version of AASHTO [37], the Q-factor Method was adopted to account for the local buckling reduction while in 2017 version, the Effective Width Method was adopted to replace the Q-factor Method. In addition, Direct Strength Method, which was proposed by Schafer and Pekoz [38] and extended by many researchers [39,40,41], was adopted in AISI [42] as an alternative to Effective Width Method for the design of cold-formed steel compression members under coupled buckling. To develop Direct Strength Method for welded box section compression member, many experimental and numerical studies have been contributed. Kwon et al [43,44,45] have conducted researches on the welded compression members with different and the modified Direct Strength Method was proposed based on the original one. In addition, Shen [46] extended the Direct Strength Method to the welded compression members made of high strength steel. However, the Direct Strength Method adopted in recent design code is only suitable for cold-formed compression member. The design formula against the local buckling in various codes are summarized in **Table. 1.2**.

Table.1.2 Reduction factor for local buckling

Design code	Reduction factor ρ
Ref [30]	$\frac{b_e}{b}=\begin{cases}1 & R\le 0.4\\ \left[1+(1+\varepsilon_0)/R^2\right]/2-\sqrt{\left[1+(1+\varepsilon_0)/R^2\right]^2/4-1/R^2} & R>0.4\end{cases}$
Ref [31]	$\rho_{crl}=\begin{cases}1 & R\le 0.7\\ \left(\frac{0.7}{R}\right)^{1.19} & R>0.7\end{cases}$
Ref [32]	$\frac{b_e}{b}=\begin{cases}1 & b/t\le \lambda_r\sqrt{F_y/F_{cr}}\\ \left(1-c_1\sqrt{\frac{F_{el}}{F_{cr}}}\right)\sqrt{\frac{F_{el}}{F_{cr}}} & b/t>\lambda_r\sqrt{F_y/F_{cr}}\end{cases}$
Ref [33]	$\rho=\begin{cases}1 & R\le 0.5+\sqrt{0.085-0.055\psi}\\ \frac{R-0.055(3+\psi)}{R^2} & R>0.5+\sqrt{0.085-0.055\psi}\end{cases}$

1.2.2 Influence of initial deflections for steel compression members

Many researches have revealed that steel compression members consist of thin plate were susceptible to buckling instability due to high slenderness and width-thickness. It is also well known that such kind of structures are sensitive to the initial deflections [47,48,49,50]. However, initial deflections are unavoidable during manufacturing and assembling procedure and their value are random in a wide range. Even a tiny initial deflection will result in significant decrease on the load-bearing capacity [51,52,53,54,55,56].

In previous researches focusing on unstiffened box section columns, the amplitude of initial deflections was measured prior to the experiments. In Usami's experiment [57], amplitudes of overall initial deflection on 19 welded box section columns were measured. The maximum overall initial deflection was L/1590 and the average was L/3850, where L was the column length. In Rasmussen's research [58] with six welded box section columns measured, their maximum and average amplitudes were L/546 and L/1172, respectively. Somodi and Kövesdi [59] had measured initial deflections on 49 welded steel columns made of various steel grades. The results show that a total of 23 columns had overall initial deflection amplitudes larger than L/1000 and the average value of total 49 columns is L/945. In Shi's experiment [60], amplitudes of local initial deflection on four welded stub columns were measured. The maximum and average were b/341 and b/512, respectively, where b was the width of the plate.

However, these values are much different from those allowed in some specifications such as overall initial deflection of L/1000 in JTG D64, JRA and EC3, L/1500 in AASHTO. As for amplitude of local initial deflection, b/150 is adopted in JRA while EN1993-1-5 [61] suggests b/200 in the numerical analysis. In addition, b/200 is also adopted in GB50205 [62] as construction tolerance.

On the other hand, many numerical studies aimed at investigating the influence of the initial deflections have been also contributed. By means of numerical analysis, Degée [63] investigated the influence of residual stress, local and overall initial deflection on the load-bearing capacity of rectangular box section columns. It was found that FE model with residual stress, local initial deflection of b/1000 and overall initial deflection of L/1000 into consideration could provide an accurate replication to experimental results.

In addition, the FE model considering local initial deflection of *b*/250 and overall initial deflection of *L*/725 gave close load-bearing capacity as that of FE model with residue stress.

Kwon [64] investigated the effect of local initial deflection on load-bearing capacity of welded RHS columns undergoing coupled buckling. The increase of the local initial deflection from *b*/2000 to *b*/100 resulted in the reduction of the load-bearing capacity corresponding to 28.5%. In Inose's study [65], the increase of the initial deflection from *b*/450 to *b*/150 led to the reduction of load-bearing capacity of welded box section columns up to 11.4%.

Ban [66] studied the influence of the overall initial deflection on the overall buckling behavior of welded box section steel columns. The increase of overall initial deflection from *L*/2500 to *L*/1000 resulted in a decrease of load-bearing capacity by about 7% on average. Coelho [67] conducted a series of numerical analyses to investigate the sensitivity of the load-bearing capacity to imperfection. Models with four different amplitude of the overall initial deflection, which are *L*/1000, *L*/500, *L*/250 and *L*/125, were analyzed. The increase of the overall initial deflection resulted in the 40% decrease of load-bearing capacity.

Kang [68] studied the effect of overall initial deflection on load-bearing capacity of welded steel box columns by selecting two different values i.e. *L*/1000 and *L*/500 with the normalized slenderness ratios from 0.8 to 1.8. The results revealed that with the increase of the overall initial deflection, the average and maximum of reduction on load-bearing capacity were about 7.2% and 9.4% respectively. Moreover, the influence of the overall initial deflection showed to be related to the normalized slenderness ratio. The maximum reduction appeared at the normalized slenderness ratio of 1.25. Lu Yang [69] carried out numerical analysis on load-bearing capacity of box section columns with normalized slenderness ratio from 0.2 to 1.6 and ratio of width to thickness equal to 20 and 60. The value of *L*/2000, *L*/1000 and *L*/500 were prepared for the overall initial deflection while *b*/500, *b*/200 and *b*/100 were introduced to local initial deflection. Finally, maximum influence of 10% was found with the different amplitude of initial deflections. More importantly, Lu Yang emphasized that the local initial deflection have the more obvious influence on the structure with high normalized width-thickness ratio while overall initial deflection affects the slender column more obviously.

Wang et al. [70] conducted a research on initial deflection sensitivity of the column due to different steel grade. Overall initial deflection of $L/1000$ was prepared for columns made of Steel Q235 and Q460. The results indicate that the columns made of high strength steel tends to be less sensitive to the influence of initial deflection than the columns made of the normal strength steel.

With respect to the stiffened box section columns, measurement targeting on the initial deflections had also been contributed. In Nakai's tests conducted on 9 columns [71], amplitudes of overall initial deflection on test specimens were measured. Their maximum is L/333 and average is L/661. Usami [72] conducted experiment on 14 stiffened box section columns, their maximum is $L/550$ and average is $L/867$ for the overall initial deflection; the maximum value is $b/330$ and average is $b/534$ for the local initial deflection. In previous research conducted by Murakoshi. et.al [73] three kinds of amplitude (i.e. $L/1000$, $L/3000$, $L/5000$) of the overall initial deflection were considered on the columns with different normalized slenderness ratio. It is found that the amplitude of the initial deflection has great influence on the ultimate strength of the stiffened box section columns. As the amplitude of the initial deflection increases from $L/5000$ to $L/1000$, the ultimate strength decreases at most 11.7%. In addition, the decrement on ultimate strength caused by initial deflection becomes more severe with the increase of the normalized slenderness ratio.

1.3 Objectives and layout of the dissertation

The main objective conducted in this dissertation is to make a comparison on the stability design of steel compression members with welded box cross section among major codes and develop formulae on the quantitative influence of initial deflections on load-bearing capacity for such kind of structures. The dissertation consists of six chapters as follows:

Chapter 1 gives the background and objectives of the research together with the overview of the previous researches carried out in the related field. In addition, the layout was given.

In Chapter 2, provisions concerning about stability design of steel compression member for steel bridge in those codes adopting the Partial Factor Design Method including Chinese code *Specification for Design of Highway Steel Bridge*, Japanese code

Specification for Highway Bridges, American code *AASHTO LRFD Bridge Design Specification*, European code *Eurocode 3*: *Design of Steel Structures - Part 2: Steel Bridges*, are outlined first. Nominal strengths related to the buckling parameters slenderness and width-thickness ratios following these codes are calculated and compared with each other. Safety factor performed as a function of ratio of live load to dead load is developed. In addition, design strength defined as nominal strength divided by resistance factor and allowable strength defined as nominal strength divided by safety factor are also discussed. The results may offer a reference for the revision of the design criteria for steel compression member in steel bridges.

In Chapter 3, previous experiments relating to the load-bearing capacity of steel columns with welded box cross section under compression were collected. The FE models to analyze the load-bearing capacity of this kind of columns with residual stress as well as local and overall initial deflections into consideration were developed. Evaluation on accuracy of the developed FE models are carried out by comparing with the experimental results. The FEA results show good agreement with experimental results. Therefore, the developed FE models can be used for further parametrical analysis.

In Chapter 4, it concentrated on the quantitative influence caused by local and overall initial deflections on the load-bearing capacity of steel columns with welded unstiffened box cross section under compression. A variety of the normalized width-thickness and slenderness ratios were considered to cover the possible diverse range of columns. Various combinations of amplitude of the local and overall initial deflections were prepared for FE models. Based on the results of parametric analyses, initial deflection influence coefficient is proposed as a function of the initial deflections and the normalized width-thickness and slenderness ratios to describe the quantitative influence caused by the difference in amplitude of the local and overall initial deflections on the load-bearing capacity. The accuracy of proposed formulae was verified by comparing with the experimental and FEA results.

In Chapter 5, it focused on the quantitative influence caused by local and overall initial deflections on the load-bearing capacity of steel columns with welded stiffened box cross section under compression. Stiffened box section columns under axial compression were chosen as a target for FE analysis with a wide range of the normalized width-thickness and slenderness ratios into consideration. Furthermore, various combinations

of amplitude of the local and the overall initial deflections are analyzed. In addition, applicability of the formulae developed to predict their influence on ultimate strength of unstiffened box section columns to stiffened box section columns was discussed.

In Chapter 6, the main conclusions of this dissertation are summarized. In addition, the points which worth to be studied in the future work are figured out.

The layout of this dissertation is given in **Fig.1.2**.

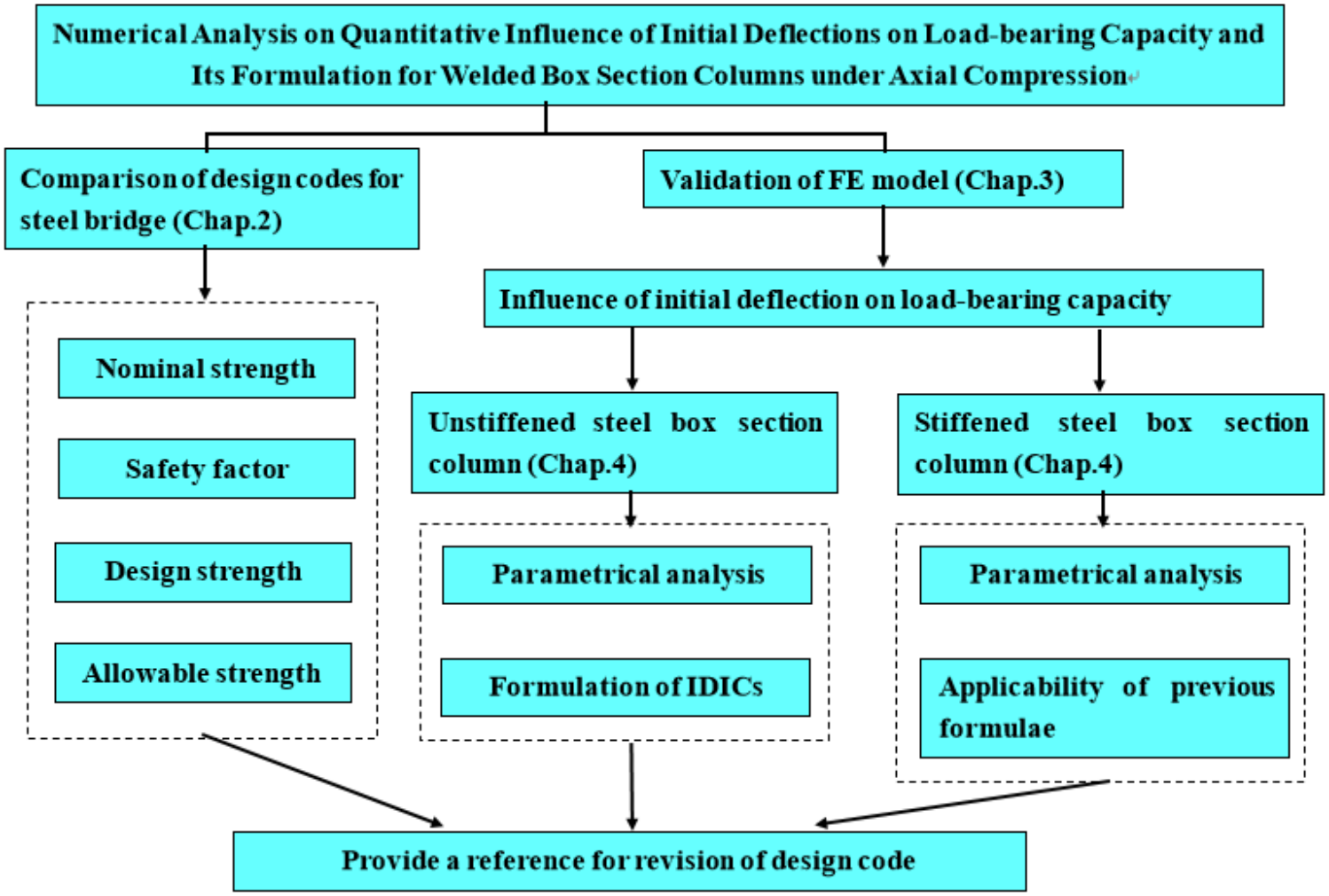

Fig. 1.2 Layout of the dissertation

CHAPTER 2

Comparison among Major Codes for Stability Design of Steel Compression Members in Steel Bridge with Partial Factors taken into Consideration

2.1 Introduction

Steel compression members are widely used in the actual bridge construction such as bars of truss girder or arch ribs [74]. However, due to high slenderness and width-thickness ratios, these kind of structures are more susceptible to buckling instability failure than strength failure.

To prevent buckling instability failure, both overall stability [75,76] of the columns and local stability [77] of the plate need to be considered during the design procedure. Based on a number of experiment and numerical analysis, various countries have drawn up their own design codes for stability of steel bridge. However, the calculation methods of stability design differ greatly among different codes.

In this chapter, provisions concerning about stability design of steel compression member for steel bridge in those codes adopting the Partial Factor Design Method including Chinese code *Specification for Design of Highway Steel Bridge*, Japanese code *Specification for Highway Bridges*, American code *AASHTO LRFD Bridge Design Specification*, European code *Eurocode 3*: *Design of Steel Structures - Part 2: Steel Bridges*, are outlined first. Nominal strengths related to the buckling parameters slenderness and width-thickness ratios following these codes are calculated and compared with each other. Safety factor performed as a function of ratio of live load to dead load is developed. In addition, design strength defined as nominal strength divided by resistance factor and allowable strength defined as nominal strength divided by safety factor are also discussed. The results may offer a reference for the revision of the design criteria for steel compression member in steel bridges.

2.2 Outline of design for nominal strength in each code

2.2.1 Chinese code: Specification for Design of Highway Steel Bridge

Against the instability, nominal strength in JTG D64 can be expressed by two parts with local and overall buckling taken into consideration. One is the overall buckling stability coefficient expressed by the normalized slenderness ratio. The other is the potential reduction in capacity due to local buckling, which is considered through effective width. To make a definitive comparison among codes listed in this research, the non-dimensional nominal strength, which is the nominal strength normalized by the

compressive strength is used as follows,

$$\bar{\sigma}_{cr} = \varphi(\lambda) \cdot \frac{A_e}{A_g} \tag{2.1}$$

where $\bar{\sigma}_{cr}$ is the non-dimensional nominal strength, A_g is the gross area of the cross-section, A_e is the effective cross-sectional area, φ is overall buckling stability coefficient, λ is the normalized slenderness ratio.

2.2.2 Japanese code: Specification for Highway Bridges

Design in JRA for the nominal strength can be performed as a product format consisting of the non-dimensional local buckling stress determined by the normalized width-thickness ratio and the non-dimensional overall buckling stress expressed by the normalized slenderness ratio without local buckling as follows,

$$\bar{\sigma}_{cr} = p_{crg} \cdot p_{crl} \tag{2.2}$$

where p_{crg} is the non-dimensional buckling stress without local buckling, p_{crl} is the non-dimensional local buckling stress.

2.2.3 American code: AASHTO LRFD Bridge Design Specification

With respect to Design in AASHTO, **t**he non-dimensional overall buckling stress is related to the normalized slenderness ratio. On the other hand, the reduction factor caused by the local buckling is considered through the ratio of effective area to gross area as follows,

$$\bar{\sigma}_{cr} = \frac{P_{cr}}{P_0} \cdot \frac{A_e}{A_g} \tag{2.3}$$

where P_{cr} is the nominal compressive resistance, P_0 is the nominal yield resistance.

2.2.4 European code: Design of Steel Structures - Part 2: Steel Bridges

In EC3, the effective width method is employed in the design of steel structure. With respect to the calculation of reduction factor due to overall buckling, the ratio of effective area to gross area is used to modify the normalized slenderness to account for the interaction between local and overall buckling as shown in Eq. (5). Furthermore, the ratio

of effective area to gross area is multiplied by the reduction factor to determine the final non-dimensional nominal strength as follows,

$$\bar{\sigma}_{cr} = \rho \cdot \chi(\bar{\lambda}) \tag{2.4}$$

$$\bar{\lambda} = \sqrt{\rho} \cdot \lambda \tag{2.5}$$

where, ρ is the reduction factor for local buckling which can be performed as the ratio of effective area to the gross area, χ is the reduction factor for overall buckling, $\bar{\lambda}$ is a modified slenderness ratio.

2.2.5 Comparison on overall and local buckling reduction factor among those codes

To provide a definitive comparison among the four codes, the formulae are detailed in the subsequent sections for a column with welded square cross section. The non-dimensional nominal strengths according to those formulae listed in those codes are plotted in **Fig. 2.1** (a) to (d) with the horizontal and vertical axis set as the normalized slenderness and width-thickness ratios, respectively. The parameters λ and R are defined as follows,

$$\lambda = \frac{1}{\pi}\sqrt{\frac{\sigma_y}{E}}\frac{L}{r} \tag{2.6}$$

$$R = \frac{b}{t}\sqrt{\frac{12(1-\upsilon^2)}{k\pi^2}\frac{\sigma_y}{E}} \tag{2.7}$$

where, σ_y is the nominal yield stress, E is Young's Modulus, L is the length of the column, r is the radius of gyration, b is the width of the plate, t is the thickness of the plate, v is the Poisson's ratio, and k is the buckling coefficient.

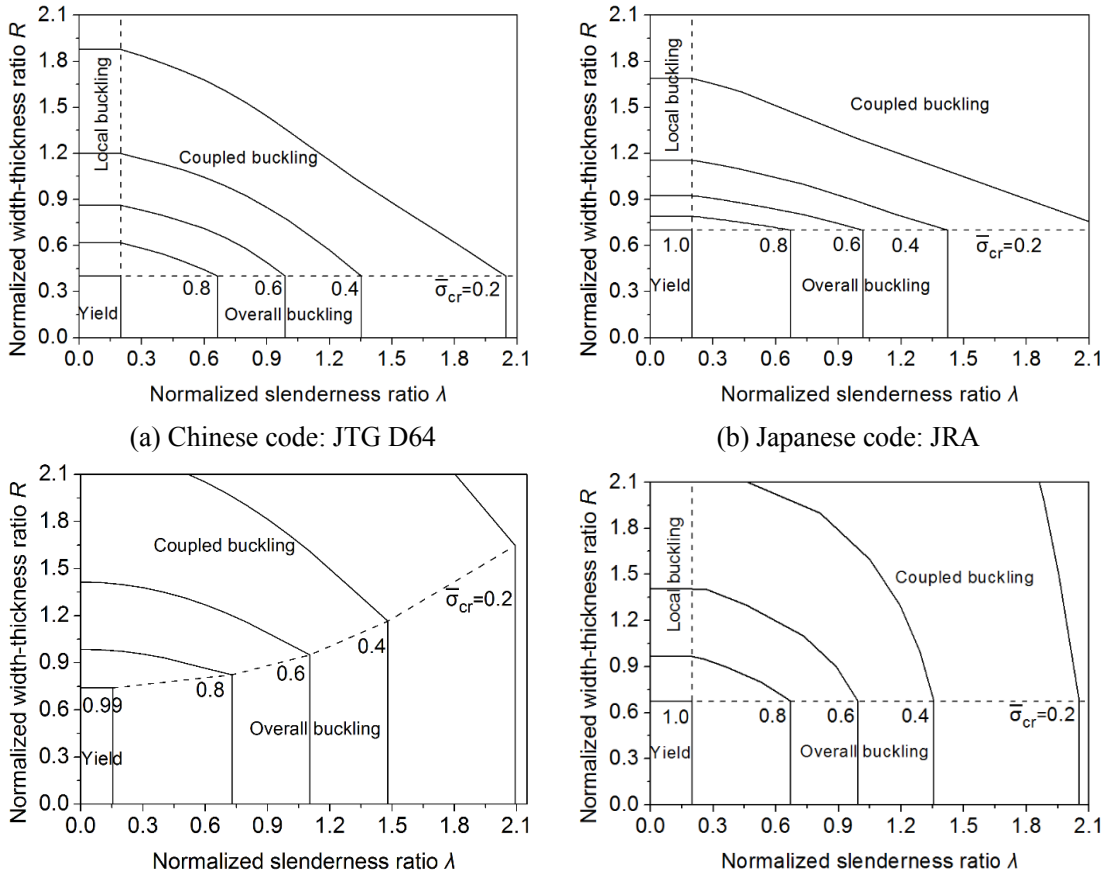

(a) Chinese code: JTG D64

(b) Japanese code: JRA

(c) American code: AASHTO

(d) European code: EC3

Fig.2.1 Non-dimensional nominal strength based on the four codes

As investigated in previous research, the initial deflections are unavoidable in practice and have significant effect on the ultimate strength of the structures. The initial deflections can be divided into two parts. One is the overall initial deflection along the columns length; the other is the local initial deflection on the plate. Referred to practice in different country, different initial deflections were considered in the strength formulae mentioned above. Among these codes, 1/1000 of the length is adopted as allowable overall initial deflection in JRA, JTG D64 and EC3, while 1/1500 of the length is adopted in AASHTO. The buckling curves for the box section columns, in which only overall buckling is considered, are compared in **Fig. 2.2(a)**. It can be found that when the normalized slenderness ratio λ is lower than 0.2, the EC3 and JTG D64 provide the highest estimate of nominal strength. In the range of λ from 0.2 to 1.5, nominal strength calculated by AASHTO is slightly higher than other three codes. A possible reason is that the

allowable overall initial deflection is smaller than other codes. When $\lambda \geqslant 1.0$, the JRA give higher nominal strength than EC3 and JTG D64.

To consider the influence of local buckling, the notion of effective width is adopted in the AASHTO, EC3 and JTG D64. The design formulae following AASHTO and EC3 are developed based on Winter formula [78] and then slightly modified. Although in Winter formula, initial deflection and residual stress are considered, the detailed value is unknown. On the other hand, design following JTG D64 uses the Perry formula to calculate the local buckling reduction factor. In JRA, local buckling reduction factor is obtained based on the Euler curve and located at the conservative side of the experimental results. As for the local initial deflection in FE model, it is recommended as 1/200 of the plate width in JTG D64 and EC3, while 1/150 of plate width is allowed in JRA. In this part, the load buckling reduction factor is defined as the ratio of effective area to gross area for JTG D64, AASHTO and EC3. The local buckling reduction factor is plotted with normalized width-thickness ratio in **Fig. 2.2(b)**. It can be observed the local buckling reduction factors following AASHTO and EC3 are approximately the same and higher than that following JRA and JTG D64. On the other hand, in the range of R from 0.4 to 1.0, JRA provides higher value than JTG D64 while it will be contrary with R larger than 1.0.

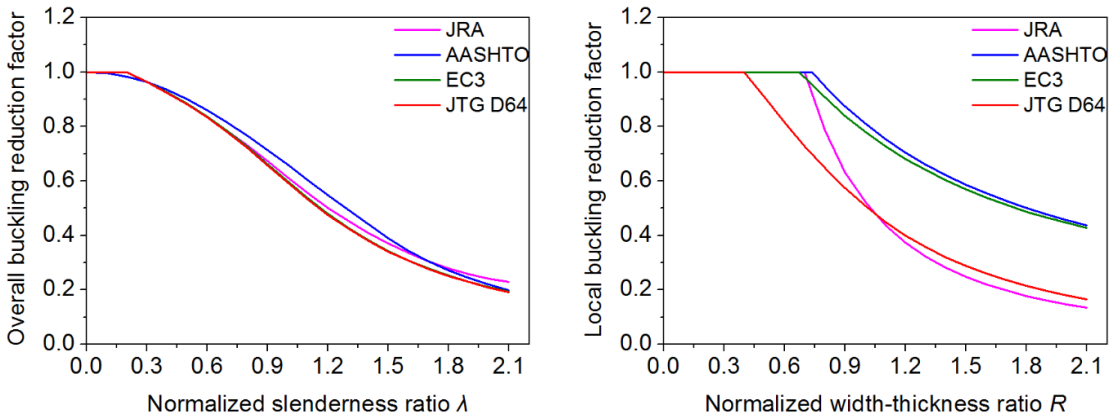

(a) Overall buckling (b) Local buckling

Fig. 2.2 Comparison among the four codes on reduction factor

2.2.6. Comparison of nominal strength among these codes

The non-dimensional nominal strength calculated by the design codes are plotted with normalized slenderness and width-thickness ratios as shown in **Fig. 2.3**. It can be seen that in general, the nominal strength generally decreases with the increase of normalized slenderness ratio λ. When the R-value is at low level(i.e. $0.5 \leq R \leq 0.7$), the nominal strengths following JRA, AASHTO and EC3 show good agreement with each other, while the calculation following JTG D64 provide lower results than others. The reason is that local buckling reduction is considered in JTG D64 when R-value exceeds 0.4. With the increase of R-value, the nominal strengths calculated according to AASHTO, EC3 and JRA are different since the local buckling is taken into consideration. In the range of R-value from 0.9 to 1.5, for compression member with low or high λ-value (i.e. $\lambda \leq 0.5$ or $\lambda > 1.5$), AASHTO gives nominal strength closed to that in EC3. This phenomenon is similar to that as shown in **Fig.2.2** since the failure mode is controlled by local buckling in the low level of λ-value while overall buckling plays a more important role in the area of high λ-value. With respect to the area of medium λ-value (i.e. $0.5 < \lambda \leq 1.5$), AASHTO provides the highest nominal strength. The results following EC3 are lower than that of AASHTO while higher than JRA and JTG D64. When the R-value goes to exceed 1.5, AASHTO gives nominal strength closed to that in EC3. With R-value equal to 0.9, nominal strength following JRA is higher than that of JTG D64. As the R-value exceeds 0.9, nominal strengths based on the two codes show agreement with each other.

In addition, FE analysis concerning about the nominal strength for the steel compression member was conducted. The steel column with unstiffened box cross section was chosen as a target in FE model with 0.25 of yield stress for residual stress, 1/150 of plate width for local initial deflection and 1/1000 of column length for the overall initial deflection into consideration. The FE model building would be described in detail in Chapter 3. In this part, the FEA results were plotted and compared with formulae results as shown in **Fig. 2.3**. It can be seen that for the stage that local buckling is not supposed to occur (i.e. R=0.5), therefore, FEA results show good agreement with the formula results based on AASHTO, EC3 and JRA while higher than that of JTG D64. At the point of R-value equal to 0.7, the formula results start to be different with the FEA results. For the λ

<1.0, design following AASHTO, EC3 and JRA provide higher nominal strength than the FEA results. In the range of *R*-value from 0.9 to 2.1 and λ-value from 0.2 to 2.1, the results calculated according to AASHTO and EC3 are higher than the FEA results. JRA and JTG D64, on the other hand, offer the lower strength than the FE analysis. In general, the results based on EC3 correspond better with the FEA results than others.

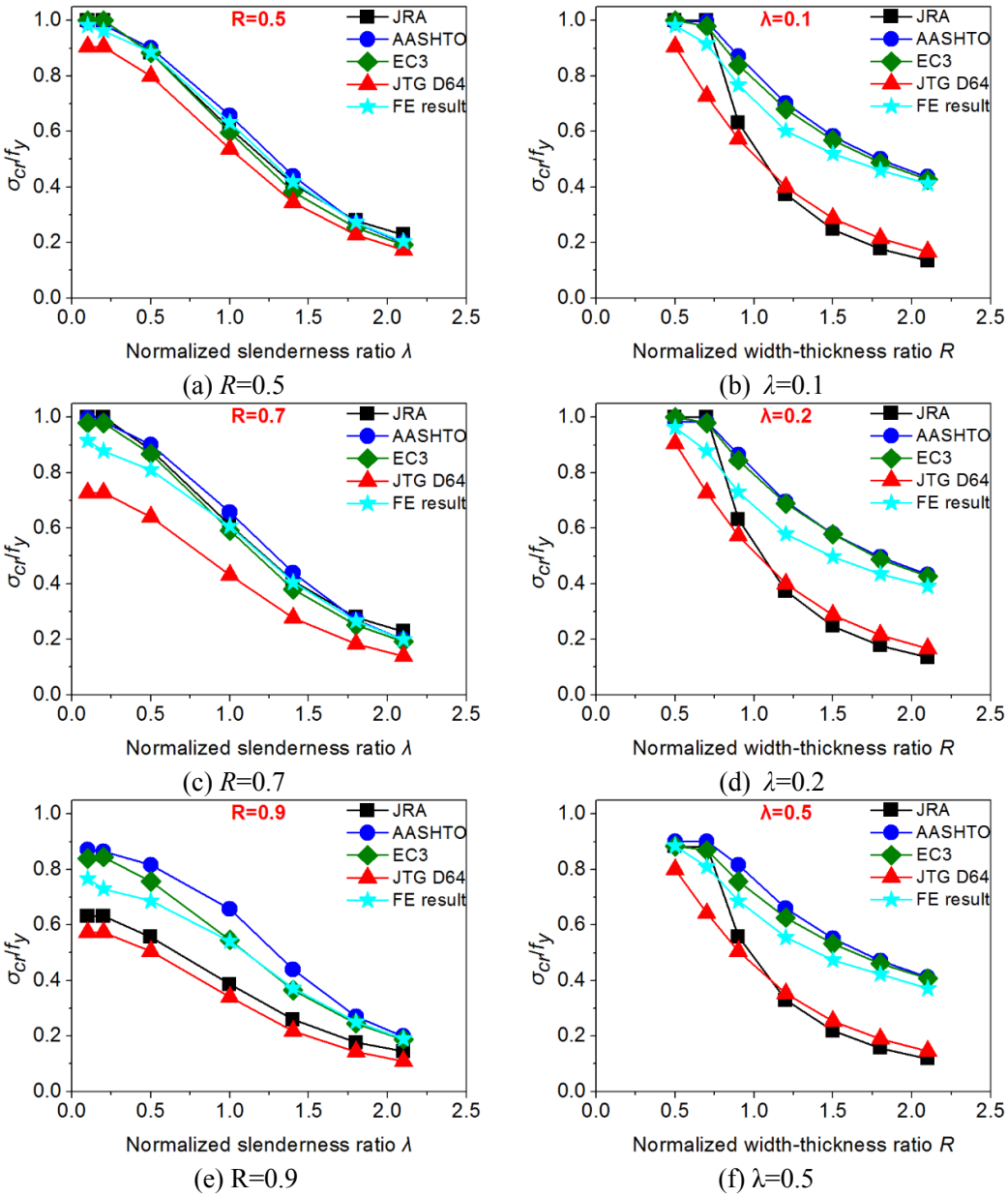

(a) *R*=0.5 (b) λ=0.1

(c) *R*=0.7 (d) λ=0.2

(e) R=0.9 (f) λ=0.5

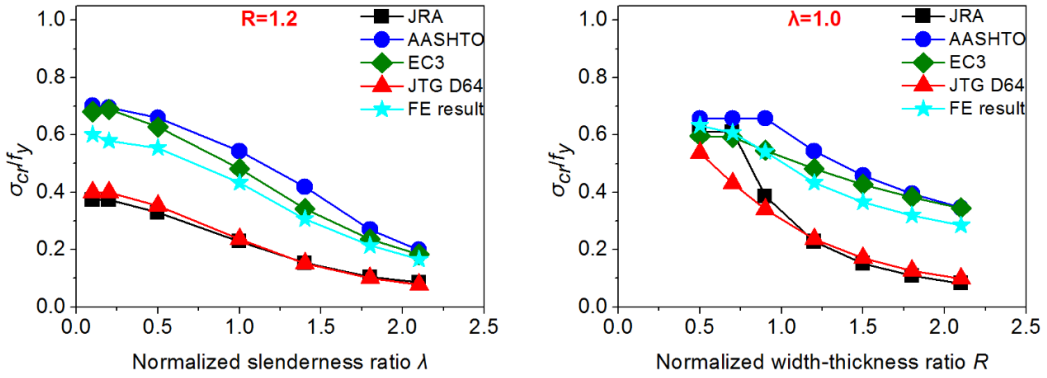

(g) R=1.2

(h) λ=1.0

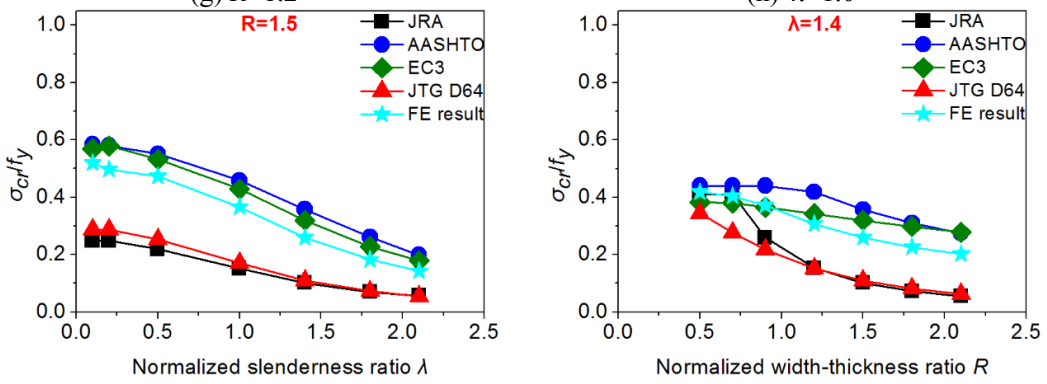

(i) R=1.5

(j) λ=1.4

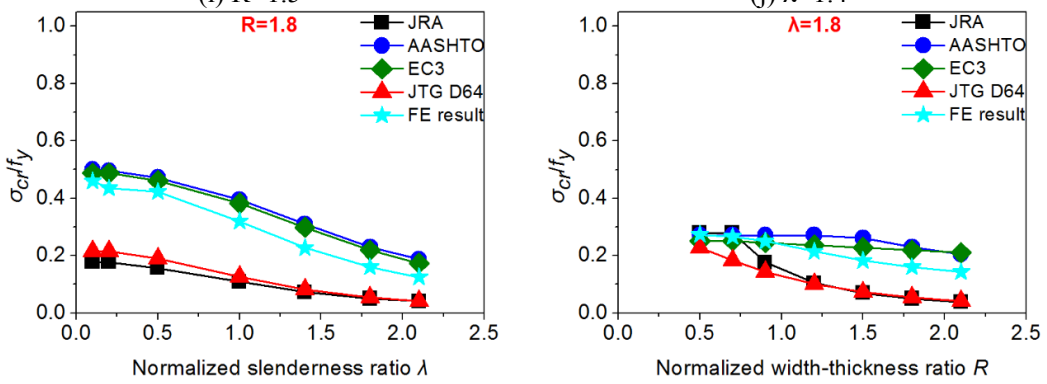

(k) R=1.8

(l) λ=1.8

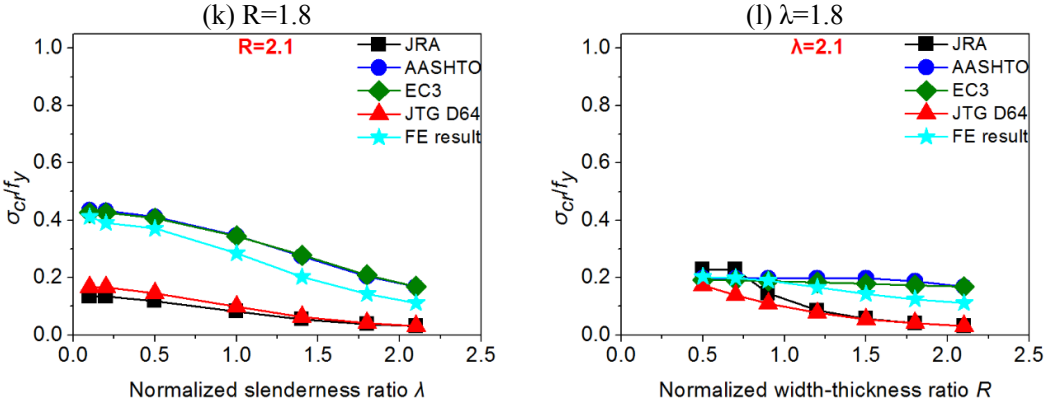

(m) R=2.1

(n) λ=2.1

Fig. 2.3 Comparison of the nominal strength among the codes

2.3 Outline of Partial Factors Design in these codes

Design following the provisions by the partial factor design method satisfies the requirement when the design strength equals or exceeds the required strength based on the combination of actions. In addition, the resistance is scaled down while actions are scaled up against the uncertainties of material property, variable action, design error, construction errors and so on. The design shall be performed as:

$$S = R_D \tag{2.8}$$

where S is the required strength using the actions combination following the Partial Factor Design Method, R_D is design strength.

So far, the partial factor design method has been widely adopted in many national design codes to replace the allowable design method. However, the provisions for the partial factors differ greatly in different design codes. Therefore, four codes adopted the partial factor design method were listed and compared with each other to investigate their difference on partial factors.

2.3.1 Design following the four codes

In Chinese code JTG D64, the partial factor design method is provided for the steel bridge design. It should be mentioned that the partial factors follow the provisions of *JTG D60*: *General Specifications for Design of Highway Bridges and Culverts* [79] and the formula shall be performed as follows,

$$\gamma_0(\sum_{i=1}^{m}\gamma_{Gi}G_{ik} + \gamma_{Q1}\gamma_{L1}Q_{1k} + \psi_c\sum_{j=2}^{n}\gamma_{Qj}\gamma_{Lj}Q_{jk}) \le \frac{R_K}{\gamma_R} \tag{2.9}$$

where, G_{ik} is the characteristic value of permanent action, Q_{1k} and Q_{jk} are the characteristic values of primary variable action and subsidiary variable action, respectively; γ_0 is the structural importance factor, γ_{Gi} is the permanent action partial factor, γ_{Q1} and γ_{Qj} are the primary and subsidiary variable action partial factor, respectively; γ_{L1} and γ_{Lj} are the primary and subsidiary action modifying coefficient according to design working life, respectively; ψ_c is the combination factor for variable action, R_k is the nominal strength of structural resistance, γ_R is the resistance partial factor.

In JRA, design for limit state condition 3 shall be performed as follows,

$$\sum S_i(\gamma_{pi}\gamma_{qi}P_i) \le \xi_1\xi_2\Phi_{RU}R_U \tag{2.10}$$

where, S_i is the required strength based on the combination of the actions, R_U is the nominal strength of structural resistance, respectively; γ_{pi} is the action combination factor, γ_{qi} is the action partial factor, P_i is the characteristic value of action, ξ_1 is the investigation and analysis factor, ξ_2 is the member and structure partial factor, Φ_{RU} is the resistance factor.

In AASHTO, design shall be performed as follows,

$$\sum \eta_i\gamma_iQ_i \le \phi R_n \tag{2.11}$$

where, η_i is the load modifier equal to 1.0 for conventional design, γ_i is the action partial factor, Q_i is the characteristic value of action, Φ is the resistance factor, R_n is the nominal strength of structural resistance.

In EC3, the design shall be performed as follows,

$$\gamma_G G_k + \gamma_Q Q_k + \sum_{i=2}^{n}\gamma_{Qi}\psi_i Q_{ki} \le \frac{R_K}{\gamma_M} \tag{2.12}$$

where, G_k is the characteristic value of permanent action, Q_k and Q_{ki} are the characteristic value of primary variable action and subsidiary variable action, respectively; R_k is the nominal strength of structural resistance, γ_G is the permanent action partial factor, γ_Q and $\gamma_{Q\mathrm{i}}$ are the primary variable action partial factor and subsidiary variable action partial factor, respectively; ψ_i is the combined factor for variable action, γ_M is the resistance partial factor.

2.3.2 Comparison of safety factors

Considering that the design theory and the formula format in the codes are similar, the load and resistance partial factors can be formulated as a unified format, which is similar to the allowable stress design method. In this study, the combination of a permanent action and the primary variable action (i.e. dead load and live load) is considered for simplicity. Therefore, the safety factor K can be formulated as follows,

$$S = \gamma_0(\gamma_D D + \gamma_L L) = \gamma_0\frac{\gamma_D + \rho_D\gamma_L}{1+\rho_D}(D+L) \le R_D = \frac{R_S}{\gamma_S} \tag{2.13}$$

$$D + L \le \frac{R_S}{K} \tag{2.14}$$

$$K = \gamma_S \gamma_0 \frac{\gamma_D + \rho_D \gamma_L}{1 + \rho_D} \tag{2.15}$$

where, D is the dead load, L is the live load, ρ_D is the ratio of live load to dead load, R_S is nominal strength, γ_S is the resistance partial factor, R_S/γ_S is the design strength, R_S/K is the allowable strength.

It should be mentioned that R_S is the unified symbol concerning about the nominal strength which is performed as R_k, R_U and R_n in **Eqs. (2.9)-(2.12)**. In addition, non-dimensional nominal strength $\bar{\sigma}_{cr}$ can be obtained through the R_S-value normalized by the gross area compressive strength (i.e. f_yA). γ_S is unified symbol concerning about the resistance factor which is performed as γ_R, $1/\xi_1\xi_2\Phi_{RU}$, $1/\Phi$ and γ_M in **Eqs. (2.9)-(2.12)**. The partial factors in the codes are listed in **Table.2.1**. In addition, two structural importance factors (i.e. 1.1 and 1.0), which considered for two design levels according to the severe extent if the bridge is damaged, are introduced to the calculation of safety factors. They are safety level I (abbreviate as JTG D64 I) and safety level II (abbreviate as JTG D64 II) correspond to very severe extent and relatively severe extent.

Table.2.1 The partial factors in the four codes

	Partial factors			
Country	γ_0	γ_D	γ_L	γ_s
JRA	1.0	1.05	1.25	1.307
AASHTO	1.0	1.25	1.75	1.053
EC3	1.0	1.05	1.35	1.1
JTG D64 I	1.1	1.2	1.4	1. 25
JTG D64 II	1.0	1.2	1.4	1. 25

To make a definitive comparison on the safety factors, an appropriate range of ratio of live load to dead load ρ_D should be considered. Hansell and Viest [80] reported that the ρ_D is a function of dynamic load allowance IM and bridge span length, and proposed the following equation for the estimation of ρ_D:

$$\rho_D = \frac{1}{0.0433(1+IM)L} \tag{2.16}$$

where IM is the dynamic load allowance equal to 0.33 in AASHTO, L is the bridge span.

Considering the bridge with the span larger than 5m, ρ_D would be less than 3.47. Therefore, the ratios of live to dead load ρ_D ranging from 0.1 to 3.5 were considered for safety factors and their influence is illustrated in **Fig.2.4**. It can be seen that the safety factor increases as the ρ_D-value increases from 0.1 to 3.5 for all codes. The increasing tendency is approximately the same among JTG D64, JRA and EC3. Moreover, The JTG D64 I provides the highest safety factors than others, and then is JTG D64 II and JRA in the order, while the EC3 offers lowest safety factors than other codes. Safety factors following AASHTO increase more quickly along with the increase of ρ_D-value than other codes. With ρ_D-value less than 0.25, safety factors according to AASHTO is lower than JRA. In the range from 0.25 to 2.0, safety factor following AASHTO locates between JTG D64 II and JRA. When the ρ_D-value exceeds 2.0, safety factor according to AASHTO is higher than that of JTG D64 II while lower than JTG D64 I.

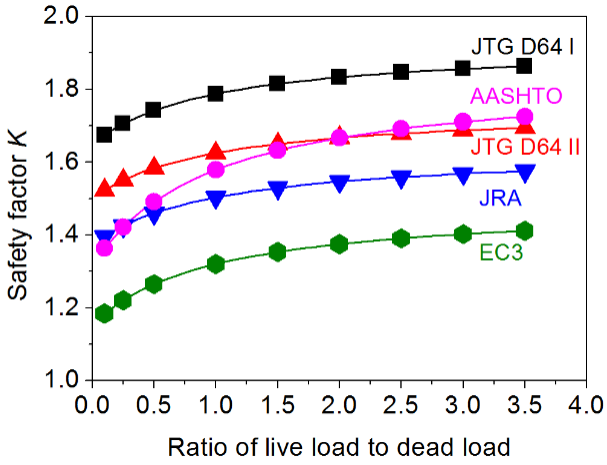

Fig. 2.4 Comparison of safety factors

2.4 Comparison of nominal strength combined with partial factors

2.4.1 Comparison of design strength

Design strength following the design codes is defined as the nominal strength divided by the resistance factor, which the value is larger than 1.0 as listed in **Table. 2.1**.

Among those codes, JRA offers the highest resistance factor, and then is JTG D64 and EC3 in the order, while AASHTO gives a lower value than other codes. The design strength is plotted with λ-value and R-value as shown in **Fig. 2.5**. When the resistance factor is considered, the decreasing tendency of design strength related to the increase of λ-value and R-value is similar to that of nominal strength as shown in **Fig. 2.3**. The difference occurs on the value of design strength. The figures show that in the whole range of λ-value (0.1 to 2.1) and R-value (0.5 to 2.1) considered in this research, generally, the AASHTO provides the higher design strength than that calculated according to EC3. In addition, the difference on design strength following AASHTO and EC3 becomes more obvious than that in nominal strength. JRA and JTG D64 offer conservative results than AASHTO and EC3. In the range of $R \leq 0.9$, JRA provides higher design strength than JTG D64. When the R-value equal or exceeds 1.2, with $\lambda \leq 1.0$ JTG D64 gives higher design strength than JRA. In the range of $\lambda > 1.0$, design strengths following JRA and JTG D64 show good agreement with each other.

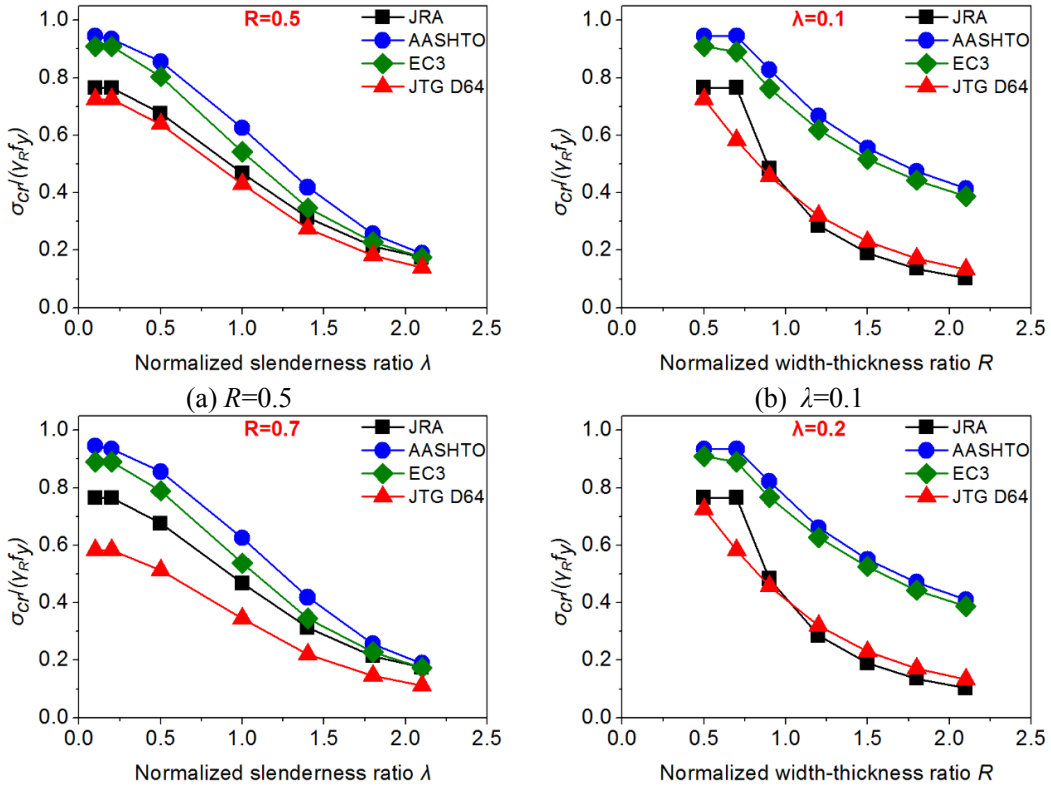

(a) R=0.5 (b) λ=0.1

(c) R=0.7 (d) λ=0.2

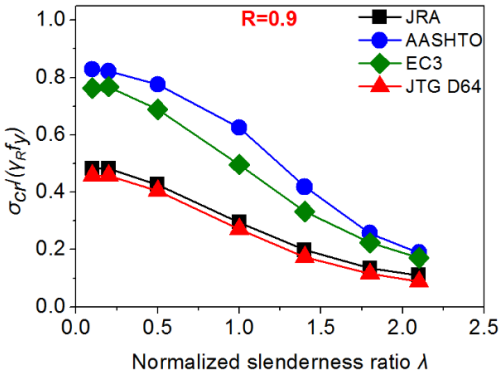

(e) R=0.9

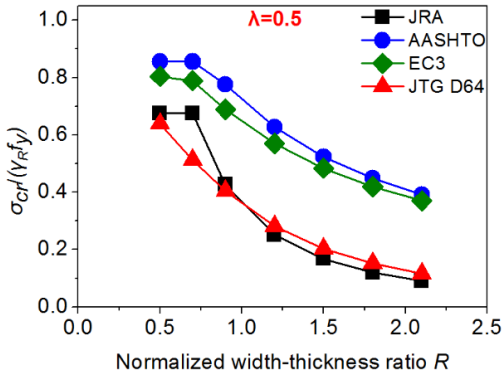

(f) λ=0.5

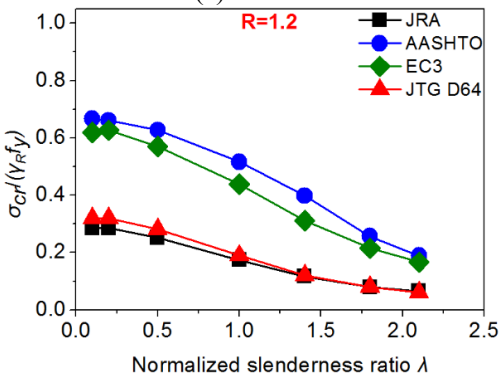

(g) R=1.2

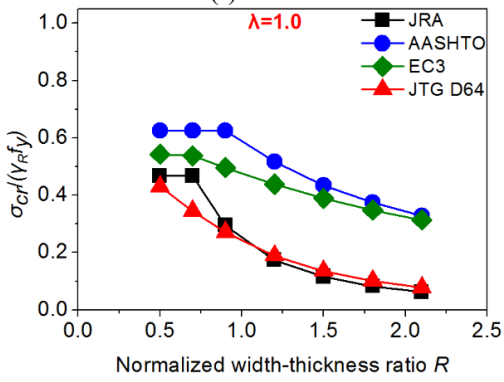

(h) λ=1.0

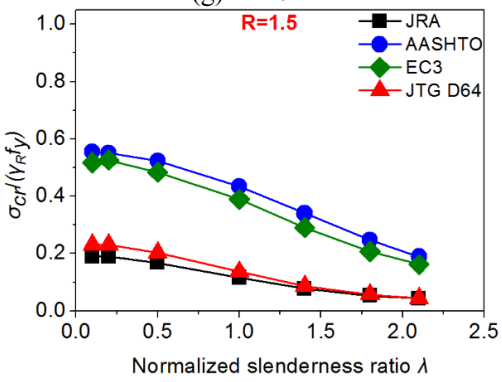

(i) R=1.5

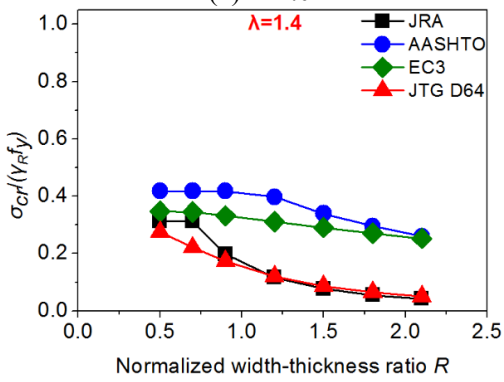

(j) λ=1.4

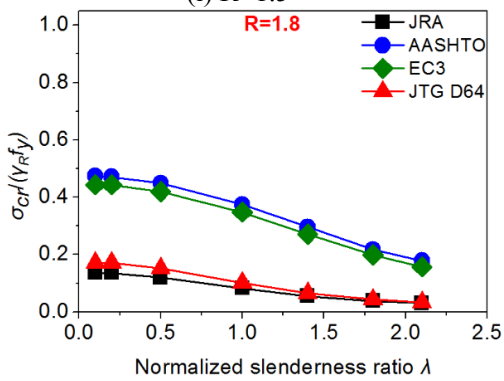

(k) R=1.8

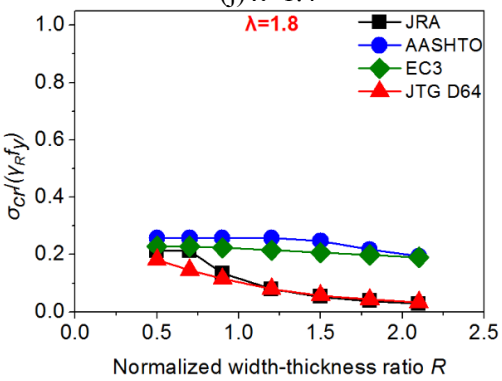

(l) λ=1.8

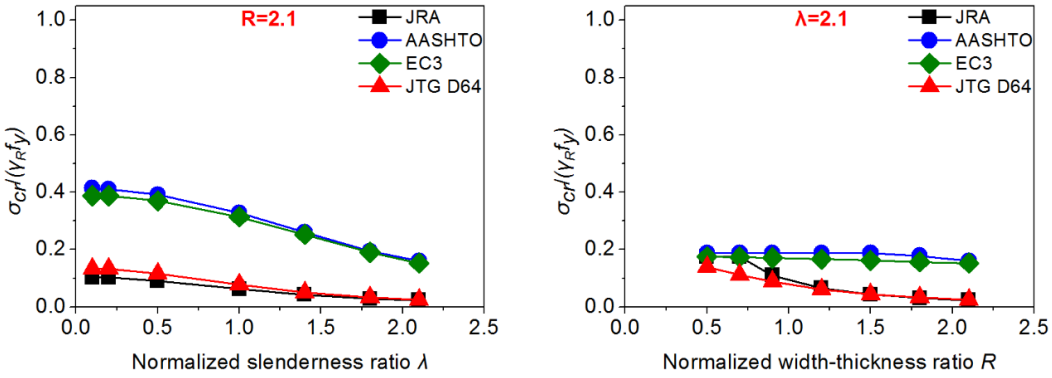

(m) R=2.1 (n) λ=2.1

Fig. 2.5 Comparison of the design strength in the codes

2.4.2 Comparison of allowable strength

To provide a definitive comparison among these codes, the format in the Partial Factor Design Method has been transformed into that in Allowable Strength Design Method as shown in **Eqs. 2.13-2.15**. Allowable strength in this study is defined as the nominal strength divided by the safety factor performed as **Eq. 2.15**. The ratios of live to dead load ρ_D equal to 0.3 and 1.2 are considered in this part. According to **Eq. 2.16**, ρ_D-values of 0.3 and 1.2 correspond to the span lengths of near 60m and 15m, respectively, which is frequently used. The safety factors $K_{0.3}$ and $K_{1.2}$ are listed in **Table. 2.2**.

Table. 2.2 The safety factors in the four codes

	Country				
ρ_D	JRA	AASHTO	EC3	JTG D64 I	JTG D64 II
0.3	1.433	1.437	1.231	1.713	1.558
1.2	1.515	1.603	1.335	1.800	1.636

The allowable strength under safety factor $K_{0.3}$ is plotted in **Fig. 2.6**. It can be seen that the decreasing tendency of allowable strength related to the increase of λ-value and R-value is similar to that of nominal strength as shown in **Fig. 2.3**. The difference occurs on the value of allowable strength among four codes. In the range of λ-value less than 1.0, EC3 provides the highest allowable strength than others due to the lower safety factor value while JTG D64 gives a higher safety factor resulting conservative allowable strength. In the range of $R \leq 0.9$, allowable strengths following AASHTO and JRA locate

between EC3 and JTG D64. In addition, AASHTO and JRA offer closed allowable strength with $R \leq 0.7$, while in the range of $R \geq 0.9$ JRA gives a lower allowable strength than AASHTO due to high local buckling reduction considered in JRA. With respect to the area of $R \geq 1.2$, allowable strengths following JRA and JTG D64 show good agreement with each other.

When the λ-value goes to exceed 1.0, in the range of $R \leq 1.5$, closed allowable strength can be obtained from EC3 and AASHTO. In the range of $R > 1.5$, however, EC3 gives slightly higher allowable strength than that of AASHTO. On the other hand, allowable strength following JRA is approximately equal to that of AASHTO and EC3 with $R \leq 0.7$ and lower than the two codes with $R > 0.7$. When R-value goes to exceed 1.2, JRA offers allowable strength closed to JTG D64, which is conservative in the four codes.

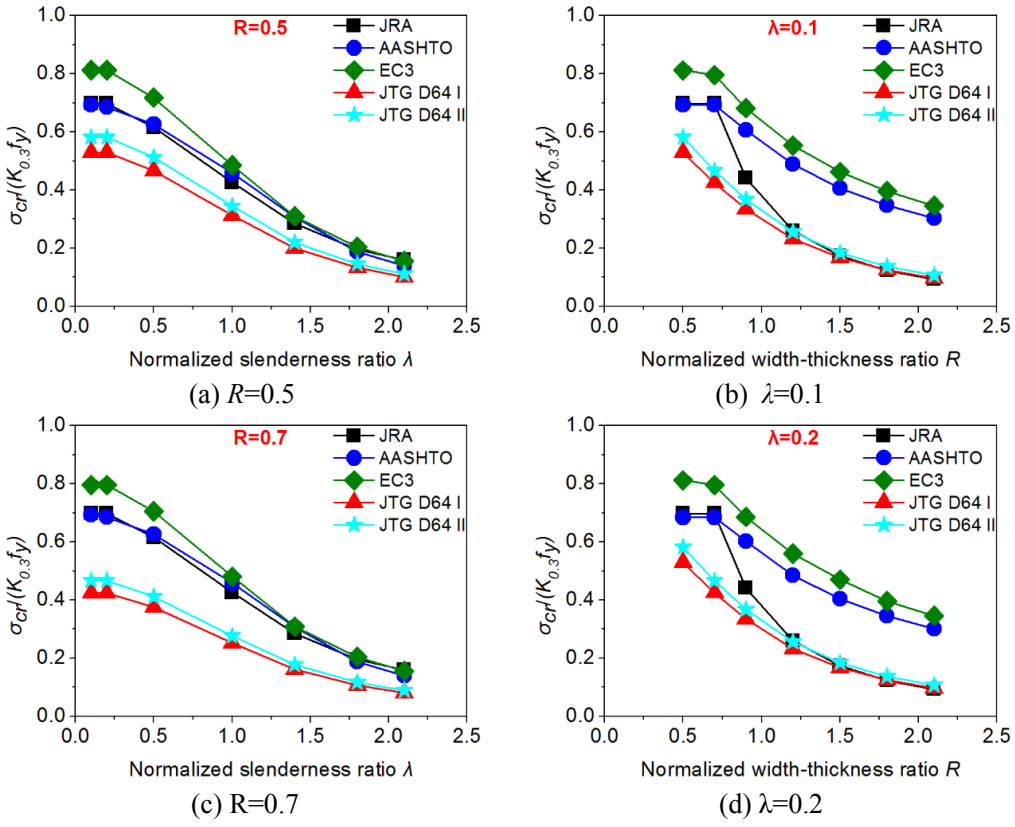

(a) R=0.5 (b) λ=0.1

(c) R=0.7 (d) λ=0.2

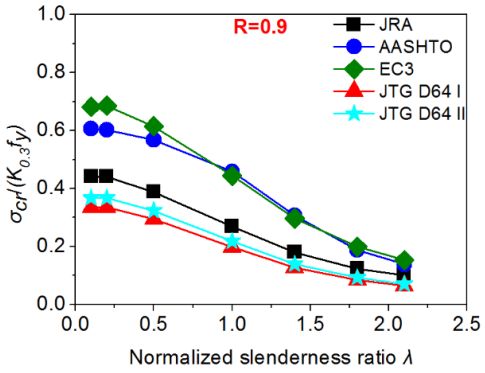

(e) R=0.9

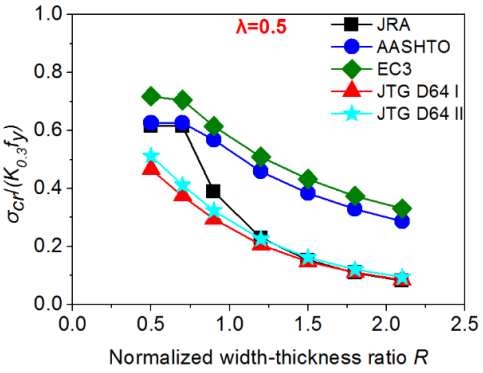

(f) λ=0.5

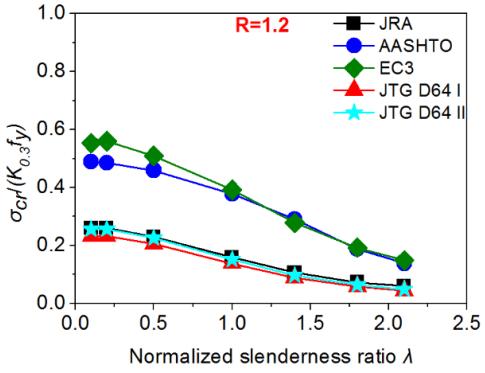

(g) R=1.2

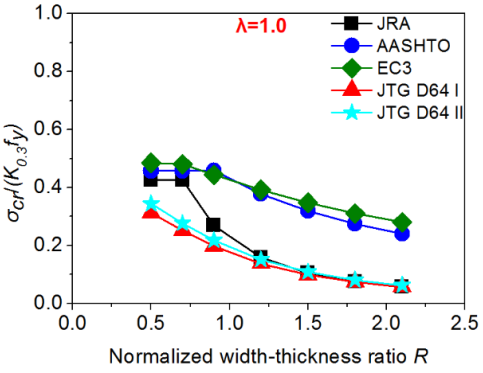

(h) λ=1.0

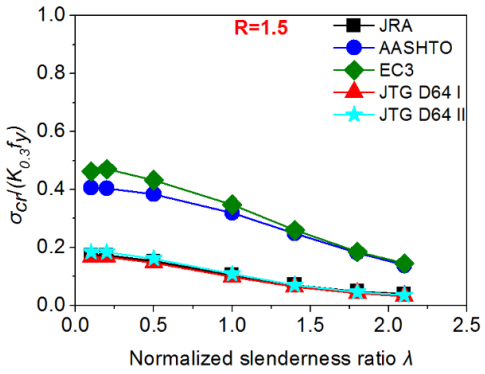

(i) R=1.5

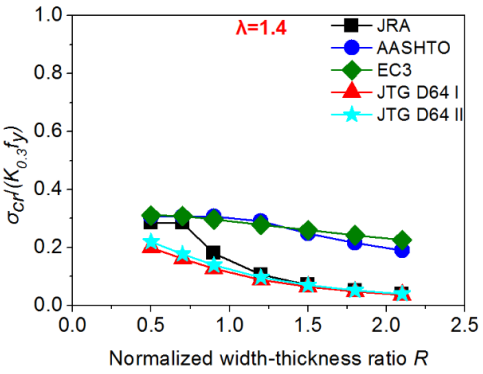

(j) λ=1.4

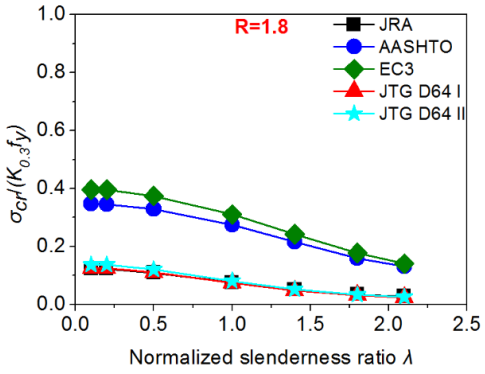

(k) R=1.8

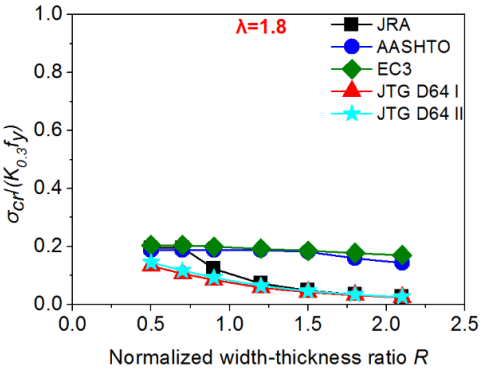

(l) λ=1.8

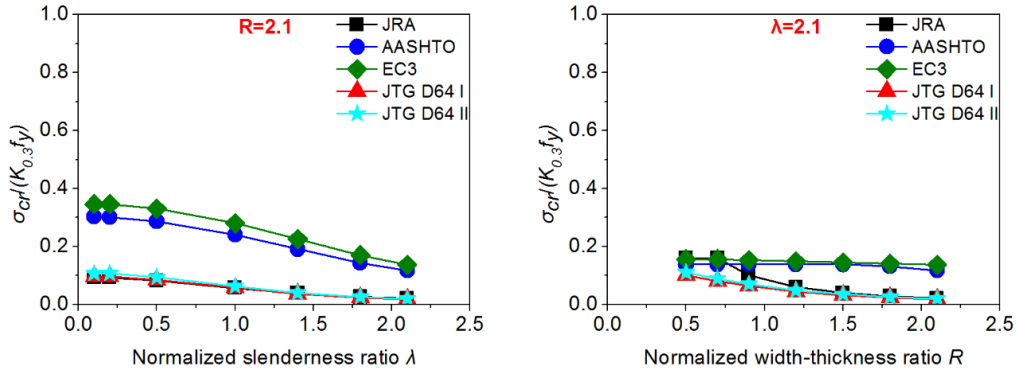

(m) R=2.1 (n) λ=2.1

Fig. 2.6 Comparison among codes on the nominal strength combined with safety factor $K_{0.3}$

The allowable strength with safety factors $K_{1.2}$ is shown in **Fig. 2.7**, respectively. Generally, when the increasing safety factors are considered, the allowable strength continue to decrease than that under $K_{0.3}$. The tendencies of comparison among the four codes are similar with each other.

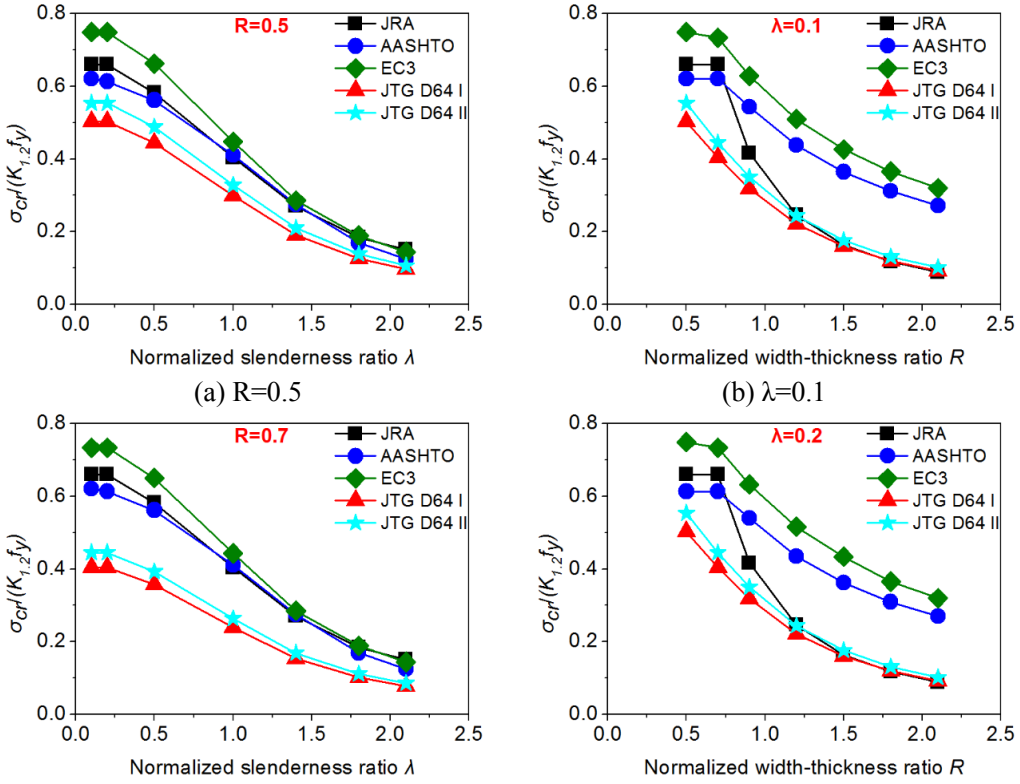

(a) R=0.5 (b) λ=0.1

(c) R=0.7 (d) λ=0.2

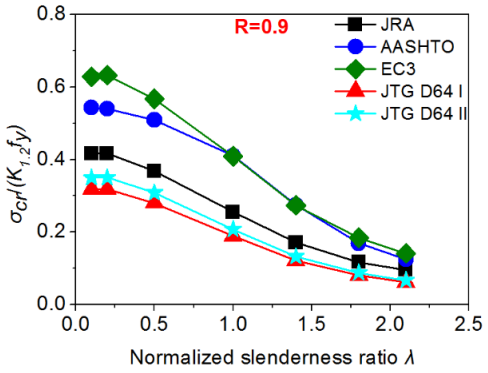

(e) R=0.9

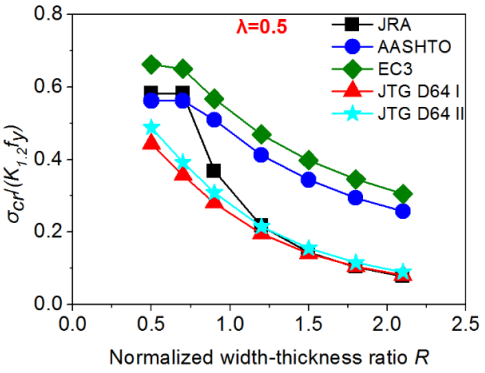

(f) λ=0.5

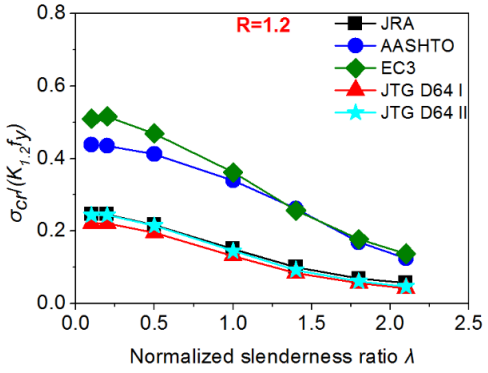

(g) R=1.2

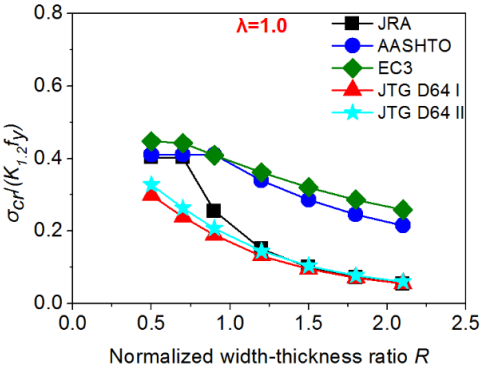

(h) λ=1.0

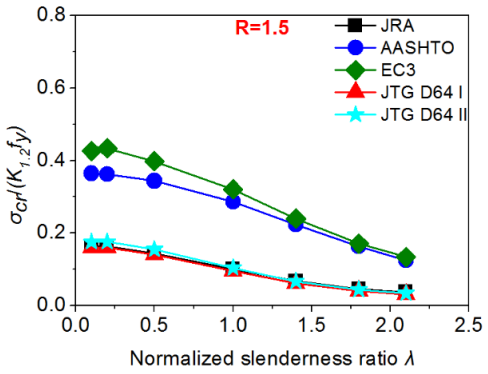

(i) R=1.5

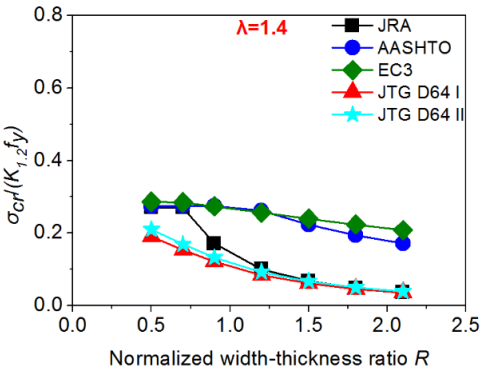

(j) λ=1.4

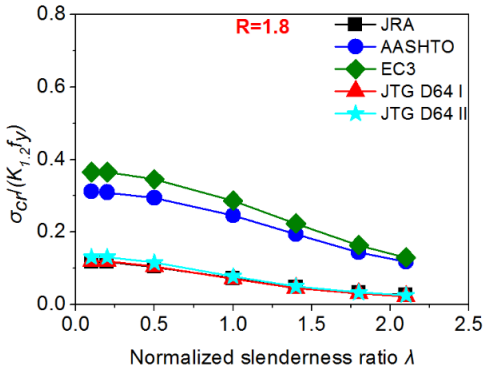

(k) R=1.8

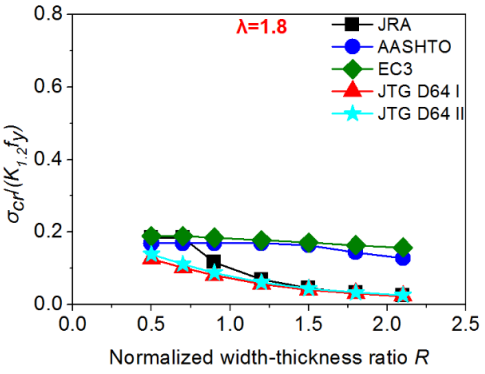

(l) λ=1.8

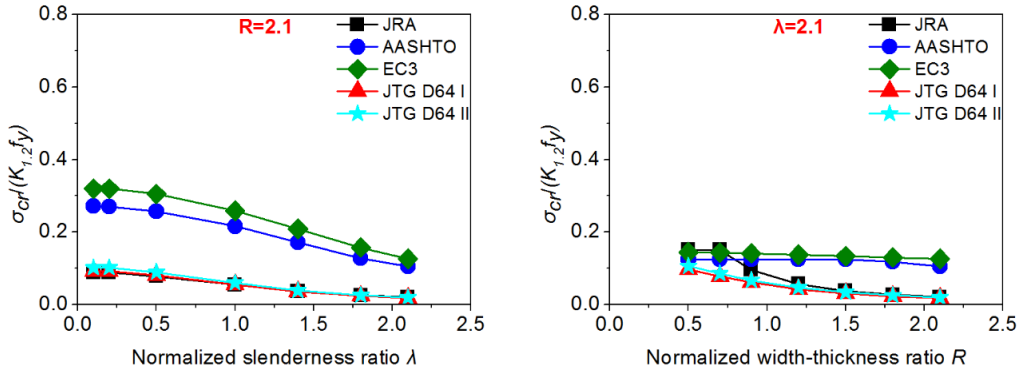

(m) R=2.1 (n) λ=2.1

Fig. 2.7 Comparison among codes on the nominal strength combined with safety factor $K_{1.2}$

2.5 Summary

In this chapter, the provision for the stability of steel compression member in the four codes adopting the Partial Factor Design Method are investigated. To provide a definitive comparison, the formulae are detailed into the case of the column with an unstiffened welded square box-section. The nominal strength of this structure based on the design codes is calculated and compared with the FEA results. The design strengths and safety factors among the four codes are discussed. Further, the allowable strength is compared to investigate the difference among those codes. The main conclusions can be summarized as follows.

(1) In the range of $0.5 \leq R \leq 0.7$, closed nominal strengths can be obtained from AASHTO, EC3 and JRA, while JTG D64 gives a lower nominal strength due to local buckling reduction considered from $R > 0.4$.

(2) When the local buckling reduction is considered (i.e. $R \geq 0.9$), the nominal strength following AASHTO is higher than that of EC3, while the results in JRA and JTG D64 are on the conservative side of EC3. In addition, the results following EC3 correspond with the FEA results better than others.

(3) Safety factor increases along with the increase of ρ_D-value. JTG D64 I provides the highest safety factors, and then is JTG D64 II and JRA in the order, while EC3 offers lowest safety factors.

(4) In the case of ρ_D-value less than 0.25, safety factors based on AASHTO is smaller than JRA. In the range from 0.25 to 2.0, safety factor following AASHTO locates between JTG D64 II and JRA. When the ρ_D-value exceeds 2.0, AASHTO gives higher safety

factors than JTG D64 II.

(5) Design strength following AASHTO is highest, and then is that of EC3 in the order, while JRA and JTG D64 offer conservative results.

(6) Allowable strength following EC3 is higher than that in AASHTO in major part due to lower safety factor considered in EC3, while high safety factor in JTG D64 results in further conservative allowable strength than other codes.

(7) Considering ρ_D of 0.3 and 1.2, it does not change the comparison tendency of allowable strength among the four codes.

CHAPTER 3

Validation of Numerical Analysis on Load-bearing Capacity for the Welded Steel Box Section Columns under Axial Compression

3.1 Introduction

Although many researchers have conducted experimental and numerical analysis on the load-bearing capacity of steel compression members, the quantitative influence of local and overall initial deflections on load-bearing capacity is still not clear. To reveal the quantitative influence, a large amount of FE models needs to be carried out. Therefore, FE model, in which the residual stress and initial deflections is considered, to replicate accurate load-bearing capacity of the structure similar to that in experiment need to be developed.

In this chapter, previous experiments relating to the load-bearing capacity of the unstiffened box section columns were collected. The general-purpose FEA software MSC.Marc [81] was applied to the numerical analyses with the measured residual stress and initial deflections into consideration. The validation of the developed FE model was verified by comparison between FEA and experimental results. Therefore, the developed FE model will be used for further parametrical analysis.

3.2 Previous experiments

Many researches focus on the load-bearing capacity of unstiffened box section columns under axial compression have been conducted. Part of the experimental columns were collected in this part. Degée et al. conducted the experiments of six columns (S-series) [63]. Two specimens (W-series) were tested by Pavlovčič et al. [82]. Somodi and Kövesdi [59] also carried out twelve column tests; ten of them (W3-series) were introduced in this paper except two columns due to unknown residual stress value. All of the above-mentioned specimens were made of S355 steel. To further cover wider ranges of width-thickness and slenderness ratios, eight specimens (R-series) made of HT80 steel having high width-thickness and slenderness ratios tested by Usami [57] were also considered in FE model validation. Cross-section is presented in **Fig. 3.1** and dimensions of all specimens are listed in **Table. 3.1**. Two specimens were prepared for each dimension except Pavlovčič's test. It should be noted that in Somodi's test, plate thickness of some A-specimen is a little different from B-specimen, the upper value is for the A-specimen and the other is for the B-specimen.

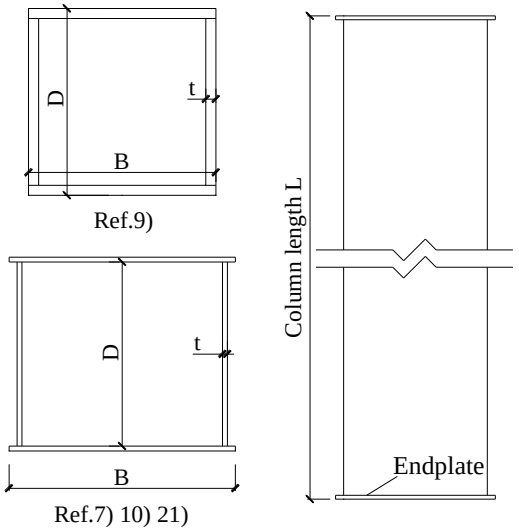

Fig. 3.1 Test specimens

Table. 3.1 Dimensions of experimental specimens

Specimen	B (mm)	D (mm)	t (mm)	L (mm)	L_B (mm)	σ_y (MPa)	E (GPa)	λ	R
S1a/b	282	230	6	2200	2500	390	187	0.35	0.9
S2a/b	282	230	6	3700	4000			0.55	0.9
S3a/b	282	230	6	4900	5200			0.72	0.9
W-S	200	152	4	3650	4000	373.4	205	0.82	0.95
W-L	200	152	4	4850	5200			1.07	0.95
W3-120-6-1800A/B	120	120	6.2	1800	1940	411		0.60	0.43
W3-120-6-2500A/B	120	120	6.2/6.1	2500	2640	411		0.80	0.43/0.44
W3-120-6-2800A/B	120	120	6.3	2800	2940	411	210	0.90	0.42
W3-150-6-2800A/B	150	150	6.1	2800	2940	393		0.70	0.55
W3-80-5-2000A/B	80	80	5.1/5.3	2000	2140	415		0.99	0.34/0.33
R-50-22	151	94.2	6	2090	-	741	215	0.91	0.69

R-50-27	181	116	6	2570	0.93	0.84
R-50-33	217	144	6	3140	0.92	1.03
R-50-38	247	166	6	3610	0.92	1.18
R-50-44	283	193	6	4180	0.93	1.36
R-65-22	151	94.4	6	2720	1.19	0.68
R-65-27	181	116	6	3340	1.20	0.84
R-65-33	217	143	6	4080	1.20	1.03

The initial deflection was measured prior to the experiment as listed in Table.2. The maximum measured local initial deflection on the plate was *b*/250 in Degée's test, *b*/520 in Pavlovčič's test while local initial deflection was not measured for W3-series and R-series specimens. The overall initial deflection for W3-series specimens listed in **Table. 3.2** is the sum of out-of-straightness deflection and load eccentricity. The columns were tested under the pin-ended condition which can rotate only around one axis.

Table. 3.2 Measured initial deflections

Specimen	w_{l0}	w_{g0}	Specimen	w_{l0}	w_{g0}
S1a	*b*/250	*L*/2800	R-50-22	-	*L*/2538
S1b		*L*/2500	R-50-27		*L*/1938
S2a		*L*/4000	R-50-33		*L*/20833
S2b		*L*/4000	R-50-38		*L*/4081
S3a		*L*/4350	R-50-44		*L*/7246
S3b		*L*/3700	R-65-22		*L*/4132
W-S	*b*/520	*L*/1825	R-65-27		*L*/2604
W-L		*L*/1426	R-65-33		*L*/8928
W3-120-6-1800A	-	*L*/534	W3-120-6-2800B	-	*L*/387
W3-120-6-1800B		*L*/416	W3-150-6-2800A		*L*/733
W3-120-6-2500A		*L*/1068	W3-150-6-2800B		*L*/475
W3-120-6-2500B		*L*/1740	W3-80-5-2000A		*L*/1159
W3-120-6-2800A		*L*/491	W3-80-5-2000B		*L*/721

Where w_{g0} and w_{l0} are the amplitudes of overall and local initial deflections, respectively.

3.3 Validation of FE modelling

3.2.1 FE modelling

The general-purpose FEA software MSC.Marc was applied to the numerical analyses of load-bearing capacity of unstiffened box section columns. There are so many element type in Marc. Different elements possess different stiffness matrix. With reasonable element type accurate simulation can be carried out. Under numerical analysis, geometry and material nonlinear need to be considered. Meanwhile initial deflection and residual stress should be considered. Given by different slenderness and thickness, the interaction between local and global buckling will occur in some specimens. And the use of post buckling strength needs to be considered. Therefore, thick shell element (No.75) was used in the model. Since the meshing size and the shape of the elements have an influence on the accuracy of the calculation [83], the shape of the elements was made to be as square as possible and meshing size was made to be small enough. Moreover, considering the convenience of residual stress setting, plates were divided into twenty elements for parametric analysis as shown in **Fig. 3.2 (a)**. The von Mises yield criterion was adopted in the analysis. Bilinear model with strain hardening coefficient of $E/100$ was used to describe the material property of S355, and trilinear model based on measured material property was used for R-series specimens. The Poisson ratio was set to 0.3 and 0.24 for S355 and H80, respectively.

In order to set the boundary conditions, two nodes were set at the midpoint of the top and bottom cross-sections. The central node was set as the main node and the other nodes in the cross-section as subordinate nodes. Then the "RBE2" function was used to connect the central node (master node) with the whole nodes at the cross-section (slave nodes). The RBE2 function can make a rigid link between the master node and a list of slave nodes. The nodes were located away from the column in order to take the dimension of the test equipment into consideration as shown in **Fig. 3.2 (b)**. Considering that the columns were tested with pin-ended supports around the weak axis "y", the rotation Y was free at both top and the bottom node as shown in **Table. 3.3**. At the top node, displacement Z was set free so that the displacement loading can be applied to the top main node.

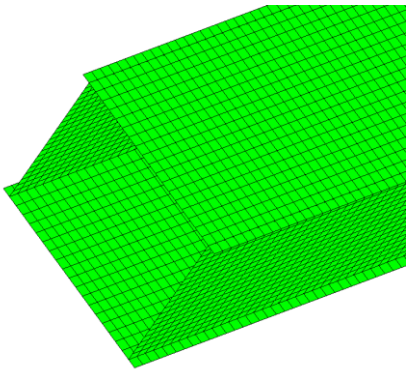

(a) Meshing profile

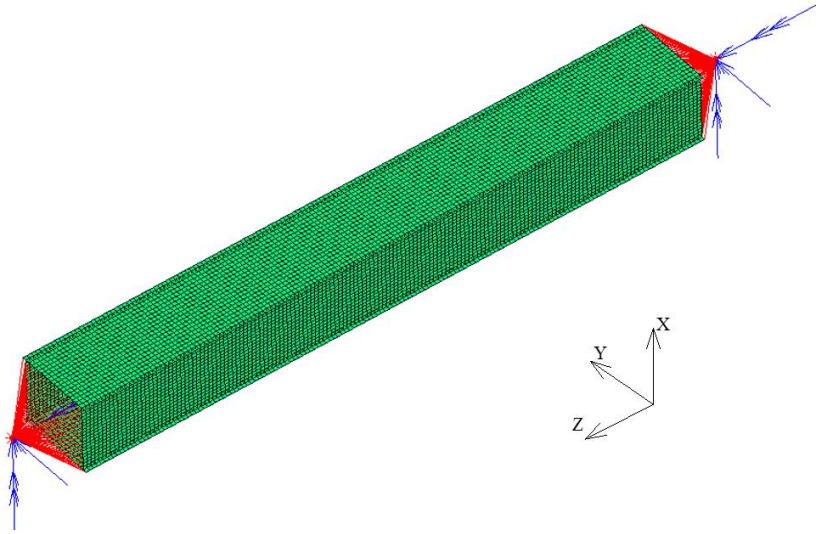

(b) Geometry and boundary condition of specimen

Fig. 3.2 FE model

Table. 3.3 Boundary conditions

DOF	T_X	T_Y	T_Z	R_X	R_Y	R_Z
Mov	Fix	Fix	Free	Fix	Free	Fix
Fix	Fix	Fix	Fix	Fix	Free	Fix

Residual stress is also one of the most important factors to the stability behavior of compression members. It was assumed to exist in every plate with compression in the middle area and tension at both sides of the plate as shown in Fig. 3.3 to be in self-equilibrium condition.

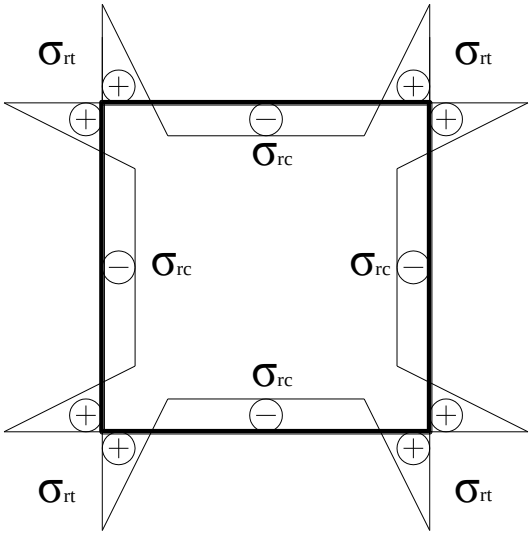

Fig. 3.3 Distribution of residual stress in the cross-section

Values of tensile and compressive residual stresses for each specimen were set as listed in **Table. 3.4**. Since less of conclusive residual stress value in Degée's research, a calibrated distribution (i.e. Model 6 in [10]), which resulted in the closest load-bearing capacity to experimental results, was used for specimens S1, S2 and S3. For the specimens tested by Somodi [9] (W3 series), the tensile and compressive residual stresses were determined referring to the values measured for specimens with the same cross section by Somodi [84]. For W-series specimens, measured compressive residual stress of 130MPa ($0.35\sigma_y$) and 160MPa ($0.43\sigma_y$) for flange and web, respectively, were used. For R-series specimens, based on measurement, 0.6 and 0.1 of yield strength was arranged for tensile and compressive residual stress, respectively. Although it is known that residual stresses are *b/t* ratio dependent values, one residual stress distribution is assumed in the parametric analysis in order to independently evaluate the influence of initial deflections on load-bearing capacity. Referring to Fukumoto's statistics [85], assumed compressive stress was set to $0.25\sigma_y$, which is the average value of 216 cases.

Table. 3.4 Residual stress used in FE model validation

Specimen	σ_{rt}/σ_y	σ_{rc}/σ_y	Specimen	σ_{rt}/σ_y	σ_{rc}/σ_y
S1a	0.6	0.04	R-50-22	0.6	0.1
S1b			R-50-27		
S2a			R-50-33		
S2b			R-50-38		
S3a			R-50-44		
S3b			R-65-22		
W-S	1.0	0.35	R-65-27		
W-L	1.0	0.43	R-65-33		
W3-120-6-1800A	1.0	0.27	W3-120-6-2800B	1.0	0.27
W3-120-6-1800B			W3-150-6-2800A		0.38
W3-120-6-2500A			W3-150-6-2800B		
W3-120-6-2500B			W3-80-5-2000A		0.45
W3-120-6-2800A			W3-80-5-2000B		

With respect to initial deflections, local and overall initial deflections were separately replicated. Images of overall along with the column length and local initial deflection on the plate are shown in **Fig. 3.4** and **Fig. 3.5**, respectively.

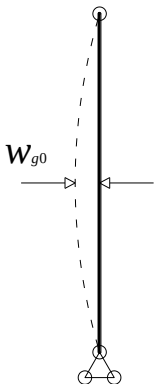

Fig. 3.4 Overall initial deflection shape

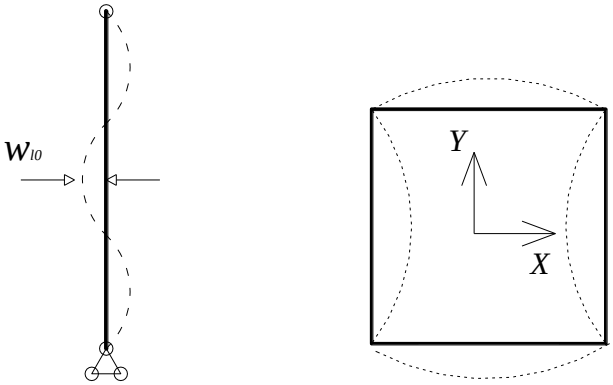

(a) Along plate width (b) On cross section

Fig. 3.5 Local initial deflection shape

When it goes to input the initial deflections into the model, the double trigonometric function shown in **Eq. 3.1** was assumed for the local initial deflection. The number of half-wave m were determined by the aspect ratio of the plate to give the minimum buckling strength according to the elastic buckling theory. Schematic illustration of initial deflections in the case of the specimen with m=3 is shown in **Fig. 3.6** as an example. Half-sinusoidal wave shape expressed by **Eq. 3.2** was assumed for the overall initial deflection. The measured amplitude of the initial deflections is used for the FE modelling. For W3-series and R-series specimens, the local initial deflection was assumed to be b/200 according to EC3 since it had not been measured.

$$\begin{cases} w_{lw} = w_{l0} \sin\dfrac{m\pi z}{a} \sin\dfrac{\pi x}{b_w} \\ w_{lf} = w_{l0} \sin\dfrac{m\pi z}{a} \sin\dfrac{\pi y}{b_f} \end{cases} \tag{3.1}$$

$$w_g = w_{g0} \sin\frac{\pi z}{L} \tag{3.2}$$

where w_{g0} is the amplitude of overall initial deflection; w_{l0} is the amplitude of local initial deflection; m is the number of half-sinusoidal wave giving the minimum buckling strength determined by the aspect ratio of the plate.

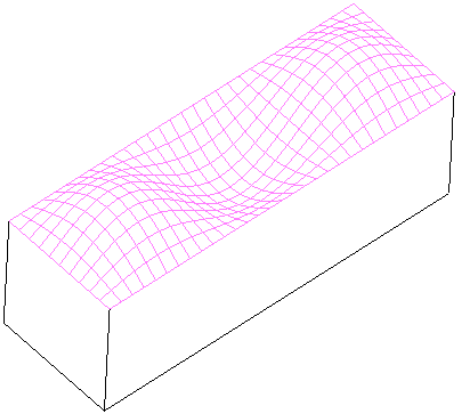

(a) Local initial deflection on one plate (m=3 as an example)

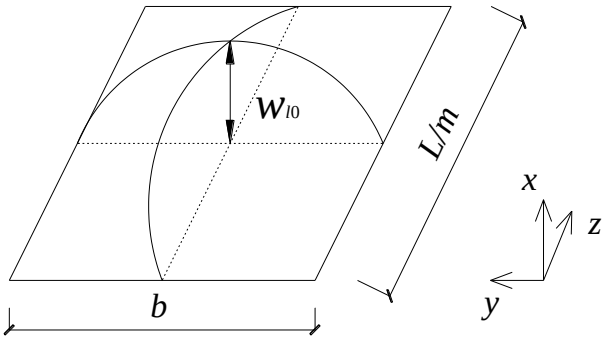

(b) Local initial deflection for half sin-wave

Fig. 3.6 Local initial deflection shape

For specimen with big width-thickness ratio, local buckling will appear under axial compression. When the specimen is locally buckled, it still possesses bearing capacity. The post buckle strength need to be considered. In elastic stage, stress versus strain is linear. Both load loading and displacement loading can be used. However, in plastic stage, few load increment may result in big displacement. In order to get accurate result, displacement loading is exerted to solve the problem in this model.

For the solution of equilibrium equation, incremental-interactive method is usually used to get accurate displacement increment. The arch length method which arch length serves as increment and interaction will reach convergence along the arch length can lead to more accurate solution. **Fig. 3.7** shows how arch length method works [86]. So arch length method is chosen in stepping procedure. Then initial fraction is set small enough to prevent from overlarge convergence ratio at the first loading step. And in nonlinear

procedure, large strain function is on.

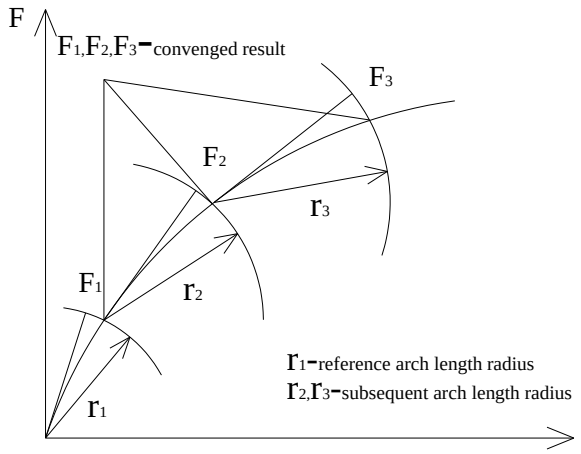

Fig. 3.7 Arch length method

3.2.2 Validation of the modelling

All the 26 columns listed in **Table. 3.1** were modeled, and their ultimate strengths were obtained. The comparison between experiment and FEA results is shown in **Fig. 3.8** and **Table. 3.5.** It can be seen that most of the FEA results for Degée's test (S-series) were a little lower than experimental results. The possible reason is that local initial deflection used in FE models is the measured maximum, which is greater than the real value for most of the specimens. For Pavlovčič test (W-series), the FEA results shows good agreement with test results. For Smodi's test (W3-series), numerical analysis provides good prediction on load-bearing capacity with a little larger deviation than that of Pavlovčič test. It can be observed that the difference between FEA and test results of W3-80-5-2000A reached up to 11.89% while difference on W3-80-5-2000B was small. Possible reason is that the same residual stresses and assumed local initial deflection were introduced for these two specimens, while their values may be different in tested specimens which resulted in 15.6% difference on load-bearing capacity (0.74 and 0.64) between them. For R-series specimens with high width-thickness ratios, it can be observed that FE results are slightly lower than test results due to the relatively large local initial deflection assumed. The average and standard deviation of errors for all specimens are 2.50% and 4.07%, respectively. Based on the above discussion, it was concluded that the model could be used in the following parametric analysis with sufficient accuracy.

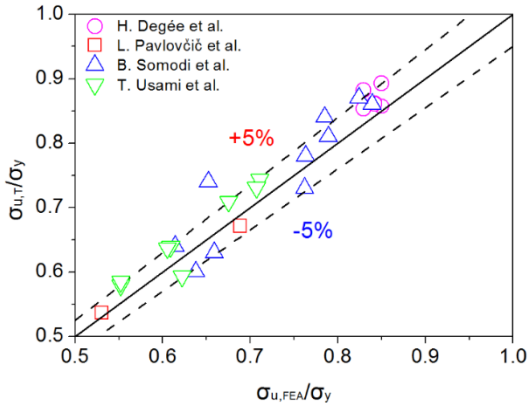

Fig. 3.8 Comparison of load-bearing capacity between experimental and FEA results

Table. 3.5 load-bearing capacity obtained by the experimental and FEA results

Specimen	σ_T/σ_y	σ_{FEA}/σ_y	Errors(%)	Specimen	σ_T/σ_y	σ_{FEA}/σ_y	Errors(%)
S1a	0.857	0.850	-0.82	R-50-22	0.743	0.711	-4.31
S1b	0.893	0.849	-4.93	R-50-27	0.731	0.707	-3.28
S2a	0.862	0.842	-2.32	R-50-33	0.709	0.675	-4.80
S2b	0.861	0.842	-2.21	R-50-38	0.639	0.609	-4.69
S3a	0.882	0.829	-6.01	R-50-44	0.579	0.552	-4.66
S3b	0.853	0.827	-3.05	R-65-22	0.593	0.622	4.89
W-S	0.671	0.689	2.68	R-65-27	0.637	0.605	-5.02
W-L	0.536	0.530	-1.12	R-65-33	0.585	0.552	-5.64
W3-120-6-1800A	0.86	0.839	-2.44	W3-120-6-2800B	0.639	0.609	-4.69
W3-120-6-1800B	0.87	0.824	-5.29	W3-150-6-2800A	0.579	0.552	-4.66
W3-120-6-2500A	0.73	0.762	4.38	W3-150-6-2800B	0.593	0.622	4.89
W3-120-6-2500B	0.84	0.785	-6.55	W3-80-5-2000A	0.637	0.605	-5.02
W3-120-6-2800A	0.63	0.659	4.60	W3-80-5-2000B	0.585	0.552	-5.64
Average Errors(%)			-2.50				
Standard DEV(%)			4.07				

3.4 Summary

In this chapter, a precise FE model to replicate the load-bearing capacity of unstiffened box section columns with a wide range of normalized slenderness and width-thickness ratios into consideration was developed. Its accuracy was proved by comparing with the experimental results. The main conclusions can be summarized as follows.

(1) Reasonable postbuckled results can be obtained by means of arc length method.

(2) Reasonbale element type, intensive meshing size as well as inputing measured residual stress and initial deflection will results in accurate prediction on the load-bearing capacity of unstiffened box section columns.

CHAPTER 4

Formulation of the quantitative influence of local and overall initial deflections on load-bearing capacity of unstiffened welded square box section columns under axial compression

4.1 Introduction

Through many researches including experimental and numerical analysis on the load-bearing capacity of unstiffened box section columns done before, it is well known that initial deflection will significantly decrease the load-bearing capacity of this kind of structures. However, the quantitative influence of initial deflections is still not clear.

So far, amplitude of initial deflections have been taken as determined value in various design codes. For example, overall initial deflection is taken as 1/1000 of column length in Japanese code *Specifications for Highway Bridges, Part II Steel Bridges and Members* while 1/150 of plate width is adopted for local initial deflection. However, amplitude of initial deflections could differ greatly due to different manufacturing and assembling method. Therefore, parametrical formulae, which targets on estimating the quantitative influence of initial deflections on load-bearing capacity for unstiffened box section columns, are worth investigating.

In this chapter, unstiffened welded square box section columns with S355 steel under axial compression were chosen as a target. Nonlinear finite element models were developed to analyze their load-bearing capacity. A variety of the normalized width-thickness and slenderness ratios were considered to cover the possible diverse range of columns. Various combinations of amplitude of the local and overall initial deflections were prepared for FE models. Based on the results of parametric analyses, initial deflection influence coefficient is proposed as a function of the initial deflections and the normalized width-thickness and slenderness ratios to describe the quantitative influence caused by the different local and overall initial deflections on the load-bearing capacity.

4.2 FE model for parametrical analysis

4.2.1 Geometric parameters

The basic FE modeling procedure was similar to the description in Chapter 3. In parametrical analysis, square cross section of 500x500mm was prepared for FE model as shown in **Fig. 4.1**. Seven different normalized slenderness and six width-thickness ratios are adopted with the range from 0.3 to 1.8 and from 0.3 to 1.5, respectively, to cover a main part of the practice. The dimension of FE models, the normalized slenderness ratio λ and normalized width-thickness ratio R are listed in **Table 4.1**. The 42 combinations of

slenderness and width-thickness ratios were listed in **Table. 4.2**.

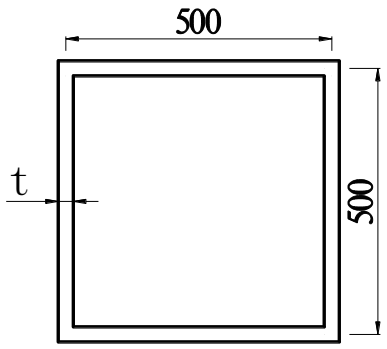

Fig. 4.1 Cross section for FE model

Table 4.1 Variable main properties of the numerical model

Parameter	Range of variable
Dimension of cross-section	500 × 500 mm
Normalized slenderness ratio λ	0.3, 0.5, 0.7, 1.0, 1.4, 1.6, 1.8
Normalized width-thickness ratio R	0.3, 0.5, 0.7, 0.9, 1.2, 1.5
Length of the column L	4572-27432 mm
Thickness of plate t	7.39-36.93 mm

Table 4.2 Combination of normalized slenderness and width-thickness ratios

R	λ						
	0.3	0.5	0.7	1.0	1.4	1.6	1.8
0.3	R03λ03	R03λ05	R03λ07	R03λ10	R03λ14	R03λ16	R03λ18
0.5	R05λ03	R05λ05	R05λ07	R05λ10	R05λ14	R05λ16	R05λ18
0.7	R07λ03	R07λ05	R07λ07	R07λ10	R07λ14	R07λ16	R07λ18
0.9	R09λ03	R09λ05	R09λ07	R09λ10	R09λ14	R09λ16	R09λ18
1.2	R12λ03	R12λ05	R12λ07	R12λ10	R12λ14	R12λ16	R12λ18
1.5	R15λ03	R15λ05	R15λ07	R15λ10	R15λ14	R15λ16	R15λ18

4.2.2 Residual stress and initial deflections

It should be mentioned that to independently investigate the influence caused by local and overall initial deflections, compressive residual stress is taken as a determined value of 0.25 yield stress, which is a the average value referring to Fukumoto's statistics

[85] relating to residual stress about 216 cases. The tensile residua stress, on the other hand, was taken equal to yield stress. The residual stress distribution input in every plate assumed for FE model in parametric analysis is shown in **Fig. 4.2**.

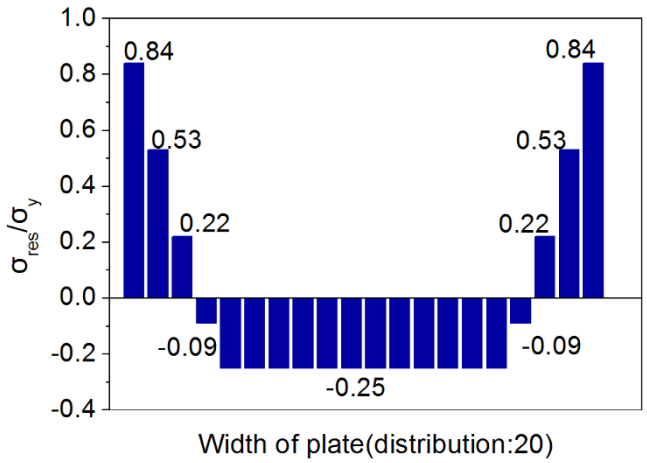

Fig. 4.2 Distribution of residual stress in every plate

To evaluate the quantitative influence of the initial deflections on the load-bearing capacity, various combinations of local and overall initial deflections were prepared for the parametrical analysis. Amplitudes of *b*/75, *b*/150 and *b*/450 were taken as local initial deflection, while amplitudes of *L*/500, *L* /1000 and *L*/3000 were set for overall initial deflection, in which nine combinations of initial deflections as shown in **Table. 4.3** result in 378 FE models for parametrical analysis. It should be mentioned that the Com5 corresponds to the combination of the allowable initial deflections in the Japanese specification.

Table. 4.3 Combinations of amplitude of initial deflections

	Com1	Com2	Com3	Com4	Com5	Com6	Com7	Com8	Com9
Local	*b*/75	*b*/75	*b*/75	*b*/150	*b*/150	*b*/150	*b*/450	*b*/450	*b*/450
Overall	*L*/500	*L*/1000	*L*/3000	*L*/500	*L*/1000	*L*/3000	*L*/500	*L*/1000	*L*/3000

4.3 Parametrical analysis results and discussion

4.3.1 Influence of local initial deflection

Results of models with the normalized width-thickness ratio R from 0.3 to 1.5 and constant normalized slenderness ratio λ of 1.0 are set as examples to show the influence of the local initial deflection. The comparison of load-bearing capacities for different local initial deflection are shown in **Fig. 4.3**. In the range of R≤0.5, the reduction on load-bearing capacity caused by increasing local initial deflection is less than 5%. In the range of R from 0.7 to 1.5, it reaches up to 19.2% at most with the increase of the amplitude of local initial deflection from b/450 to b/75.

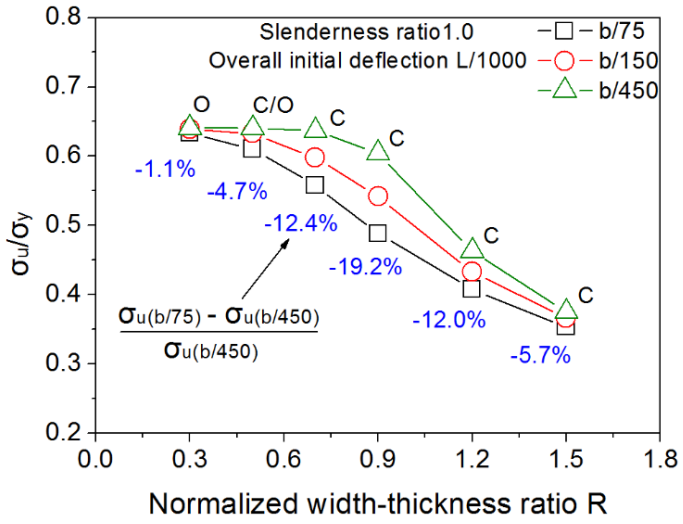

Fig. 4.3 Influence of local initial deflection on load-bearing capacity

In this study, initial deflection influence coefficient (IDIC) is introduced to describe the quantitative influence of the initial deflections and defined as a ratio of the load-bearing capacity of a model with each Com-i to that of the Com-5. The calculation of $\mathrm{IDIC_{FEA}}$ based on FEA results can be performed as follows.

$$\mathrm{IDIC_{FEA}} = \frac{F_{u,Com-i}}{F_{u,Com-5}} \tag{4.1}$$

where the F_u is the load-bearing capacity of the specimen.

Relationship between the IDIC and the amplitude of the local initial deflection normalized by the standard amplitude i.e. *b*/150 is shown in **Fig. 4.4 - 4.10**. It can be seen that IDIC decreases approximately linearly as the amplitude of local initial deflection increases. The decreasing slope is nearly the same for different amplitudes of the overall initial deflection. Therefore, linear regression analysis is conducted on the data when the amplitude of the overall initial deflection is *L*/1000.

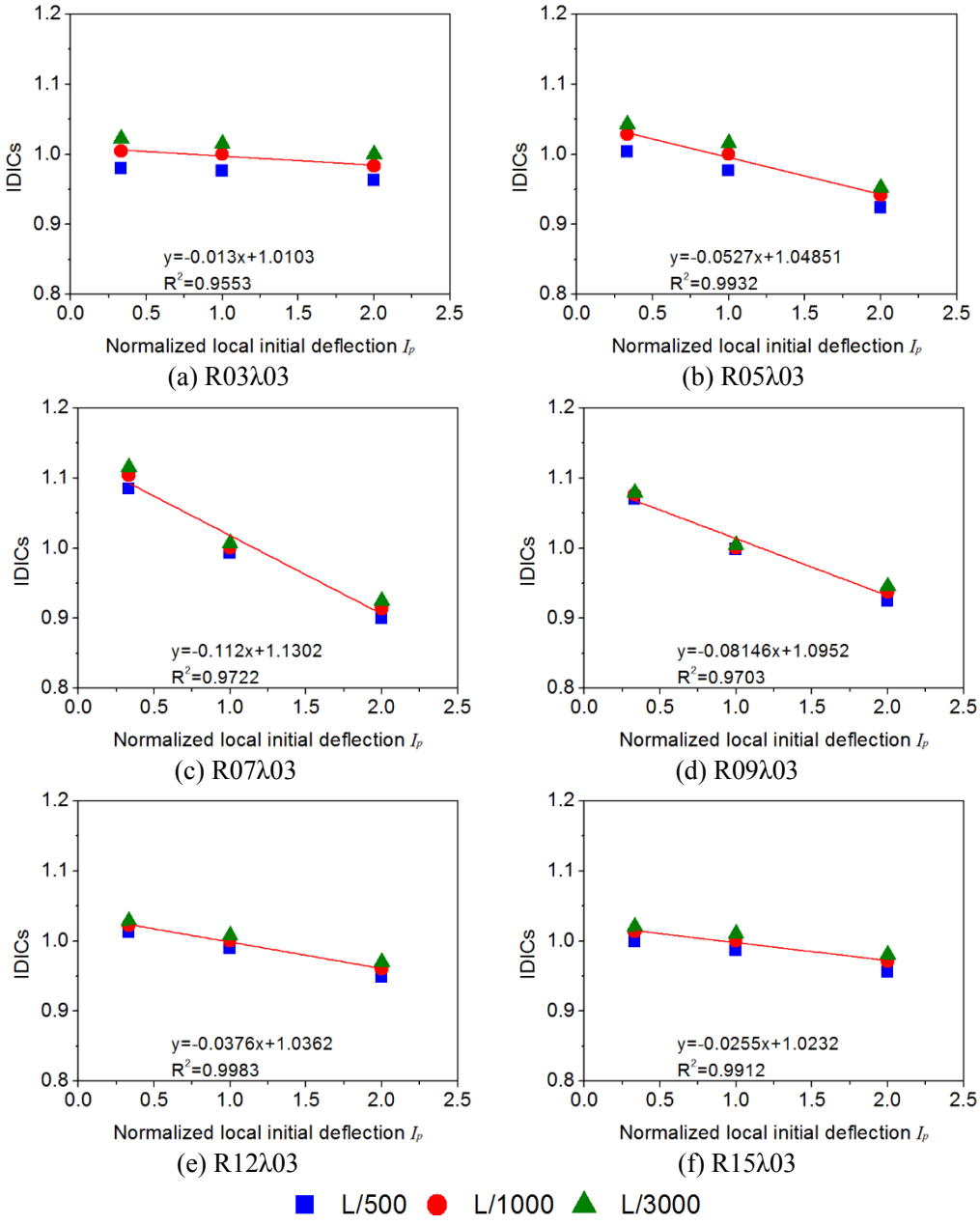

Fig. 4.4 Initial deflection influence coefficient (IDICs) versus normalized local initial deflection

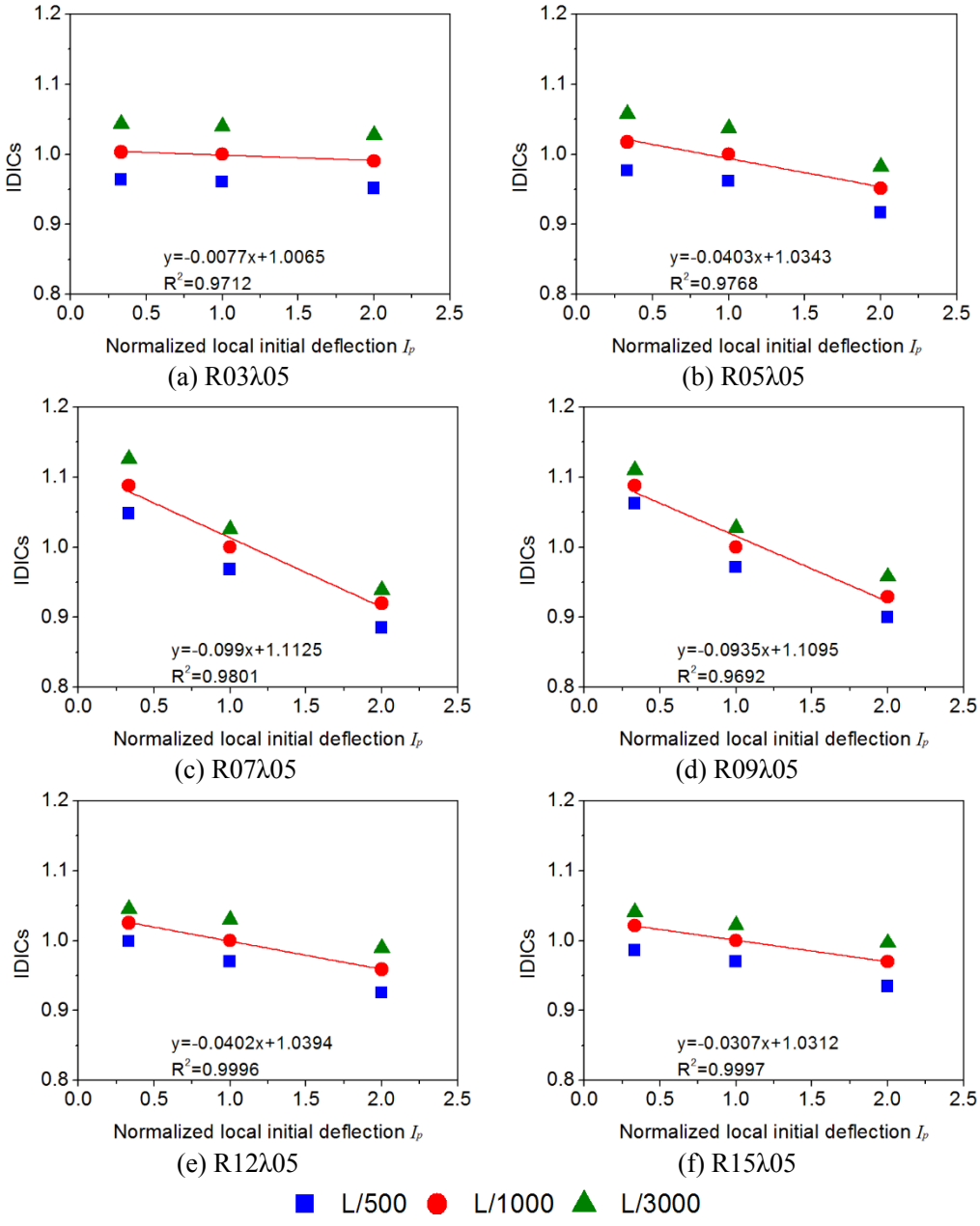

Fig. 4.5 Initial deflection influence coefficient (IDICs) versus normalized local initial deflection

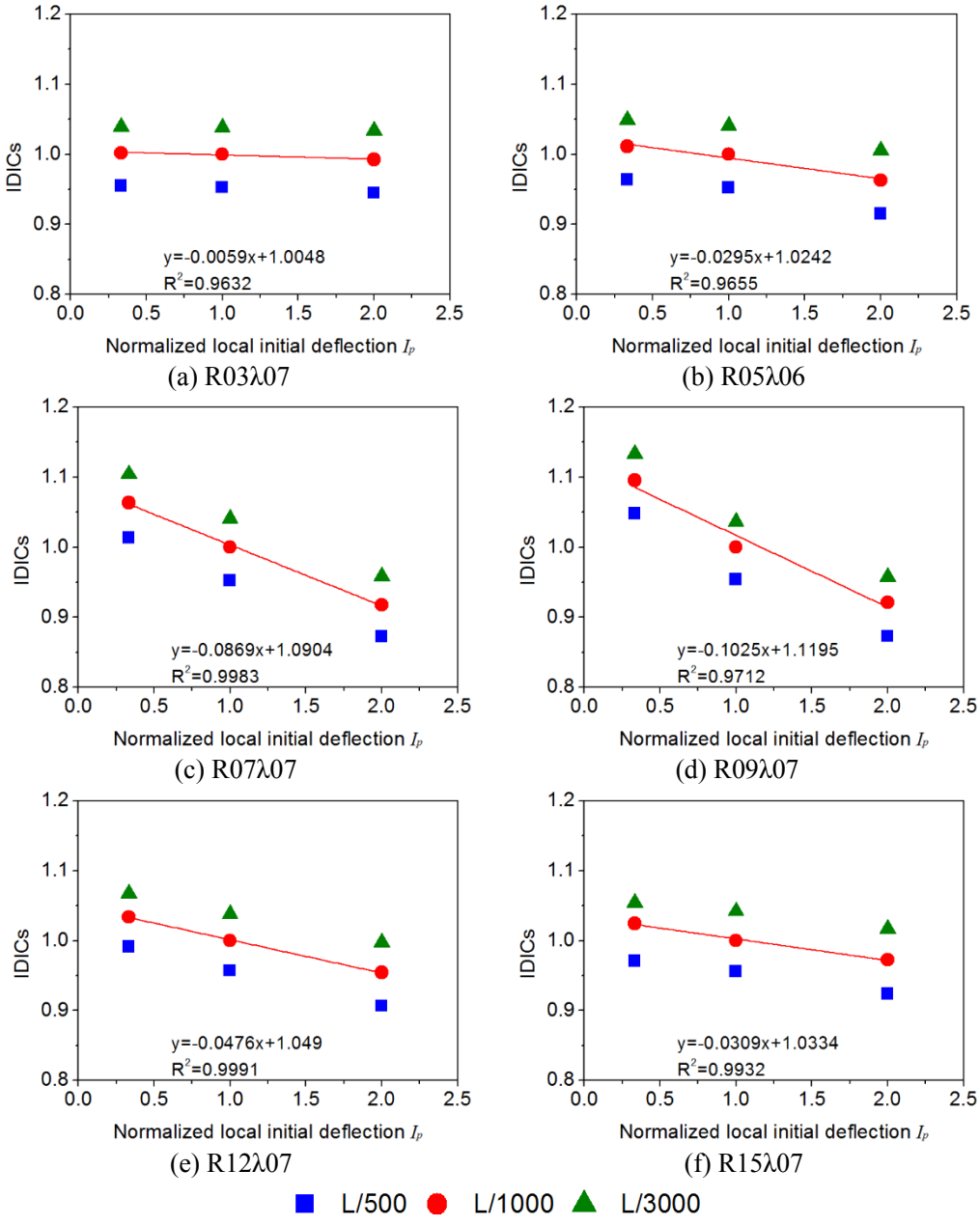

Fig. 4.6 Initial deflection influence coefficient (IDICs) versus normalized local initial deflection

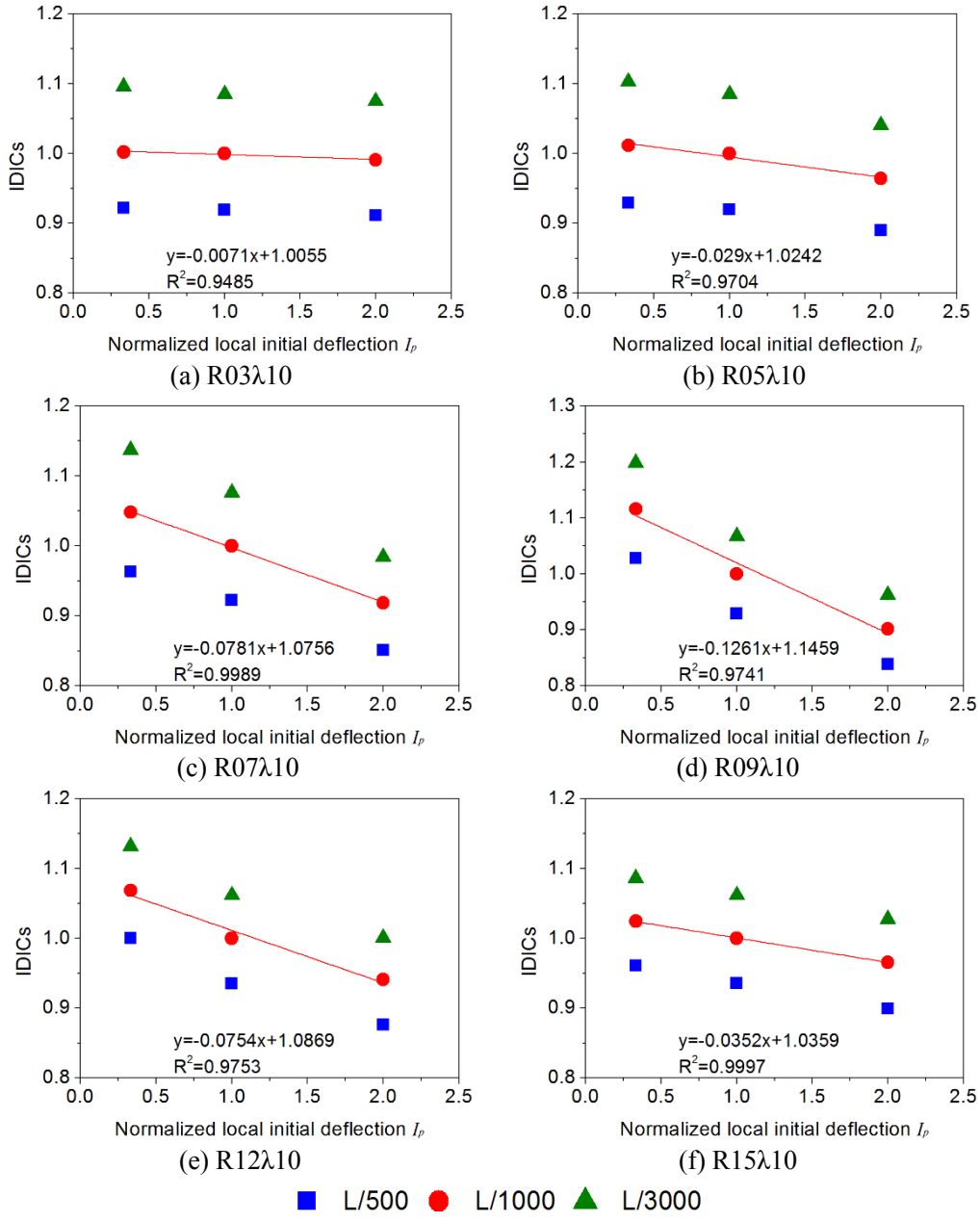

Fig. 4.7 Initial deflection influence coefficient (IDICs) versus normalized local initial deflection

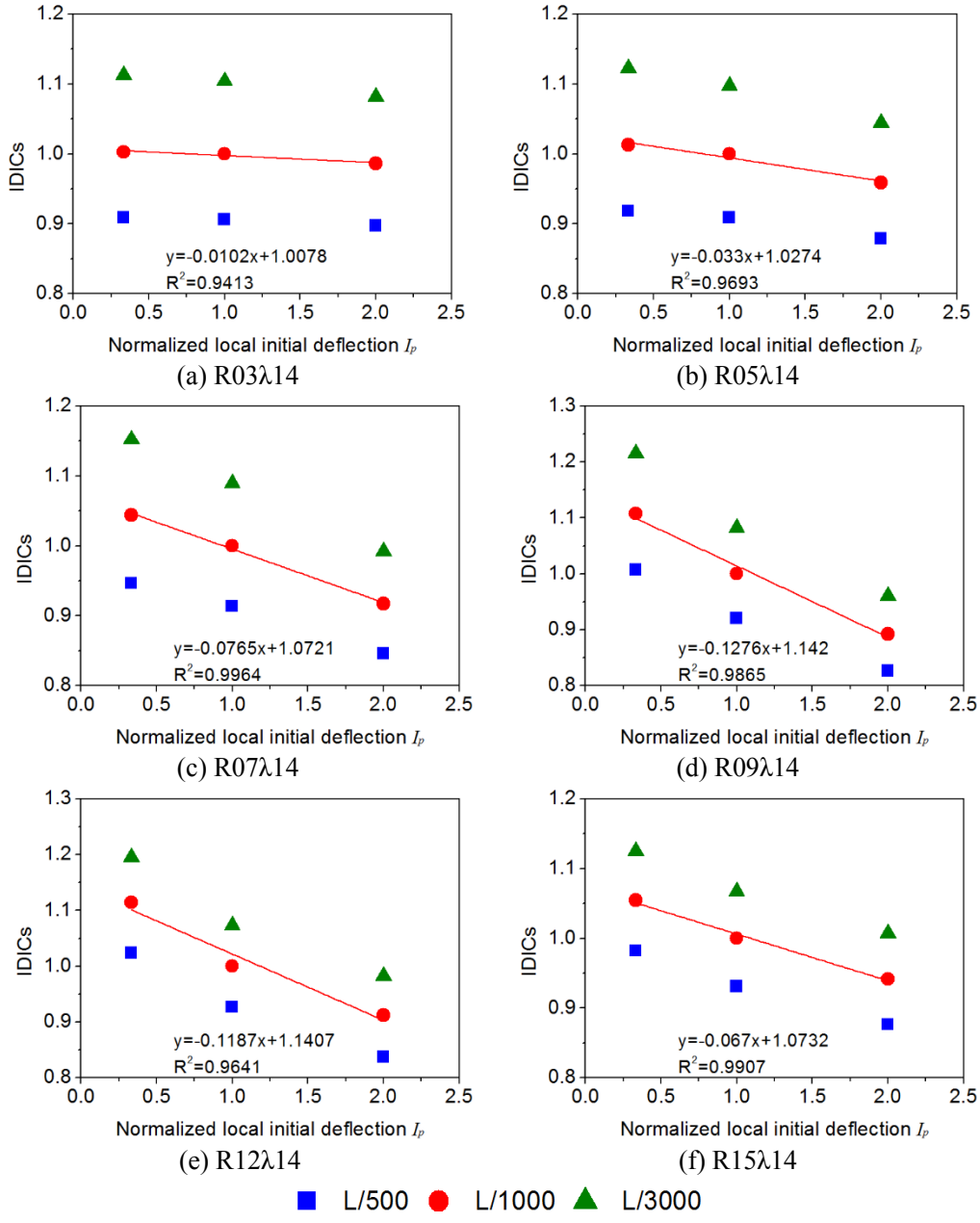

Fig. 4.8 Initial deflection influence coefficient (IDICs) versus normalized local initial deflection

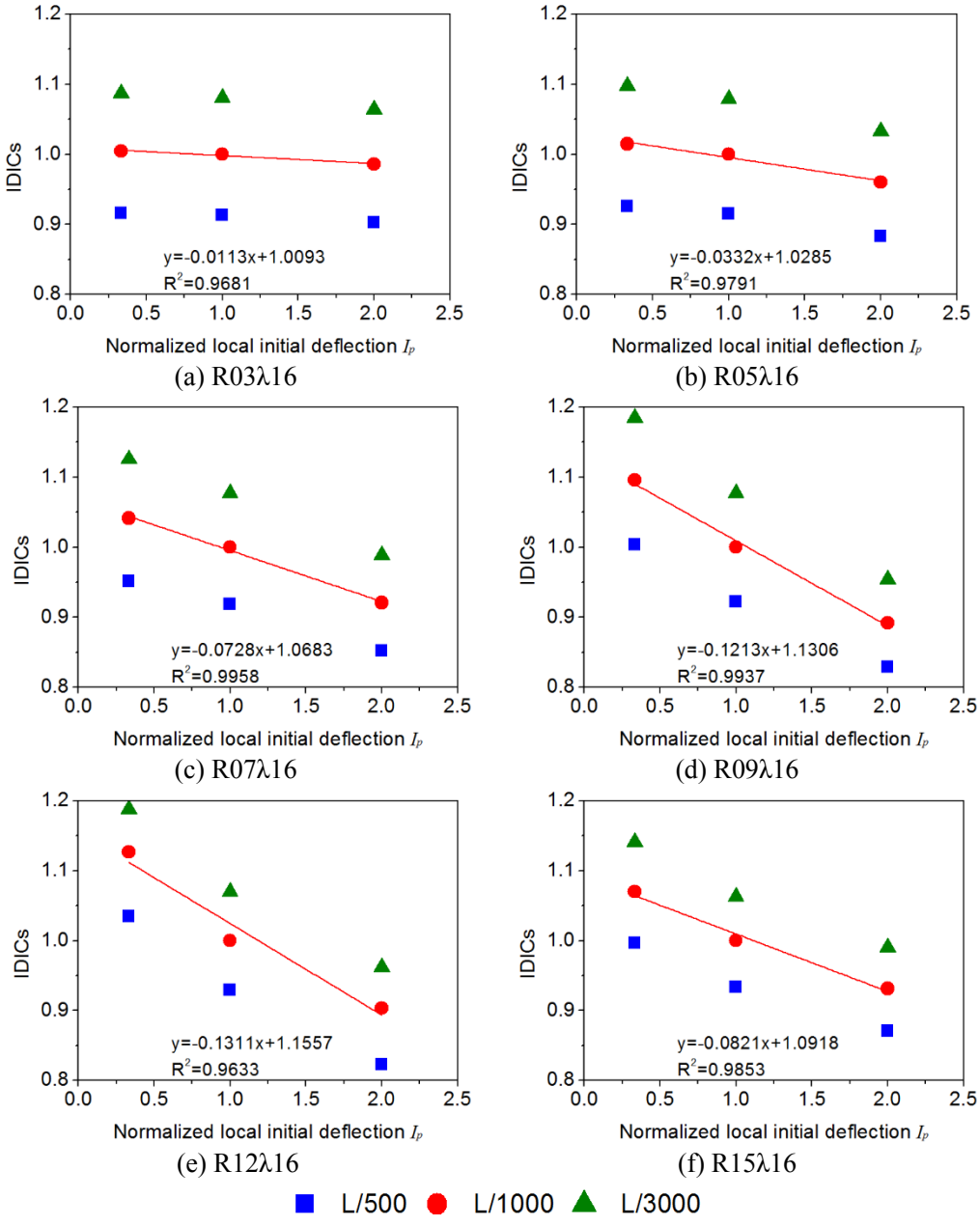

Fig. 4.9 Initial deflection influence coefficient (IDICs) versus normalized local initial deflection

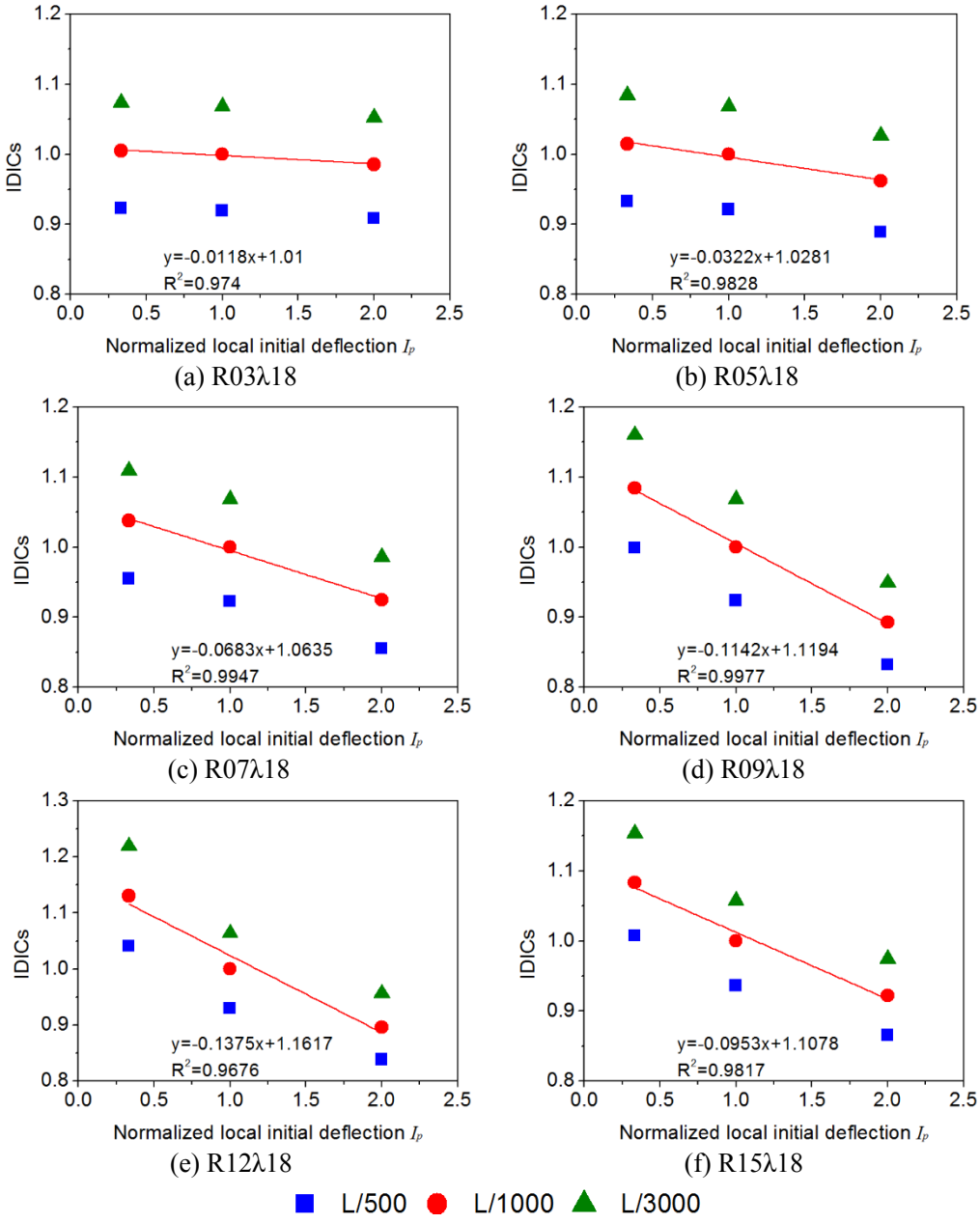

Fig. 4.10 Initial deflection influence coefficient (IDICs) versus normalized local initial deflection

The decreasing slope α is related to normalized width-thickness ratios as shown in **Fig. 4.11**, in which seven series of data with different normalized slenderness ratios are plotted. It can be seen that the decreasing slope increases first and then decreases with the increase of the normalized width-thickness ratio. Since the decreasing slope represents the reduction of load-bearing capacity by local initial deflection, the peak points show the width-thickness ratio where the reduction reaches the maximum. In addition, the peak

point of the decreasing slope α tends to move to larger width-thickness ratio with the increase of normalized slenderness ratios. When the normalized width-thickness ratio R is small (i.e., $R \leq 0.5$), the influence of the local initial deflection seems to be slight. In the range of R from 0.7 to 1.5, column strength becomes comparatively sensitive to the local initial deflection. When normalized slenderness ratio λ is small (i.e., $\lambda \leq 0.5$), the influence reaches the maximum with the decreasing slope about 0.1 at R=0.7. It corresponds to the 17.2% decrease of the load-bearing capacity. When λ is large (i.e., $\lambda \geq 1.0$), the load-bearing capacity of columns with higher R-value becomes sensitive to the local initial deflection. With R and λ equal to 1.2 and 1.8, respectively, the influence of local initial deflection reaches the maximum with the decreasing slope of 0.1375 corresponding to the 20.7% decrease of load-bearing capacity.

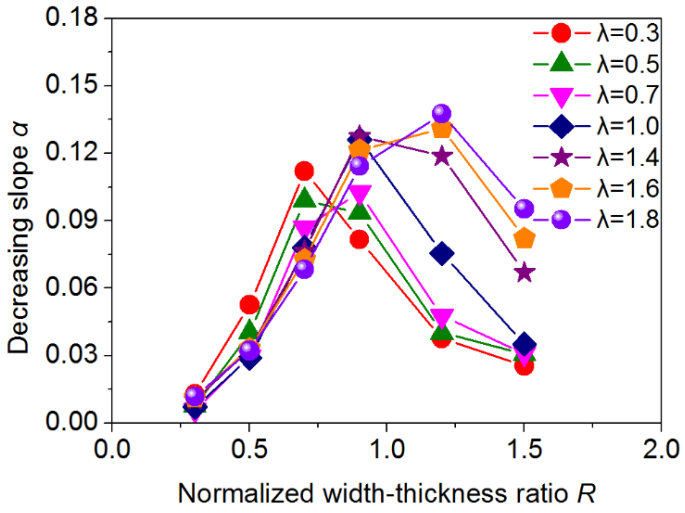

Fig. 4.11 Decreasing slope α versus normalized width-thickness ratio R

Failure modes of all FE models have been checked. They are listed in **Table. 4.4**. The symbols of "O" and "C" in the table represent overall buckling and coupled buckling, respectively. The typical buckling failure modes are demonstrated in **Fig. 4.12** taking two models as examples. The deformation of the columns is detailed at two points. One is at the point of load-bearing capacity, and the other is at the 85% of the load-bearing capacity after peak value. It can be recognized that coupled buckling or overall buckling occurs for 12 combinations of width-thickness and slenderness ratios indicated by "C/O" depending on the amplitudes of initial deflections. For these combinations, the failure

modes are detailed in **Table. 4.5**. The failure mode of R05λ05-07 and R07λ14-18 changes from overall buckling to coupled buckling with the increase of local initial deflection from b/450 to b/150. Failure mode change of R05λ09-18 occurs when increasing initial deflection from b/150 to b/75. This indicates that the amplitude of local initial deflection could change the failure mode in the normalized width-thickness ratio range from 0.5 to 0.7. The failure mode change by the local initial deflection could result in the larger reduction of load-bearing capacity by it. Therefore, it could be thought that this change is a cause inducing the movement of peak point of decreasing slope.

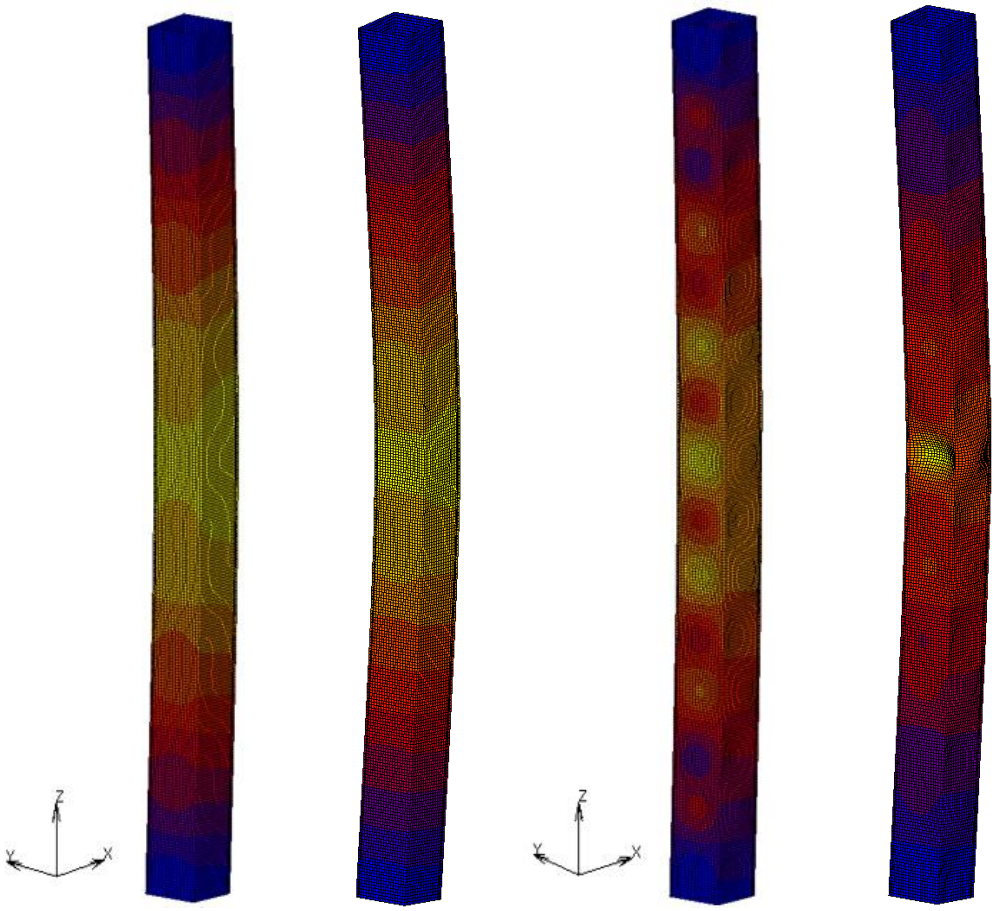

(a) at peak load (b) at 85% after peak (c) at peak load(d) at 85% after peak

Overall buckling (R03λ05) Coupled buckling (R09λ05)

Fig. 4.12 Examples of deformed shape. (Amplifying factor:5)

Table. 4.4 Failure modes in the FE models

Width-thickness ratio R	Slenderness ratio λ						
	0.3	0.5	0.7	1.0	1.4	1.6	1.8
0.3	O	O	O	O	O	O	O
0.5	C	C/O	C/O	C/O	C/O	C/O	C/O
0.7	C	C	C	C	C/O	C/O	C/O
0.9	C	C	C	C	C	C	C
1.2	C	C	C	C	C	C	C
1.5	C	C	C	C	C	C	C

Table. 4.5 Failure mode change by initial deflections

(a) R05λ05-07, R07λ14-18

Overall initial deflection	Local initial deflection		
	b/75	b/150	b/450
L/500	C	C	O
L/1000	C	C	O
L/3000	C	C	O

(b) R05λ10-18

Overall initial deflection	Local initial deflection		
	b/75	b/150	b/450
L/500	C	O	O
L/1000	C	O	O
L/3000	C	O	O

4.3.2 Influence of overall initial deflection

Results of models with the normalized slenderness ratios λ from 0.3 to 1.8 and constant normalized width-thickness ratio R of 0.9 are set as examples to show the influence of the overall initial deflection. The comparison of load-bearing capacities for different overall initial deflection are shown in **Fig. 4.13**. In the case of λ=0.3, the reduction on load-bearing capacity by increasing overall initial deflection is less than 5%. As the slenderness ratio increases, reduction on the load-bearing capacity reaches up to 15.1% at most with the amplitude of overall initial deflection increases from L/3000 to L/500.

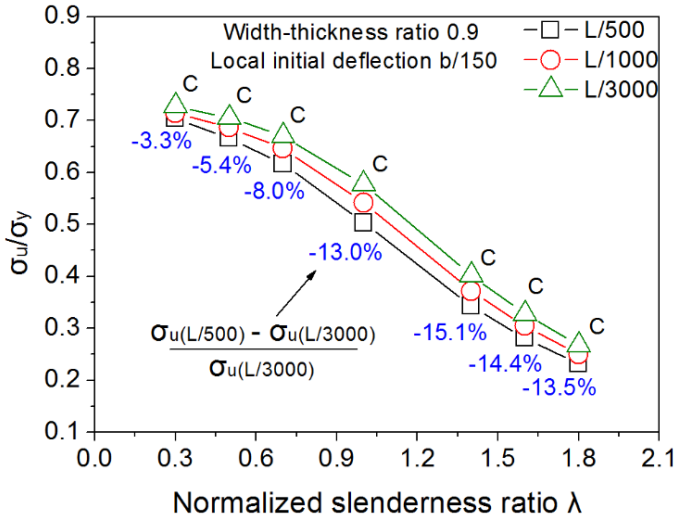

Fig. 4.13 Influence of overall initial deflection on load-bearing capacity

Relationship between the IDIC and the amplitude of the overall initial deflection normalized by the standard amplitude i.e. *L*/1000 is shown in **Fig. 4.14 – 4.19**. The similar tendency to **Fig. 4.4 - 4.11** can be seen, namely, the IDIC decreases approximately linearly as the amplitude of overall initial deflection increases, and the decreasing slope is nearly the same for different amplitudes of the local initial deflection.

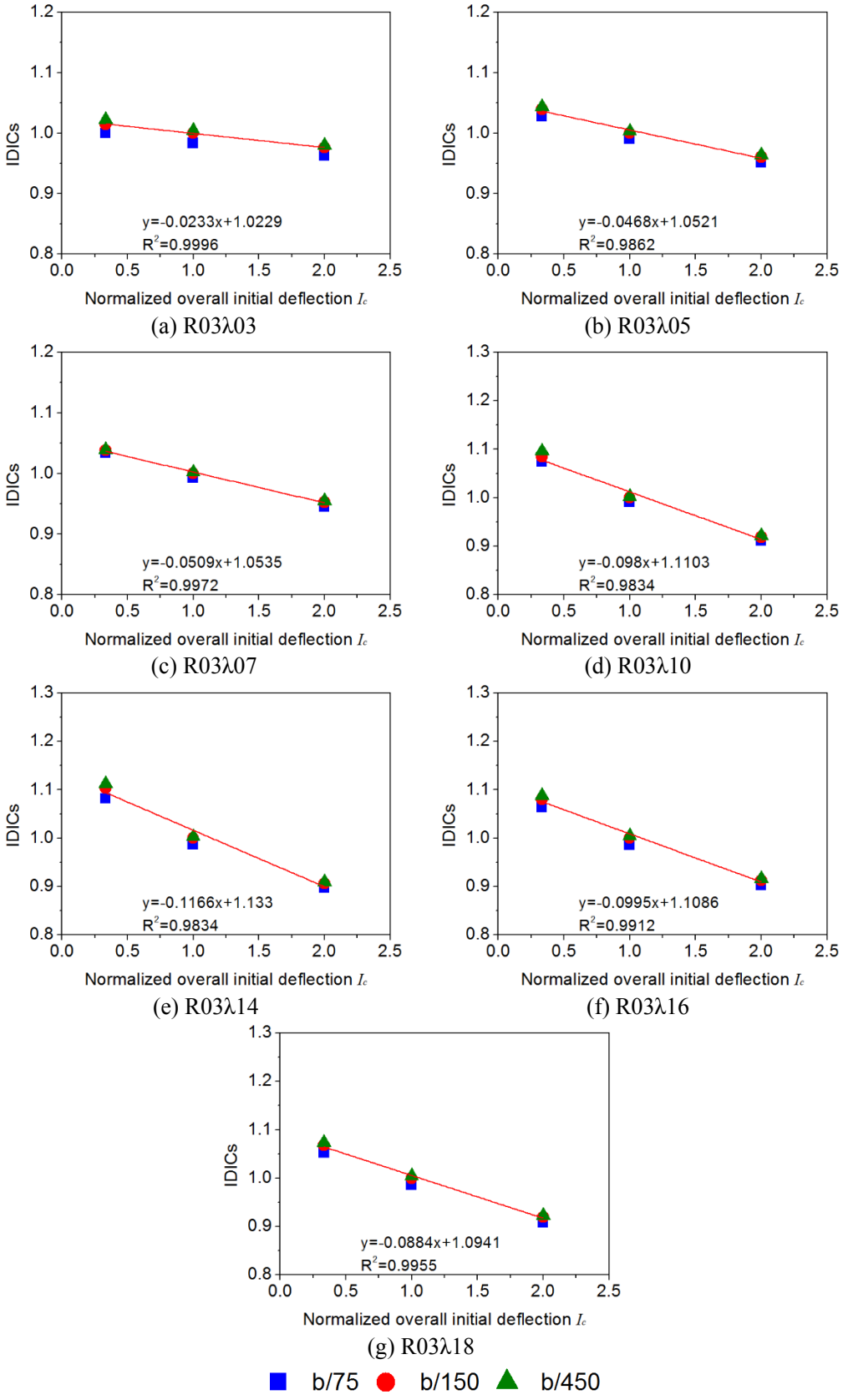

Fig. 4.14 Initial deflection influence coefficient (IDICs) versus overall initial deflection

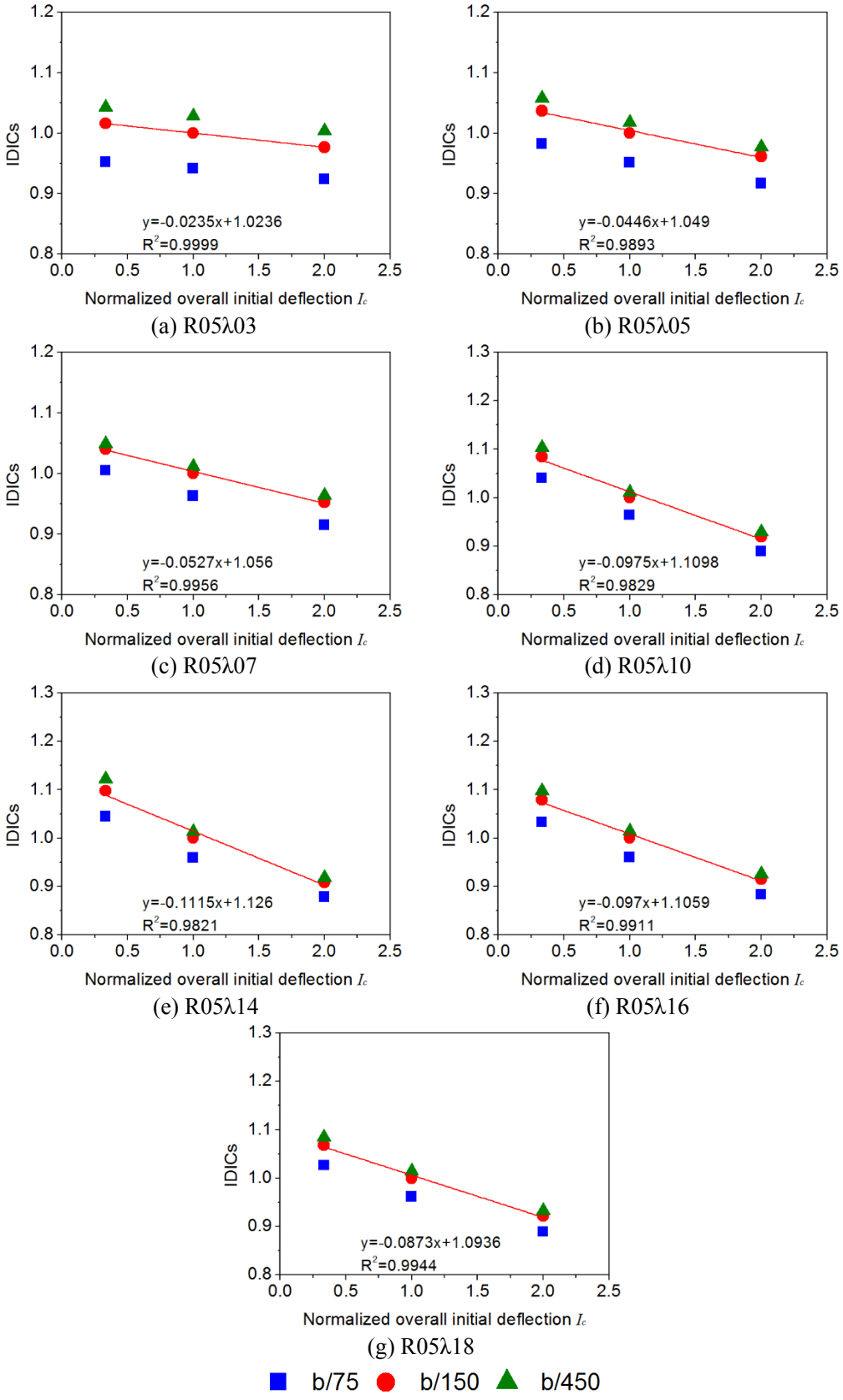

(a) R05λ03 (b) R05λ05

(c) R05λ07 (d) R05λ10

(e) R05λ14 (f) R05λ16

(g) R05λ18

Fig. 4.15 Initial deflection influence coefficient (IDICs) versus overall initial deflection

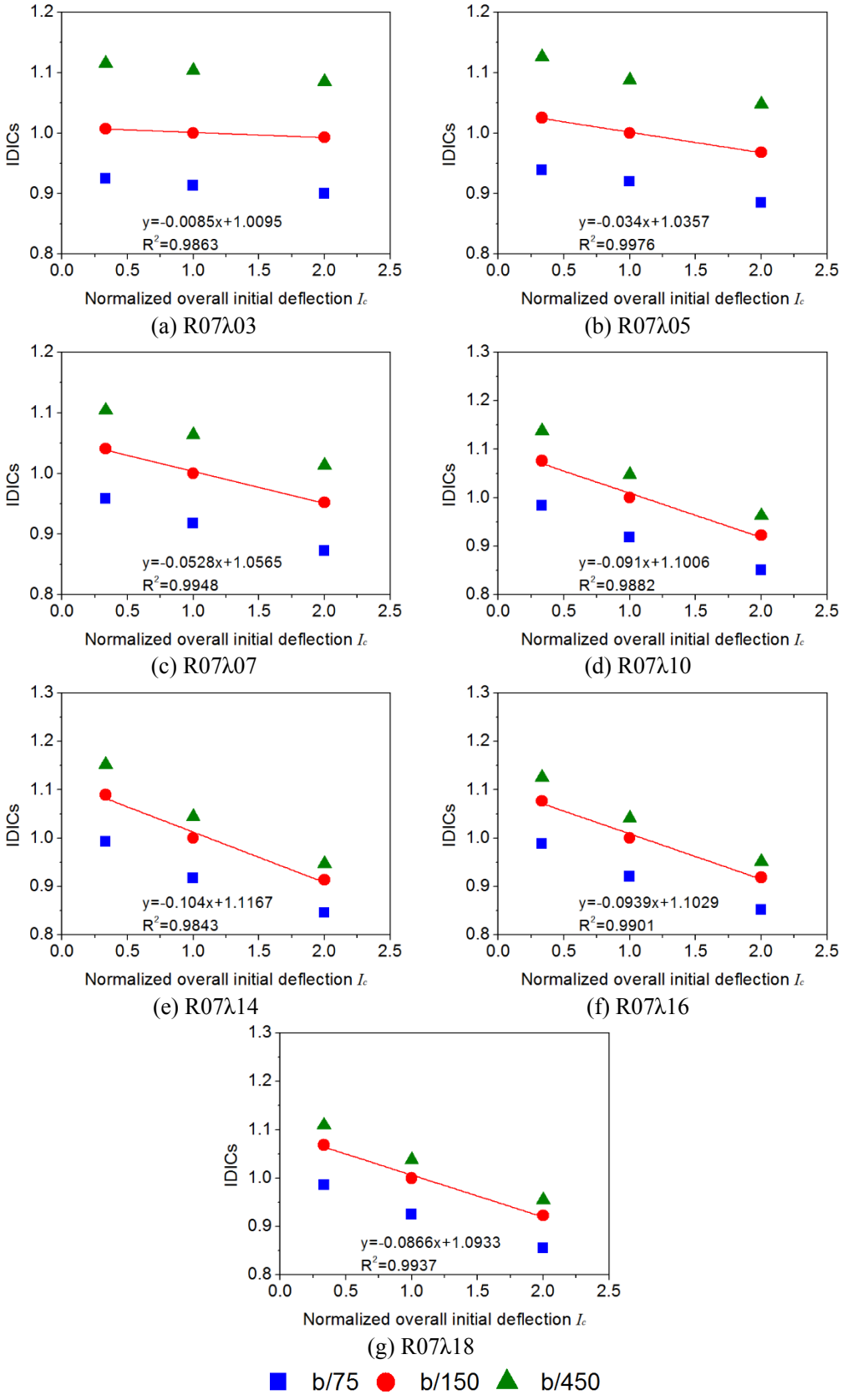

Fig. 4.16 Initial deflection influence coefficient (IDICs) versus overall initial deflection

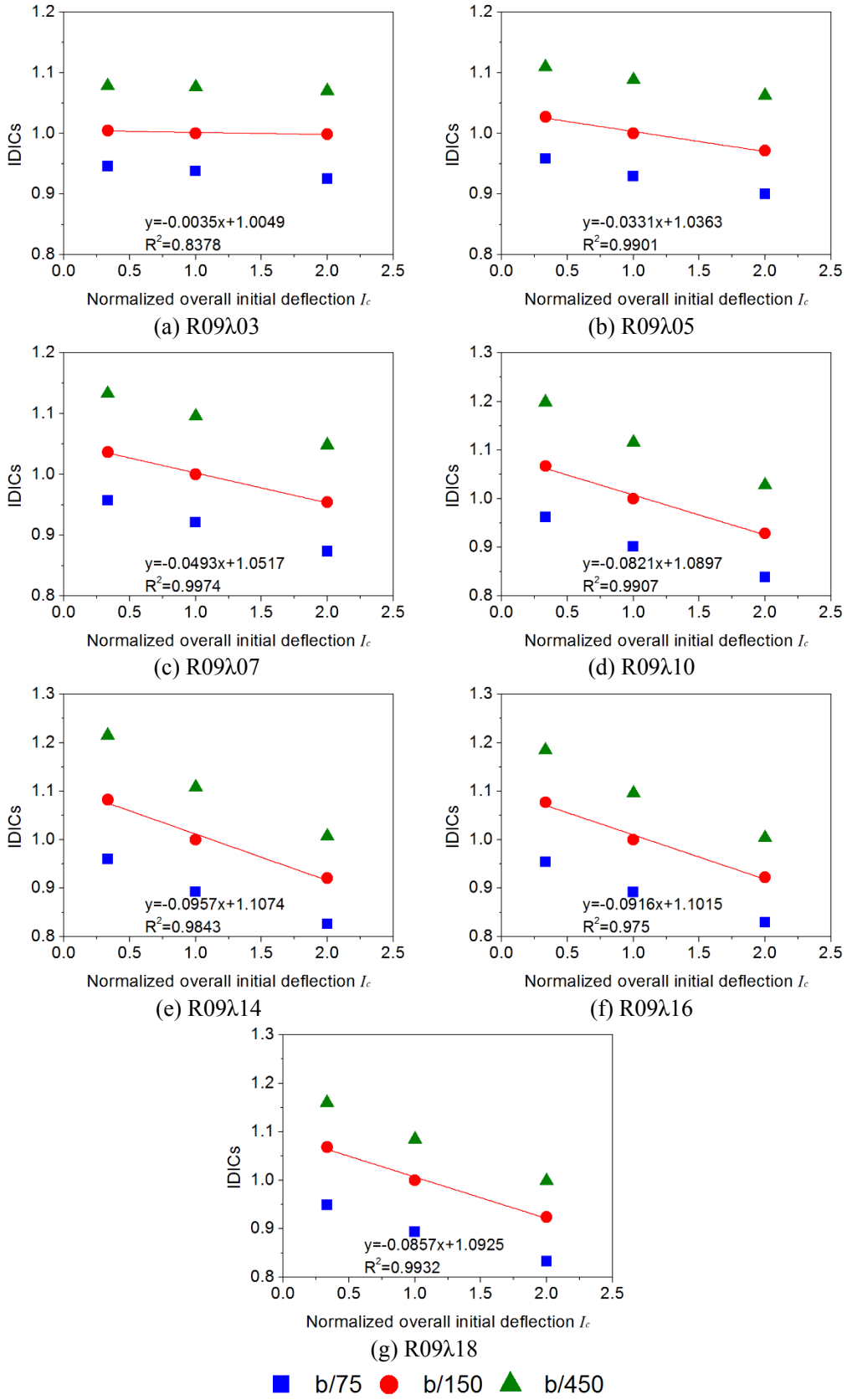

Fig. 4.17 Initial deflection influence coefficient (IDICs) versus overall initial deflection

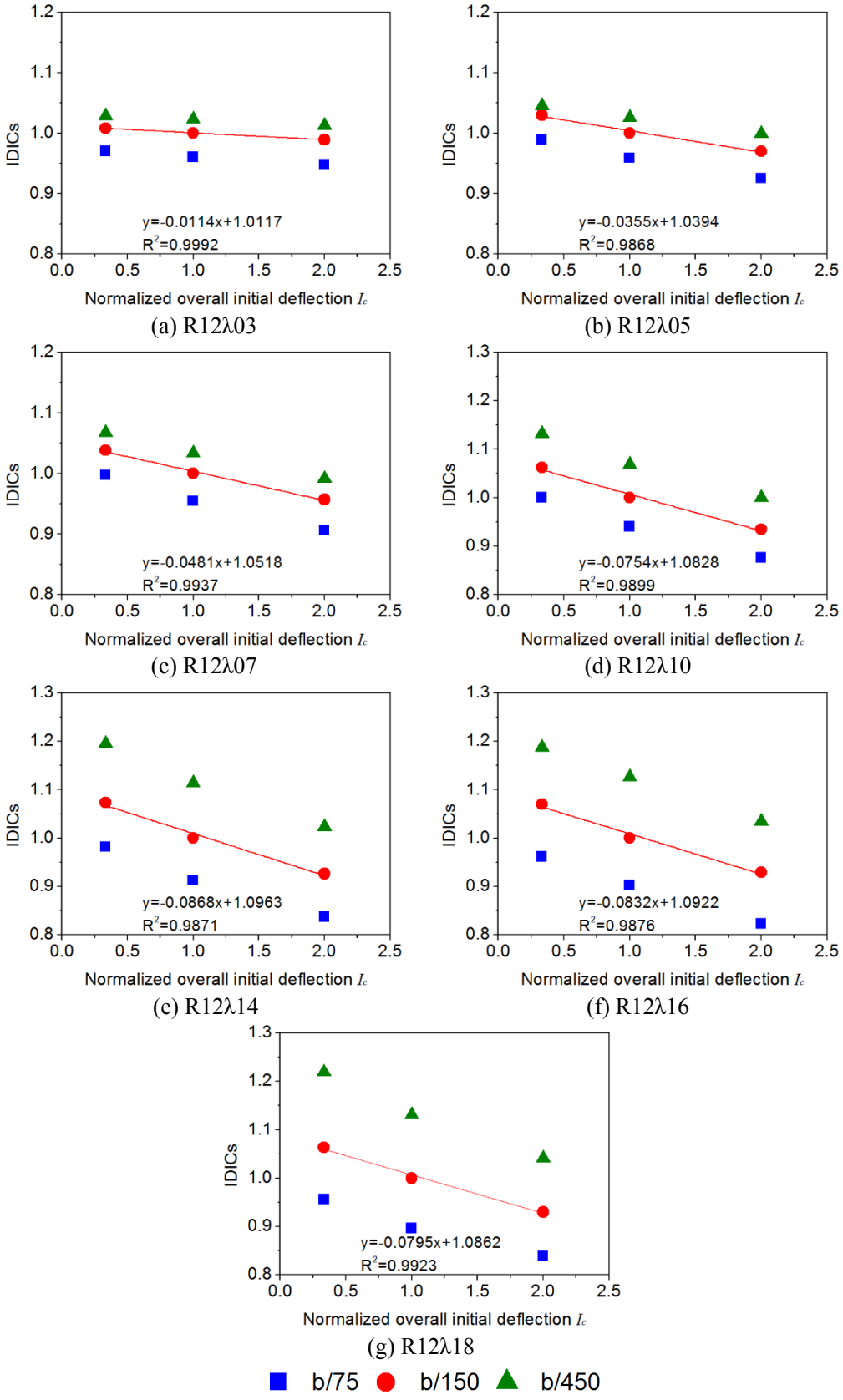

Fig. 4.18 Initial deflection influence coefficient (IDICs) versus overall initial deflection

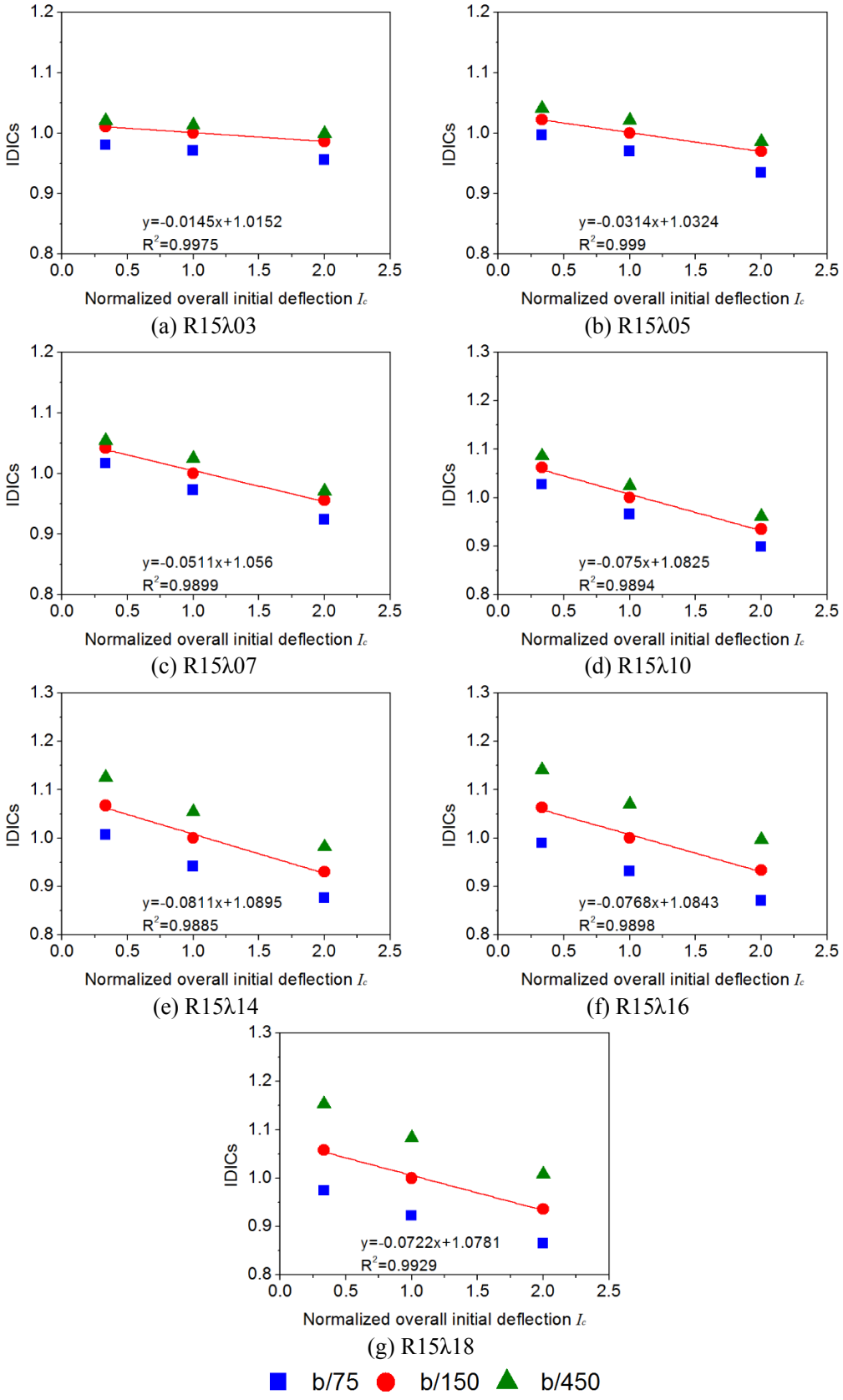

(a) R15λ03 (b) R15λ05

(c) R15λ07 (d) R15λ10

(e) R15λ14 (f) R15λ16

(g) R15λ18

Fig. 4.19 Initial deflection influence coefficient (IDICs) versus overall initial deflection

Linear regression analysis is conducted on the data when the amplitude of the local initial deflection is $b/150$. The absolute values of the decreasing slope β is related to the normalized slenderness ratio λ as shown in **Fig. 4.20** in which six series of data with different normalized width-thickness ratio R are plotted. It can be seen that the decreasing slope β increases first and then decreases with the increase of the λ-value. This tendency is similar to **Fig. 4.11**. However, being different from **Fig. 4.11**, the peak value of the decreasing slope appears at almost the same λ-value of 1.4. As shown in **Table 4.5**, the amplitude of overall deflection does not change the failure mode. This may be a cause of the difference.

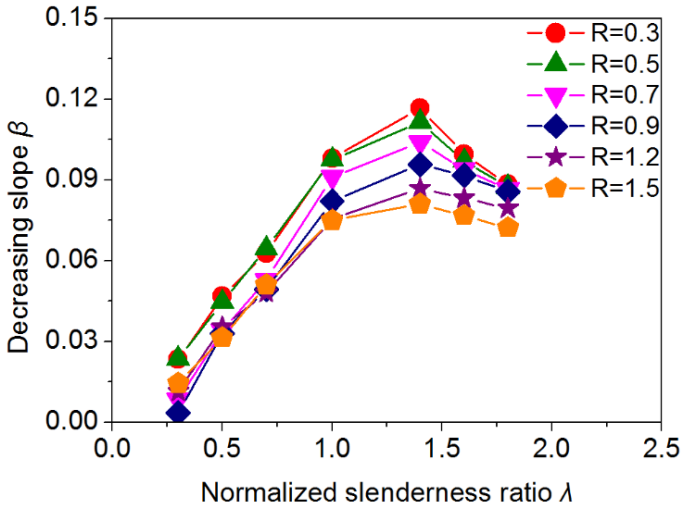

Fig. 4.20 Decreasing slope β versus normalized slenderness ratio λ

With λ from 0.7 to 1.8, column load-bearing capacity becomes comparatively sensitive to overall initial deflection. The maximum decreasing slope ranges from 0.081 to 0.1166. In addition, the influence of overall initial deflection on load-bearing capacity is related to normalized width-thickness ratio R. With the decrease of R, the influence of overall initial deflection increases. This is because column strength is mainly dominated by overall buckling when R is small. With R and λ equal to 0.3 and 1.4, respectively, the influence reaches the maximum with the decreasing slope of 0.1166 corresponding to the 17.9% decrease of load-bearing capacity.

4.4 Influence of overall initial deflection

4.4.1 Format of proposed formulae

In the previous chapter, the quantitative influence caused by the initial deflections on the load-bearing capacity was observed with a wide range of the normalized slenderness and width-thickness ratios taken into consideration. The value of IDIC tends to decrease linearly as the local or overall initial deflections increase. The decreasing slope caused by the local/overall initial deflection is nearly invariable regardless of the amplitude of the overall/local initial deflection. This fact may suggest that there is no significant coupling effect on IDIC between two initial deflections. Therefore, the IDIC can be calculated as,

$$\mathrm{IDIC} = f(R,\lambda)(I_p - 1) + g(\lambda,R)(I_c - 1) + 1 \tag{4.2}$$

In the formula, $f(R, \lambda)$ is the decreasing slope α, $g(R, \lambda)$ is the decreasing slope β; I_p is the local initial deflection normalized by the standard local initial deflection (b/150); I_c is the overall initial deflection normalized by the standard overall initial deflection (L/1000). The terms, I_p, I_c minus 1, are set to satisfy the condition that the IDIC is equal to 1 when the local and overall initial deflections are b/150 and L/1000, respectively.

4.4.2 Decreasing slope α

From the numerical results presented in **Fig. 4.11**, it can be seen that the influence of local initial deflection is related with both normalized width-thickness ratio and slenderness ratio. As the width-thickness ratio increases, the decreasing slope increases first then decreases after the peak value. In addition, the peak value of the decreasing slope α appears at different normalized slenderness ratio. Referring to **Fig. 4.11**, the decreasing slope α is assumed as **Eq. 4.3**,

$$f(R,\lambda) = p_1 * R^{(p_2 + p_3 * R)} \tag{4.3}$$

where R and λ is normalized width-thickness and slenderness ratios, respectively.

Coefficients p_1, p_2, p_3 and their determination coefficient are obtained as listed in **Table. 4.6** through the regression analysis of the above numerical results with Levenberg-Marquardt method. It is understood that the coefficients p_1, p_2, p_3 can be associated with

the normalized slenderness ratio. Relationship between the coefficients and the normalized slenderness ratio is plotted in **Fig. 4.21**.

Table 4.6 Coefficient term and determination coefficient of equation (L/1000)

Slenderness ratio λ	Coefficient term			Determination coefficient
	p_1	p_2	p_3	
0.3	-0.0749	3.1002	-5.5554	0.9143
0.5	-0.0834	3.5604	-5.4439	0.9254
0.7	-0.0915	4.2250	-5.6733	0.9478
1.0	-0.1168	4.8706	-5.6100	0.9767
1.4	-0.1320	3.9886	-3.7722	0.9924
1.6	-0.1318	3.7669	-3.2494	0.9921
1.8	-0.1289	3.6211	-2.8643	0.9906

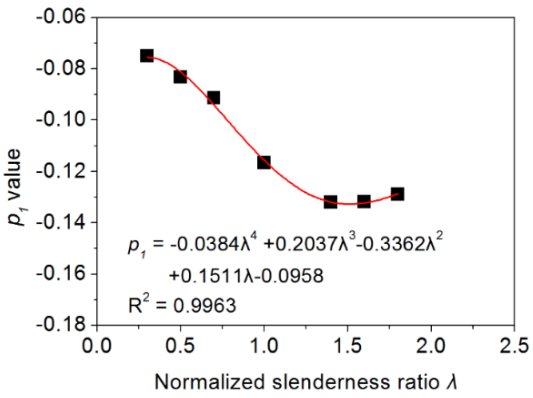

(a) Equation of p_1

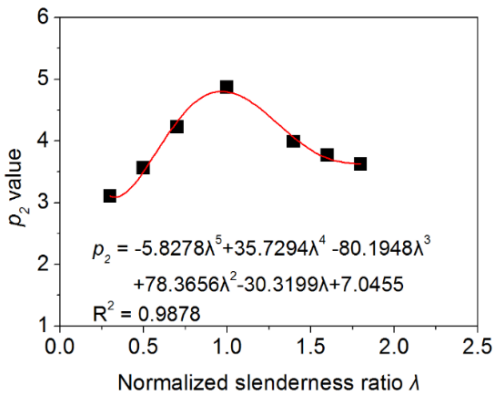

(b) Equation of p_2

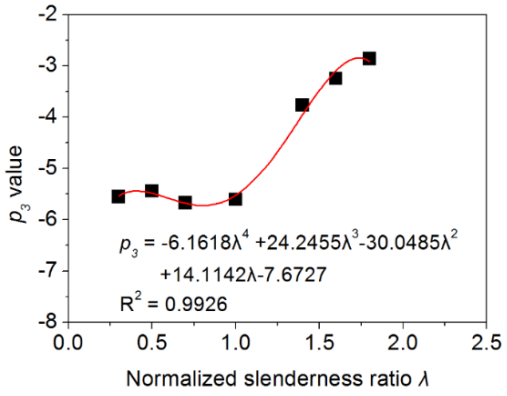

(c) Equation of p_3

Fig. 4.21 Equation of coefficient terms p_1, p_2, p_3

The authors tried several functions including linear, polynomial, logarithmic, exponential, trigonometric functions for the regression analysis. As a result, the polynomial regression was adopted since it provided comparatively accurate prediction and the formula format is simpler than others. The obtained formulae to estimate each coefficient are shown in **Eq. 4.4**.

$$\begin{cases} p_1 = -0.0384\lambda^4 + 0.2037\lambda^3 - 0.3362\lambda^2 + 0.1511\lambda - 0.0958 \\ p_2 = -5.8278\lambda^4 + 35.7294\lambda^3 - 80.1948\lambda^2 + 78.3656\lambda + 7.0455 \\ p_3 = -6.1618\lambda^4 + 24.2455\lambda^3 - 30.0485\lambda^2 + 14.1142\lambda - 7.6727 \end{cases} \tag{4.4}$$

4.4.3 Decreasing slope β

From the numerical results presented in **Fig. 4.20**, it can be seen that the influence of overall initial deflection is also related to both normalized width-thickness ratio and slenderness ratios. As the slenderness ratio increases, the decreasing slope increases first, then decreases after the peak value which is similar to that as shown in **Fig. 4.11**. The different is that the peak value of the decreasing slope appears at almost the same λ-value of 1.4. The cubic function is assumed for the decreasing slope β as **Eq. 4.5**,

$$g(\lambda, R) = q_1(\lambda - 1.4)^3 + q_2(\lambda - 1.4)^2 + q_3 \tag{4.5}$$

where R and λ are normalized width-thickness and slenderness ratios, respectively.

Coefficients q_1, q_2, q_3 and determination coefficient are obtained as listed in **Table. 4.7** through the regression analysis of the above numerical results. It is understood that the coefficients q_1, q_2, q_3 can be associated with the normalized width-thickness ratio. Relationship between the coefficients and the normalized width-thickness ratio is plotted in **Fig.4.22**. By means of the polynomial regression, the formulae to estimate these coefficients q_1, q_2 and q_3 can be performed as a function of normalized width-thickness ratio R as shown in **Eq.4.6**.

Table 4.7 Coefficient term and determination coefficient of equation (b/150)

Width-thickness ratio R	Coefficient term			Determination coefficient
	q_1	q_2	q_3	
0.3	0.0548	0.1333	-0.1124	0.9853
0.5	0.0431	0.1179	-0.1087	0.9874
0.7	0.0303	0.1126	-0.1030	0.9896
0.9	0.0248	0.0989	-0.0963	0.9834
1.2	0.0068	0.0706	-0.0866	0.9873
1.5	0.0086	0.0664	-0.0817	0.9922

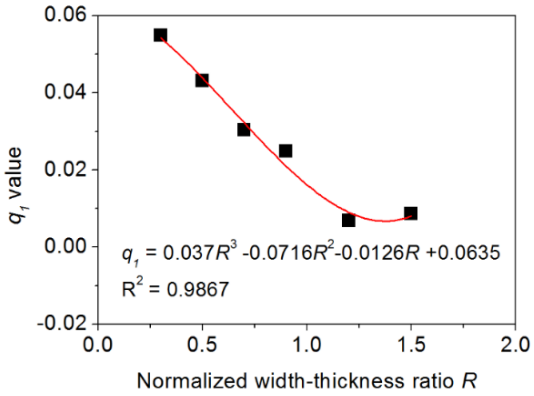

(a) Equation of q_1

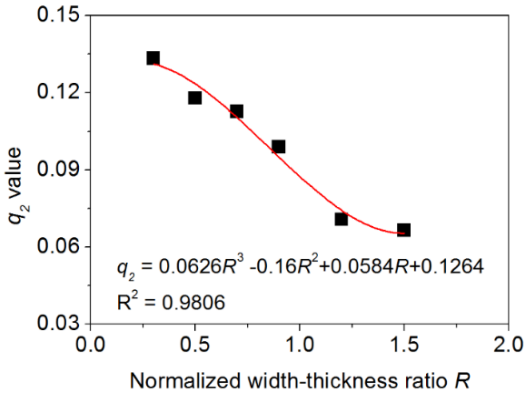

(b) Equation of q_2

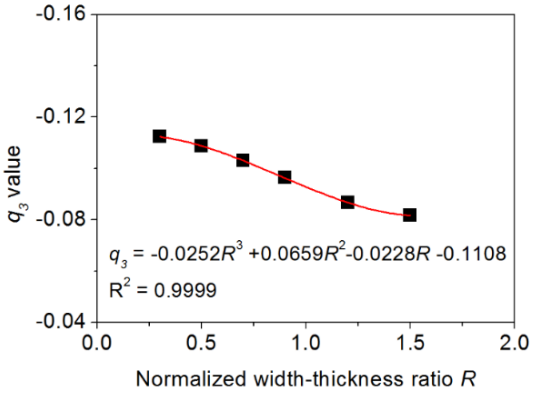

(c) Equation of q_3

Fig. 4.22 Equation of coefficient terms q_1, q_2, q_3

$$\begin{cases} q_1 = 0.037R^3 - 0.0716R^2 - 0.0126R + 0.0635 \\ q_2 = 0.0626R^3 - 0.16R^2 + 0.0584R + 0.1264 \\ q_3 = -0.0252R^3 + 0.0659R^2 - 0.0228R - 0.1108 \end{cases} \quad (4.6)$$

4.5 Validation of the proposed formulae

4.5.1 Comparison between formulae and FEA results

The IDICs obtained by the proposed formulae were compared with those by FEA for 378 models to verify the accuracy of the formulae. The comparisons are divided into seven figures by the normalized slenderness ratios as shown in **Fig. 4.23 (a)-(g)**. Additional 108 FEA results with normalized slenderness ratio of 0.9 and 1.2, which are not used in formula fitting analysis, are considered in formula verification procedure for further prove the validation of the proposed formulae as shown in **Fig. 4.24**. The absolute value of maximum errors and average errors between formulae results and FEA results are shown in **Table. 4.8** and **Table. 4.9**, respectively.

It can be seen that most of the formulae results show good agreement with FEA results with maximum errors less than 5%. Only in four cases, the formulae results are found with errors more than 5%, but less than 7%. These relatively large errors are caused by the fact that the influence tendency of initial deflections is not strictly linear. Although the accuracy can be improved by considering the quadratic function on the influence tendency, the authors do not think that it is necessary due to accurate prediction results in most cases and more complicated calculation by using quadratic function.

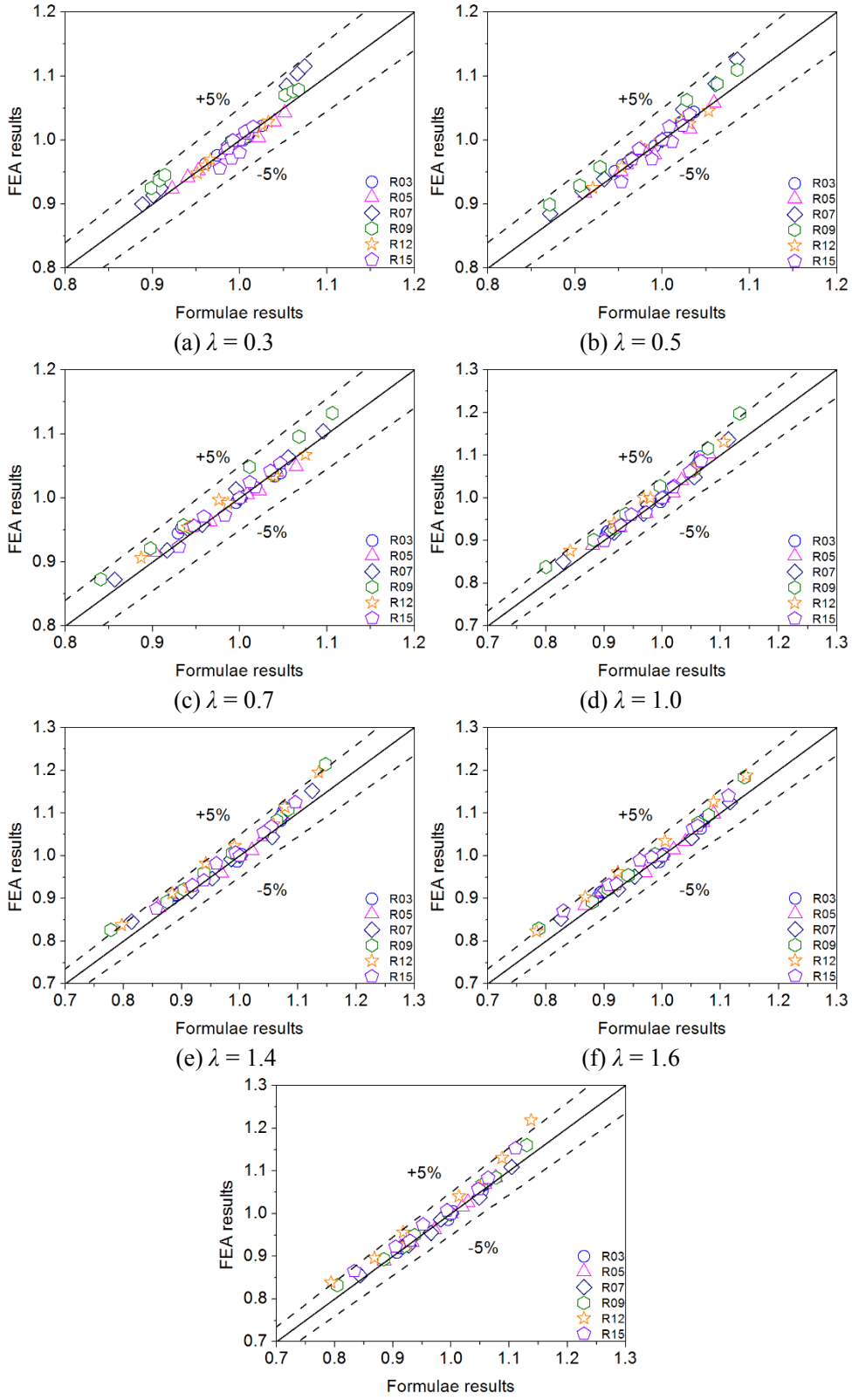

(a) $\lambda = 0.3$ (b) $\lambda = 0.5$

(c) $\lambda = 0.7$ (d) $\lambda = 1.0$

(e) $\lambda = 1.4$ (f) $\lambda = 1.6$

(g) $\lambda = 1.8$

Fig. 4.23 Comparison of IDICs between formulae and FEA results

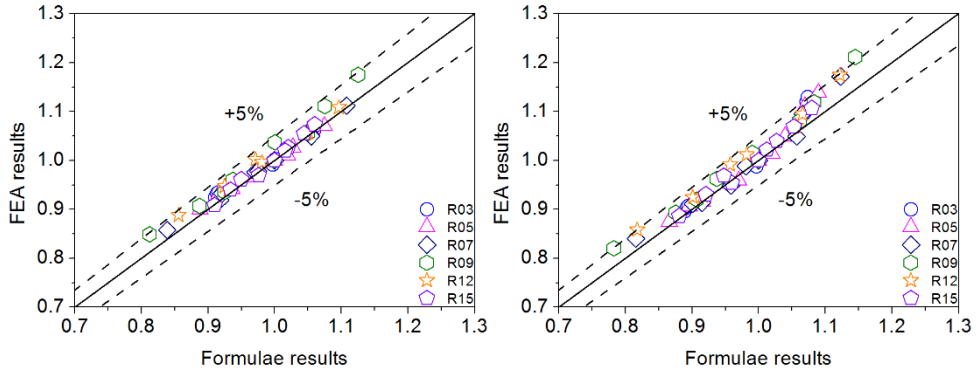

(a) $\lambda = 0.9$ (b) $\lambda = 1.2$

Fig. 4.24 Comparison of IDICs between formulae and FEA results

Table. 4.8 Maximum errors between formula and FEA results (%)

Width-thickness ratio R	Slenderness ratio λ								
	0.3	0.5	0.7	0.9	1.0	1.2	1.4	1.6	1.8
0.3	0.44	0.89	2.04	2.03	2.82	4.89	3.12	2.17	1.09
0.5	1.81	1.48	1.62	1.67	2.17	4.27	2.55	2.07	1.01
0.7	3.68	3.57	1.81	2.25	2.47	4.17	3.81	3.08	1.36
0.9	3.30	3.22	3.69	4.35	5.40	5.49	5.74	4.97	3.32
1.2	0.46	1.33	2.19	3.68	3.91	4.77	4.99	4.74	6.68
1.5	2.23	1.98	1.29	1.26	1.78	2.48	2.62	4.70	3.67

Table. 4.9 Average errors between formula and FEA results (%)

Width-thickness ratio R	Slenderness ratio λ								
	0.3	0.5	0.7	0.9	1.0	1.2	1.4	1.6	1.8
0.3	0.32	0.51	1.02	0.85	1.37	1.99	1.68	1.17	0.63
0.5	0.62	0.66	0.86	0.75	1.14	1.61	1.45	1.11	0.58
0.7	1.87	1.54	0.85	0.78	1.18	1.69	1.56	1.04	0.79
0.9	1.80	2.18	2.27	2.73	2.94	2.96	2.89	2.15	1.34
1.2	0.28	0.61	1.11	1.78	2.19	2.94	3.31	3.18	3.42
1.5	1.05	1.17	0.84	0.74	0.93	1.33	1.60	2.14	2.07

Therefore, it can be concluded that the proposed IDIC formulae have sufficient accuracy and reliability for estimating the quantitative influence of the initial deflections on the load-bearing capacity of the unstiffened welded box section columns.

4.5.2 Comparison between formulae and experimental results

Besides the comparison between formulae and FEA results, the comparison between formulae and experimental results was also conducted to evaluation the validation of the proposed formulae. To predict the load-bearing capacity of an experimental column with measured initial deflections, not only the formulae aimed at quantitative influence of various initial deflections, but also formulae target on load-bearing capacity under certain initial deflections. In this part, a simplified formula developed by Kishi [87] to calculate the load-bearing capacity under local initial deflection of $b/150$ and overall initial deflection of $L/1000$, was used. The formulae are performed as follows,

$$\sigma_{cr}/\sigma_u = 1-(0.0502\lambda^2 - 0.2485\lambda + 0.6077)(R-0.5) \tag{4.7}$$

$$\sigma_u/\sigma_y = \begin{cases} 1 & \lambda \le 0.2 \\ 1.059 - 0.258\lambda - 0.190\lambda^2 & 0.2 < \lambda \le 1.0 \\ 1.427 - 1.039\lambda + 0.223\lambda^2 & \lambda > 1.0 \end{cases} \tag{4.8}$$

where σ_{cr} is the load-bearing capacity; σ_u is the overall buckling strength of the column with the normalized slenderness ratio of λ specified in JRA; and R is the normalized width-thickness ratio.

Formulae to estimate the quantitative influence caused by the initial deflection are proposed in this study. The product between the proposed formulae in this study and the existing simplified formula from Kishi will be the load-bearing capacity of the columns with actual amplitude of initial deflections. The comparison between current formulae and experimental results [64, 84] is shown in **Table. 4.10**. Since the local initial deflection was not measured in Somodi's test [60], the test results of W3-series specimens were not used in this part. It can be seen that the existing formula considering initial deflections of $b/150$ and $L/1000$ comparatively underestimates the load-bearing capacity for all specimens. The product between existing formula and IDICs provides better prediction on the load-bearing capacity.

Table 15 Comparison between formula and experimental results

Specimen	F_T (kN)	$\bar{\sigma}_T$	$\bar{\sigma}_{cr}$	IDIC	IDIC $*\bar{\sigma}_{cr}$	$(\bar{\sigma}_{cr}-\bar{\sigma}_T)/\bar{\sigma}_T$ (%)	$(IDIC*\bar{\sigma}_{cr}-\bar{\sigma}_T)/\bar{\sigma}_T$ (%)
S1a	2053	0.857	0.730	1.0471	0.764	-14.8	-10.9
S1b	2139	0.893	0.730	1.0464	0.764	-18.3	-14.4
S2a	2065	0.862	0.711	1.0689	0.760	-17.5	-11.8
S2b	2062	0.861	0.711	1.0689	0.760	-17.4	-11.7
S3a	2114	0.882	0.684	1.0868	0.743	-22.4	-15.8
S3b	2044	0.853	0.684	1.0844	0.742	-19.8	-13.0
W-S	706	0.671	0.578	1.1068	0.640	-13.9	-4.6
W-L	564	0.536	0.468	1.1123	0.521	-12.7	-2.8

Where F_T is the experimental results, $\bar{\sigma}$ is the non-dimensional load-bearing capacity, $\bar{\sigma}_{cr}$ is calculated based on the Kishi's formula and specification formula, IDIC is an initial deflection influence coefficient.

4.6 Influence of residual stress on IDICs

For the welded box section columns, many researchers have demonstrated that residual stress would have significant influence on their load-bearing capacity [88, 89]. According to previous statistics on residual stress of 216 normal strength steel columns by Fukumoto [87], compressive residual stress was found in the range from 0 to $0.6\sigma_y$. In this section, to investigate the influence of residual stress on the relationship between initial deflection influence coefficient(IDIC) and initial deflections, specimens with short, medium and high columns length were chosen for FE analysis with compressive residual stress $0.1\sigma_y$ and $0.4\sigma_y$ into consideration. As mentioned in Section 4.3.1 and 4.3.2, the IDICs approximately linearly decreases as the amplitude of local/overall initial deflection increases. The decreasing slope is nearly the same for different amplitudes of overall/local initial deflection. Therefore, the IDICs are plotted with normalized local initial deflection under the overall initial deflection of $L/1000$ as shown in **Fig. 4.25**. It can been seen that slight influence due to different residual stress value on the relationship between IDICs and local initial deflection can be observed. In general, the slope of the plot for smaller residual stress is steeper, indicating larger influence of local initial deflection. For the columns with high slenderness ratio, the difference on IDICs becomes up to

approximately 5% with the increase of residual stress from $0.1\sigma_y$ to $0.4\sigma_y$.

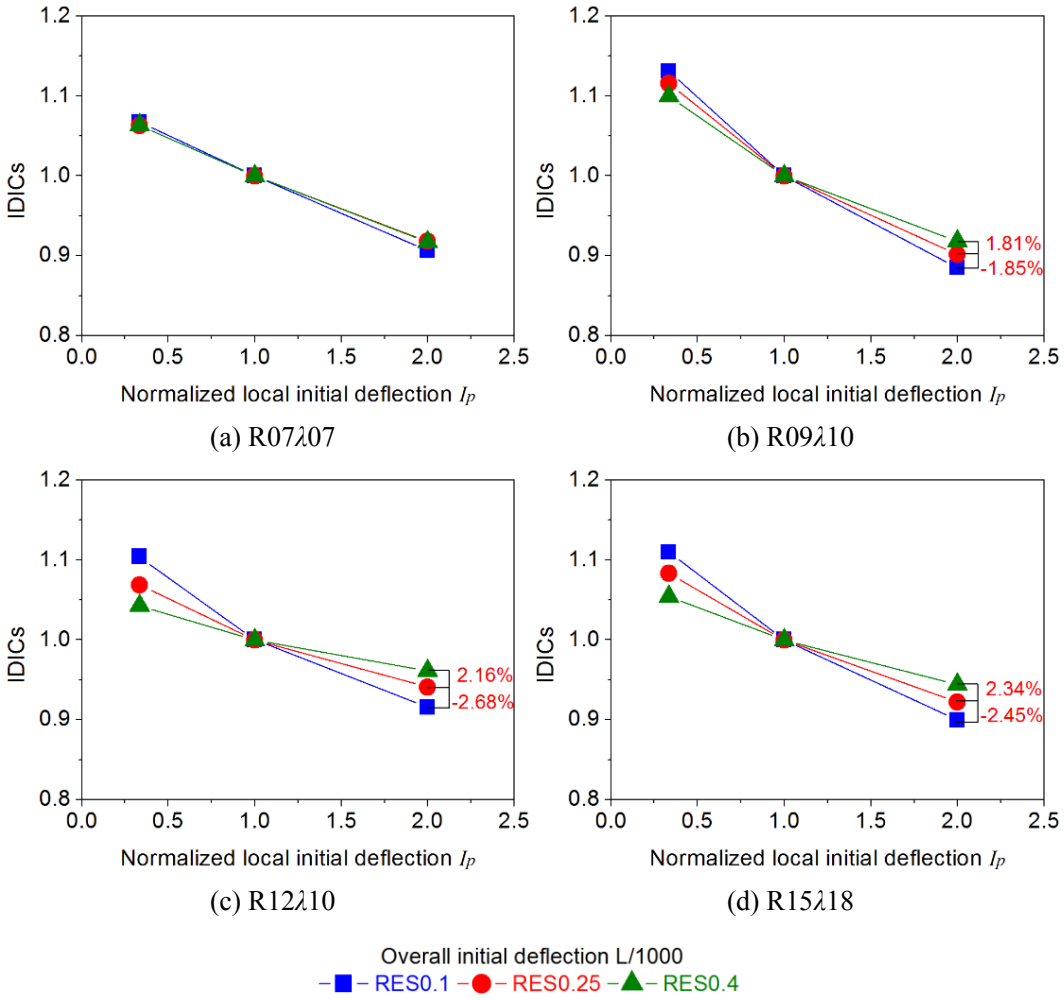

Fig. 4.25 IDICs versus normalized local initial deflection

Investigation was also carried out to study the influence of different residual stress of $0.1\sigma_y$, $0.25\sigma_y$ and $0.4\sigma_y$ on the relationship between IDICs and normalized overall initial deflection. IDICs are plotted with normalized overall initial deflection under the local initial deflection of $b/150$ as shown in **Fig. 4.26**. It can be found that the decreasing tendency of IDICs related to shows close agreement with each other under different residual stress. This result indicates that residual stress has no clear influence on the relationship between IDICs and normalized overall initial deflection.

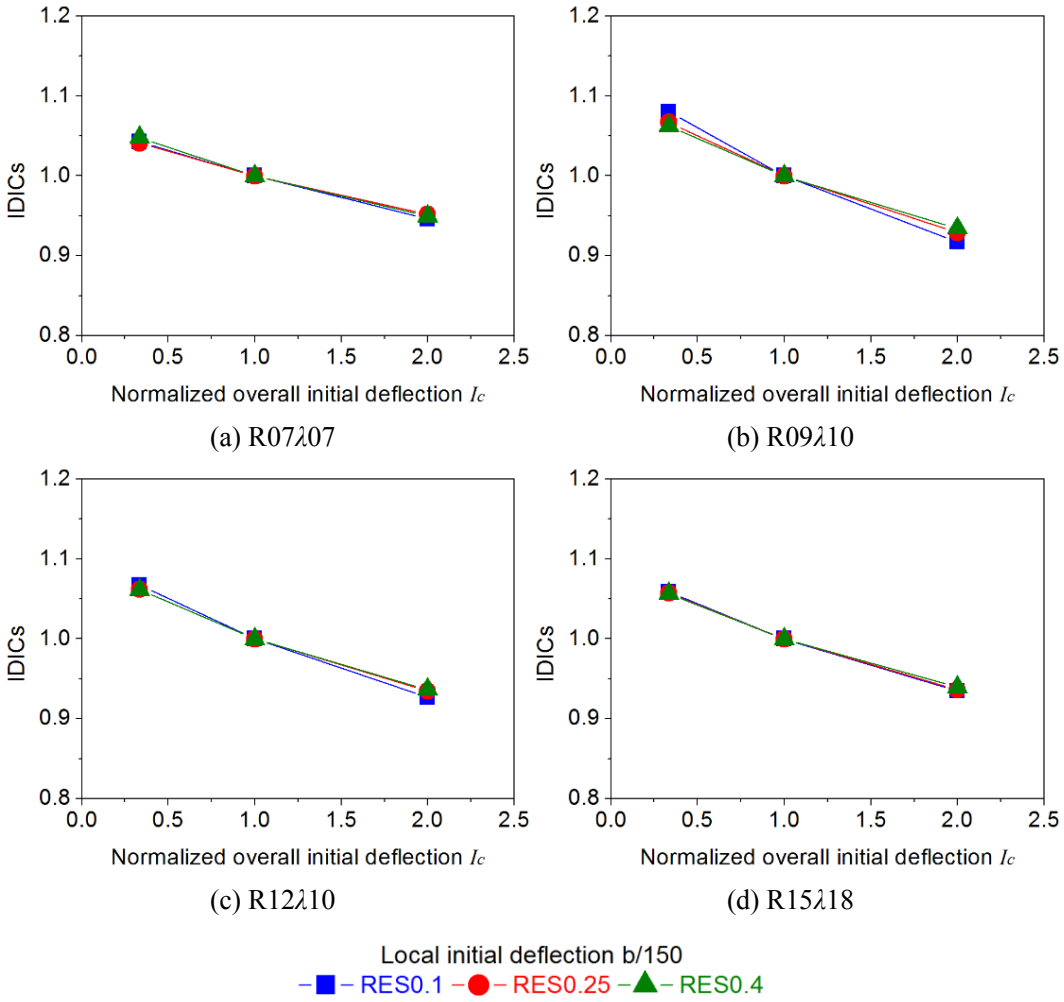

Fig. 4.26 IDICs versus normalized overall initial deflection

4.7 Summary

In this study, 486 models were analyzed to investigate the quantitative influence of the initial deflections on the load-bearing capacity of unstiffened welded square box section columns with a variety of normalized slenderness and width-thickness ratios. The main conclusions can be summarized as follows.

(1) The load-bearing capacity linearly decreases as the amplitude of local/overall initial deflection increases. The decreasing slope is nearly the same for different amplitudes of overall/local initial deflection.

(2) With the normalized width-thickness and slenderness ratios equal to 1.2 and 1.8, respectively, the influence of the local initial deflection reaches the maximum with the decreasing slope of 0.1375 corresponding to the 20.7% reduction on load-bearing capacity.

(3) With the normalized width-thickness and slenderness ratio equal to 0.3 and 1.4, respectively, the influence of the overall initial deflection reaches the maximum with decreasing slope of 0.1166 corresponding to the 17.9% reduction on load-bearing capacity.

(4) Based on numerous FEA results, the formulae for the initial deflection influence coefficient (IDIC) are developed, which describe the quantitative influence caused by the initial deflections. Compared with the FEA results, the accuracy of the formulae is verified.

(5) Compared with the experimental results, it is verified that the product between the IDIC and the simplified formula can predict the load-bearing capacity with good accuracy in the case of columns with various amplitudes of the initial deflections.

(6) The residual stress has slight influence on the relationship between IDICs and local initial deflection, while it has negligible influence on the relationship between IDICs and overall initial deflection.

The validity of the proposed formulae has been evaluated only for the conditions examined in this research. Their applicability to different cross-sections, residual stress pattern and high strength steel columns as well as wider range of initial deflection value should be studied in the future work.

Annex: An example to apply show the application procedure of the proposed formulae

Test specimen W-S in Table 1 is set as an example to improve the accuracy of prediction on the load-bearing capacity. The basic parameter of W-S is tabulated below.

Basic buckling parameter of W-S

Parameter	Value
Normalized slenderness ratio λ	0.82
Normalized width-thickness ratio R	0.95
Overall initial deflection	L/1825
Local initial deflection	b/520
σ_T/σ_y	0.671

Calculation according to Kishi's formula (**Eq. 4.7**) and design code (**Eq. 4.8**):

$$\sigma_{cr}/\sigma_u = 1-(0.0502\lambda^2-0.2485\lambda+0.6077)(R-0.5)=0.803$$
$$\sigma_u/\sigma_y = 1.059-0.258\lambda-0.190\lambda^2 = 0.72$$
$$\Rightarrow \sigma_{cr}/\sigma_y = 0.803*0.72 = 0.578$$

Calculation of IDIC according to **Eqs. 4.2-4.6**:

$$\begin{cases} p_1 = -0.0384\lambda^4+0.2037\lambda^3-0.3362\lambda^2+0.1511\lambda-0.0958=-0.1030 \\ p_2 = -5.8278\lambda^4+35.7294\lambda^3-80.1948\lambda^2+78.3656\lambda+7.0455=4.6527 \\ p_3 = -6.1618\lambda^4+24.2455\lambda^3-30.0485\lambda^2+14.1142\lambda-7.6727=-5.7214 \end{cases}$$
$$f(R,\lambda) = p_1 * R^{(p_2+p_3*R)} = -0.1072$$

$$\begin{cases} q_1 = 0.037R^3-0.0716R^2-0.0126R+0.0635=0.0186 \\ q_2 = 0.0626R^3-0.16R^2+0.0584R+0.1264=0.0912 \\ q_3 = -0.0252R^3+0.0659R^2-0.0228R-0.1108=-0.0946 \end{cases}$$
$$g(\lambda,R)=\mathrm{q}_1(\lambda-1.4)^3+\mathrm{q}_2(\lambda-1.4)^2+\mathrm{q}_3=-0.0675$$

$$\mathrm{IDIC} = f(R,\lambda)(I_p-1)+g(\lambda,R)(I_c-1)+1=1.1068$$
$$\Rightarrow \sigma_{u,formula}/\sigma_y = IDIC*\sigma_u/\sigma_y = 1.1068*0.578 = 0.64$$

Comparison with experimental results:

$$\frac{\sigma_{cr}-\sigma_{ex}}{\sigma_{ex}}=\frac{0.578-0.671}{0.671}*100\%=-13.9\%$$

$$\frac{\sigma_{u,formula}-\sigma_{ex}}{\sigma_{ex}}=\frac{0.64-0.671}{0.671}*100\%=-4.6\%$$

It can be seen that the prediction by the simplified formula tends to underestimate the load-bearing capacity of the columns due to large initial deflections considered. When the actual amplitude of initial deflections is considered into the calculation by the proposed formulae, more accurate results can be obtained.

CHAPTER 5

Influence of local and overall initial deflections on coupled buckling strength of stiffened box section columns under axial compression

5.1 Introduction

Stiffened box section compression member were determined by a wish for a high cross-section stiffness and local buckling resistance than that with unstiffened box section and usually provided for the arch ribs in steel arch bridges. However, due to high slenderness and width-thickness ratios, these kind of compression members are also susceptible to buckling instability phenomenon like that for unstiffened box section columns. In addition, initial deflections have significant influence on the load-bearing capacity.

In previous research conducted by Murakoshi. et.al [90], three kinds of amplitude (i.e. $L/1000$, $L/3000$, $L/5000$) of the overall initial deflection were considered on the columns with different normalized slenderness ratio. It is found that the amplitude of the initial deflection has great influence on the load-bearing capacity of the stiffened box section columns. As the amplitude of the initial deflection increases from $L/5000$ to $L/1000$, load-bearing capacity decreases at most 11.7%. In addition, the decrement on load-bearing capacity caused by initial deflection becomes more severe with the increase of the normalized slenderness ratio. Therefore, further numerical study focusing on the quantitative influence need to be carried out.

In this chapter, stiffened box section columns under axial compression are chosen as a target. Nonlinear finite element models are developed to analyze the load-bearing capacity of columns. A wide range of the normalized width-thickness and slenderness ratios is set to ensure the occurrence of coupled buckling instability. Furthermore, various combinations of amplitude of the local and the overall initial deflections are analyzed in this study. In addition, applicability of the formulae developed to predict their influence on load-bearing capacity of unstiffened box section columns to stiffened box section columns is discussed.

5.2 FE model for parametrical analysis

5.2.1 Main parameters of stiffened box section columns

The buckling instability of stiffened welded box section column is significantly influenced by the normalized slenderness and width-thickness ratios, λ and R_R, given by the formulae,

$$\lambda = \frac{1}{\pi}\sqrt{\frac{\sigma_y}{E}}\frac{L}{r} \tag{5.1}$$

$$R_R = \frac{b}{t}\sqrt{\frac{12(1-\upsilon^2)}{4n\pi^2}\frac{\sigma_y}{E}} \tag{5.2}$$

where σ_y is the nominal yield stress, E is the Young's Modulus, L is the length of the column, r is the radius of gyration, b is the width of the plate, t is the thickness of the plate, v is the Poisson's ratio, and n is the number of the subpanels separated by the stiffeners.

In addition to the slenderness and width-thickness ratios, the properties of the stiffener are also influential. The stiffeners' relative stiffness γ can be defined as,

$$\gamma = \frac{I_l}{bt^3/11} \tag{5.3}$$

where I_l is the moment of inertia of one stiffener with respect to the end connected to the plate.

The required stiffness in JRA is expressed as follows,

$$\begin{cases} \gamma_{req} = 4\alpha^2 n(1+n\frac{b_s t_s}{bt}) - \frac{(\alpha^2+1)^2}{n} & \alpha \leqslant \alpha_0 \\ \gamma_{req} = \frac{1}{n}\left[(2n^2(1+n\frac{b_s t_s}{bt})-1)^2 - 1\right] & \alpha > \alpha_0 \end{cases} \tag{5.4}$$

$$\alpha_0 = \sqrt[4]{1+n\gamma} \tag{5.5}$$

where b_s and t_s are the width and thickness of the stiffener, respectively, α is the aspect ratio (i.e. $\alpha = b/t$), α_0 is the critical aspect ratio.

5.2.2 Geometric parameters

To ensure the appearance of coupled buckling failure mode, the normalized width-thickness and slenderness ratios were set from 0.5 to 1.5 and 0.1 to 1.4, respectively.

Based on statistics [93] on the dimension of arch rib in 44 arch bridges in Japan, it was found that the widths of the flange and web in most investigated arch bridges are in the range from 1000 to 2500 mm and 750 to 1500 mm, respectively. Therefore, the widths of flange and web of analyzed models are set to 1500mm and 1000mm, respectively, as

shown in **Fig. 5.1**. The designated width-thickness ratios can be obtained by changing the thickness of the plate.

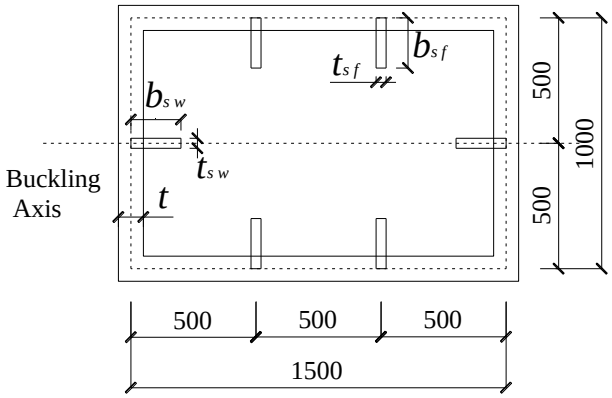

Fig. 5.1 Cross section of the specimen

In the previous study conducted by NARA [91] on the load-bearing capacity of the stiffened plate, it is found that γ/γ_{req} ratio of has great influence on the load-bearing capacity of the structure. Therefore, to prevent this effect, the value of γ was set equal to $\gamma_{req.}$ The dimension of specimens with normalized slenderness ratio of 0.1 is listed in **Table. 5.1**. Models with high λ-value of 0.5, 1.0 and 1.4 were generated by amplifying the column length with the relative factors (i.e. ratio of λ-value to 0.1). In addition, nine combinations of amplitudes of initial deflections were considered as listed in Table 2, leading to 144 FE models. Among the combinations, the one of $b_n/150$ and $L/1000$ corresponds to the allowable initial deflections in the current Japanese specification, JRA.

Table. 5.1 Dimension of specimens

Model	1	2	3	4
b (mm)	1500			
d (mm)	1000			
t (mm)	22.16	12.31	9.23	7.39
n_f	3			
n_w	2			
b_{sf} (mm)	190	120	112	89
t_{sf} (mm)	16	10.2	4.9	5
b_{sw} (mm)	170	110	102	81
t_{sw} (mm)	17	9.6	4.6	4.8
L (mm)	3108	3150	3168	3170
γ/γ_{req}	1.0	1.0	1.0	1.0
R_R	0.5	0.9	1.2	1.5
λ	0.1	0.1	0.1	0.1

5.2.3 FE model building

The general-purpose FEA software MSC.Marc was applied to the numerical analyses. Thick shell element (No.75) was used in the model. Meshing size was set to be small enough to ensure the accuracy of the results. Considering the convenience of residual stress setting, plates were divided into ten elements on every subpanel and four elements on the stiffener as shown in **Fig. 5.2(a)**. The von Mises yield criterion was adopted in the analysis. Bilinear model with yield point of 355 MPa and strain hardening coefficient of $E/100$ was used to describe the material property. The Young's modulus and Poisson ratio were set to 200 GPa and 0.3, respectively. The columns were supported under pin-ended condition with respect to the buckling axis Y as shown in **Fig. 5.2(b)**, which is the same as that in Chapter 3.

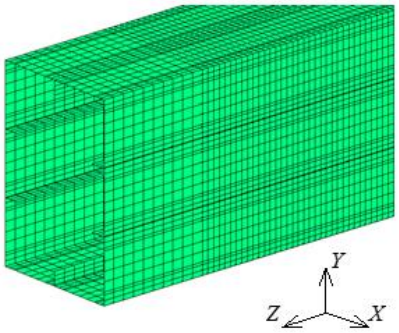

(a) Meshing profile

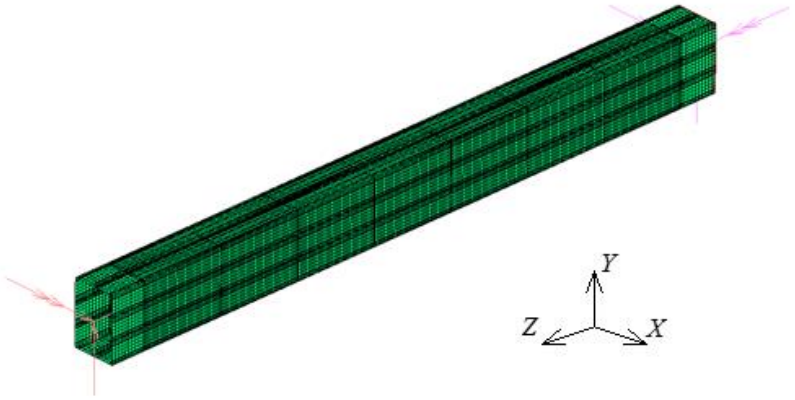

(b) Boundary condition of specimen

Fig. 5.2 Geometry and meshing in the model

Residual stress is also one of the most important factors to the stability behavior of compression members. It was assumed to exist in every plate with compression in the middle area and tension at both sides of the plate as shown in **Fig. 5.3(a)** so as to be in self-equilibrium condition. Referring to the Guidelines for Stability Design of Steel Structures [92], the residual stress of the stiffener was set as shown in **Fig. 5.3(b)**. The compressive stress σ_{rc} was set to $0.25\sigma_y$ based on Fukumoto's statistics [89].

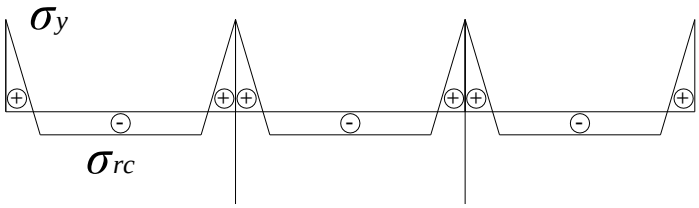

(a) On the plate

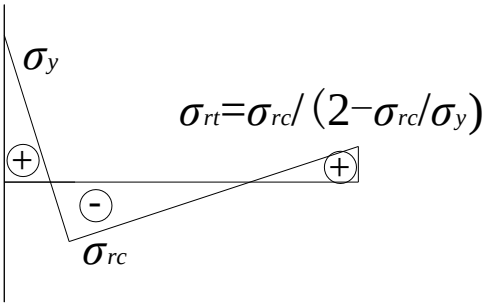

(b) On the stiffener

Fig. 5.3 Distribution of residual stress

Images of local and overall initial deflection shapes are shown in **Fig. 5.4** and **Fig. 5.5**, respectively. The double trigonometric function shown in **Eq. 5.6** was assumed for the local initial deflection. The number of half wave m was determined by the aspect ratio of the plate so as to give the minimum buckling strength according to the elastic buckling theory. Schematic illustration of local initial deflections between two diagrams is shown in **Fig. 5.4(a)**. A half-sinusoidal wave shape expressed by **Eq. 5.7** was assumed for the overall initial deflection. With respect to amplitude of initial deflections, $b_n/75$, b_n /150 and b_n /450 were taken as local initial deflection, while amplitudes of $L/500$, L /1000 and $L/3000$ were set for overall initial deflection resulting in nine combinations.

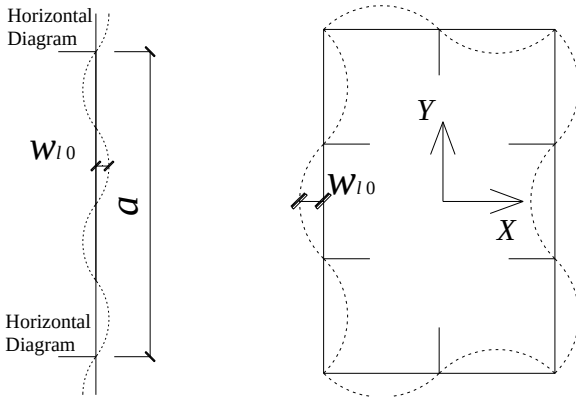

(a) Along the column length (b) On the cross section

Fig. 5.4 Local initial deflection

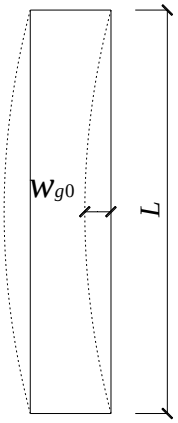

Fig. 5.5 Overall initial deflection

$$\begin{cases} w_{lw} = w_{l0} sin\dfrac{m\pi z}{a} sin\dfrac{\pi x}{b_{nw}} \\ w_{lf} = w_{l0} sin\dfrac{m\pi z}{a} sin\dfrac{\pi y}{b_{nf}} \end{cases} \tag{5.6}$$

$$w_g = w_{g0} sin\frac{\pi z}{L} \tag{5.7}$$

where w_{lw} and w_{lf} are the local initial deflections on the web and flange, respectively; w_{l0} is the amplitude of local initial deflection, m is the number of half sin-wave giving the minimum buckling strength, a is the length between two diagrams, b_{nw} and b_{nf} are the widths of subpanel between two stiffeners on the web and flange, respectively; w_g is the overall initial deflection, w_{g0} is the amplitude of the overall initial deflection.

5.3 Parametrical analysis results and discussion

In this chapter, initial deflection influence coefficient (IDIC) is also introduced to describe the quantitative influence of the initial deflections and defined as a ratio of the load-bearing capacity of a model with variable initial deflection combinations to that in specification (i.e. b_n/150, L/1000).

5.3.1 Influence of local initial deflection

The relationship between IDICs and normalized local initial deflection is plotted in **Fig. 5.6 – 5.9** with linear fitting analysis conducted on the group of points corresponding to the condition where the amplitude of overall initial deflection is L/1000. Models with λ equal to 1.4, R_R varying from 0.5 to 1.5 as shown in **Fig. 5.9**, are selected as an examples to demonstrate the reduction of load-bearing capacity caused by local initial deflection. It can be seen that IDICs decrease approximately linearly as the amplitude of local initial deflection increases. The decreasing tendency is nearly the same for different amplitudes of the overall initial deflection in each structural model. However, the decreasing tendency of IDICs shows much different in the columns with different normalized width-thickness ratios.

When the normalized width-thickness ratio R_R is small as 0.5 or large as 1.5, the local initial deflection has slight effect on the load-bearing capacity corresponding to 6.4% and 7.2%, respectively. The possible reason is that the failure of specimen with low width-thickness ratio is mainly controlled by overall buckling, while it is slightly influenced by the local initial deflection. For the specimen with high width-thickness ratio, local buckling occurs early due to the low plate stiffness even if the local initial deflection is small. In the case of columns with medium R_R-value, the local initial deflection has significant effect on the load-bearing capacity. Especially at R_R equal to 0.9, reduction on load-bearing capacity with the increase in amplitude of local initial deflection from b_n /450 to b_n /75 reaches up to 19.2%.

In addition, it should be mentioned that the decreasing slope of IDICs related to R_R also differs a lot under different normalized slenderness ratio λ. The columns with high normalized slenderness ratios tend to be more sensitive to the local initial deflection than that under low normalized slenderness ratios. The reason is that for such columns, local buckling will occurs at the early stage and later in conjunction with overall buckling lead

to failure. The columns failing in coupled buckling shows more sensitive to initial deflections.

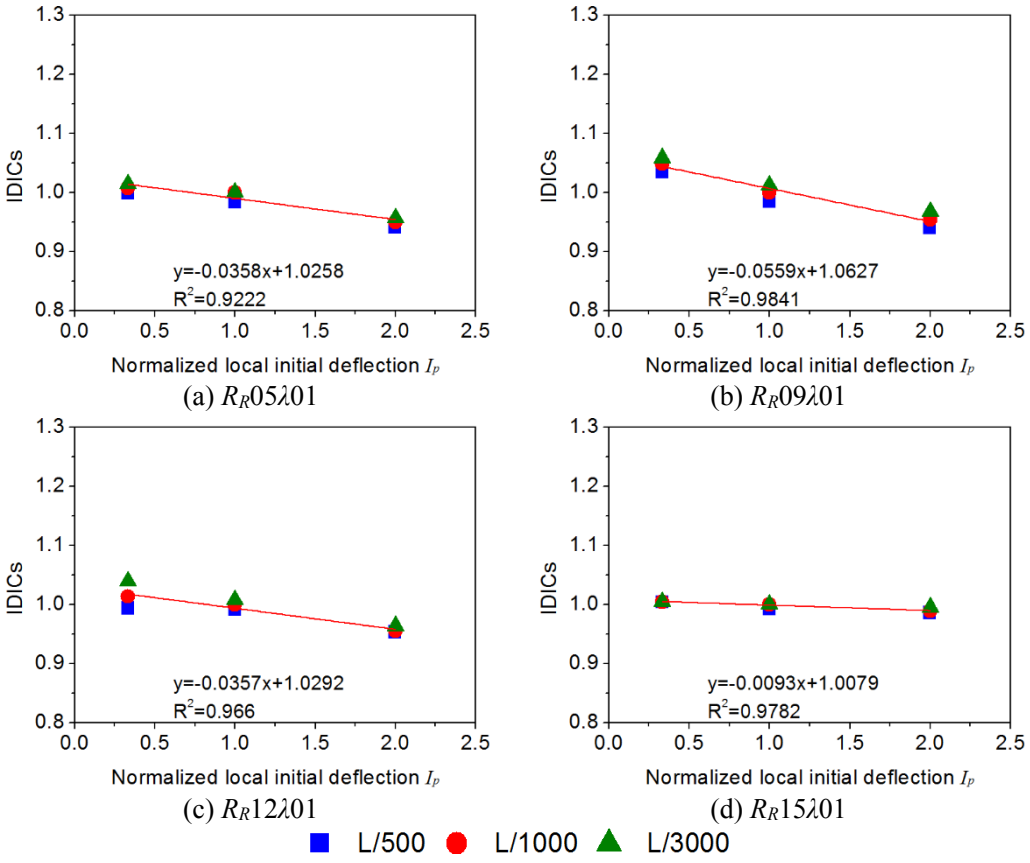

(a) $R_R05\lambda01$ (b) $R_R09\lambda01$

(c) $R_R12\lambda01$ (d) $R_R15\lambda01$

Fig. 5.6 Influence of local initial deflection

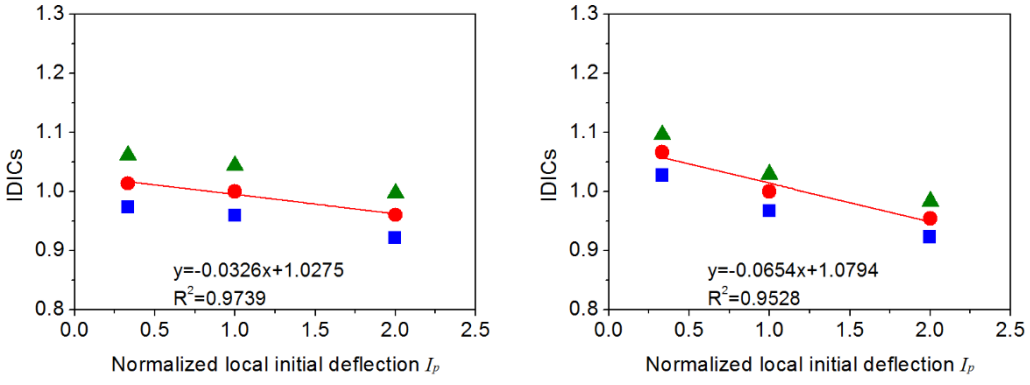

(a) $R_R05\lambda05$ (b) $R_R09\lambda05$

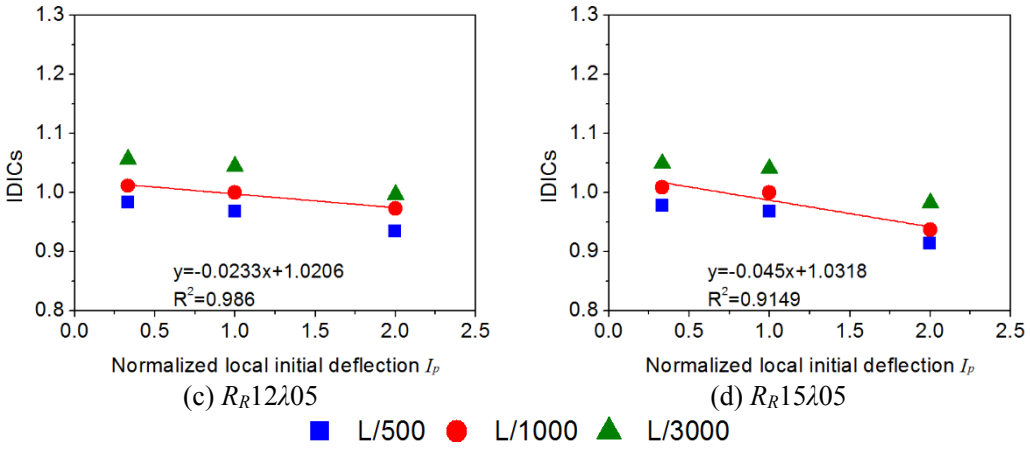

(c) $R_R12\lambda05$ (d) $R_R15\lambda05$

Fig. 5.7 Influence of local initial deflection

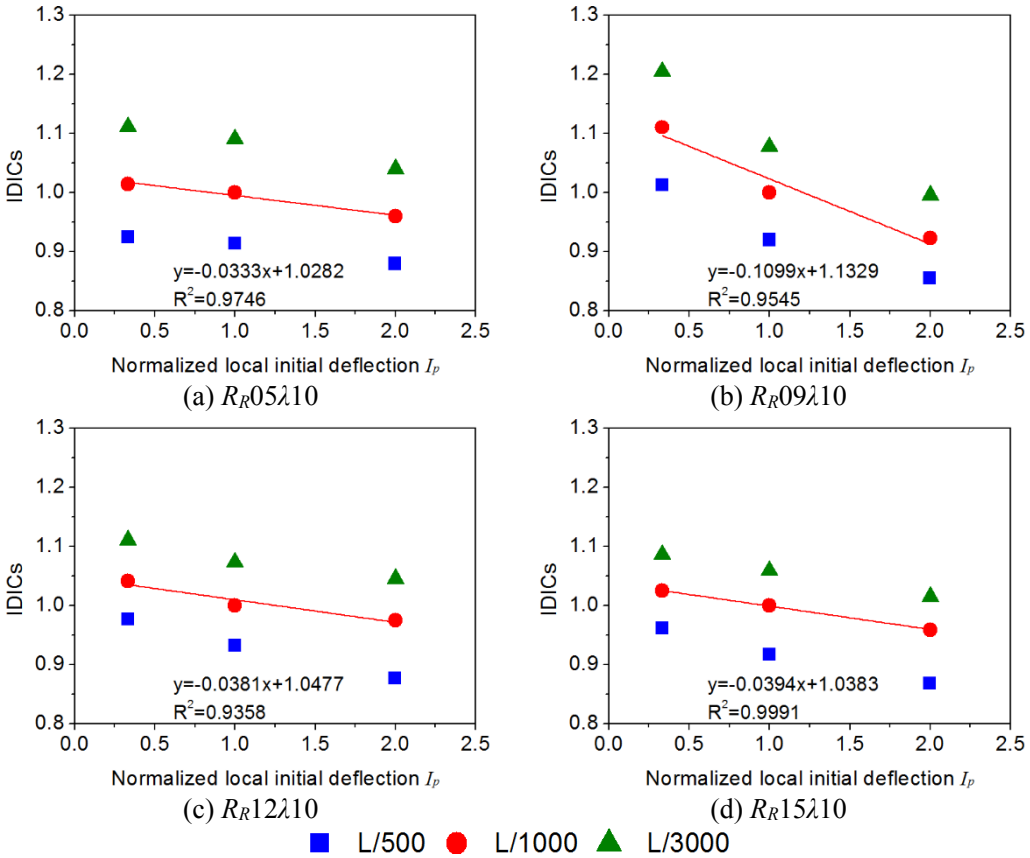

(a) $R_R05\lambda10$ (b) $R_R09\lambda10$

(c) $R_R12\lambda10$ (d) $R_R15\lambda10$

Fig. 5.8 Influence of local initial deflection

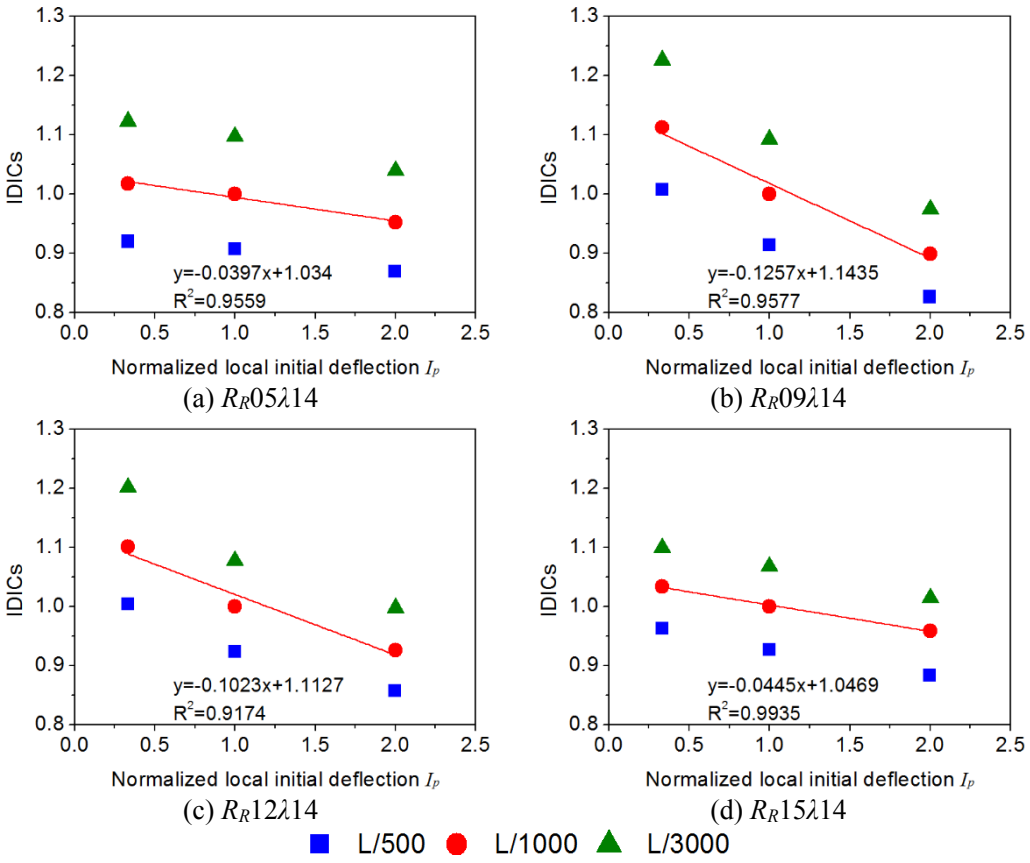

(a) $R_R05\lambda14$ (b) $R_R09\lambda14$

(c) $R_R12\lambda14$ (d) $R_R15\lambda14$

Fig. 5.9 Influence of local initial deflection

5.3.2 Influence of overall initial deflection

The relationship between IDICs and normalized local initial deflection is plotted in **Fig. 5.10 – 5.13**. Linear fitting analysis with IDICs and normalized overall initial deflection as parameter is conducted for the columns under local initial deflection of b/150. Models with normalized slenderness ratios λ from 0.1 to 1.4 and constant normalized width-thickness ratio R_R of 0.9 as shown in **Fig. 5.11** are set as examples to demonstrate the influence of the overall initial deflection on load-bearing capacity..

It can be seen that as overall initial deflection increases, IDIC decreases approximately linearly and the decreasing tendency is independent with local initial deflection. This fact indicates that there is no clearly coupled effect between the local and overall initial deflections. When the normalized slenderness ratio is small such as λ=0.1, overall initial deflection has little influence on load bearing capacity. As the normalized slenderness ratio increases, the slope of the decreasing tendency increases, which represents the increasing influence on the load-bearing capacity caused by overall initial

deflection. Reduction on the load-bearing capacity reaches up to 16.3% at most with the increase in amplitude of overall initial deflection from *L*/3000 to *L*/500.

In addition, it can be also observed that the reduction of load-bearing capacity due to local initial deflection becomes more significant as the normalized slenderness ratio increases. The possible reason is that when the normalized slenderness ratios are at low level, the failure mode is mainly controlled by local buckling. For the columns with high slenderness ratio, local buckling occurs before overall buckling, and then the coupled buckling further deteriorates the load-bearing capacity. Therefore, the influence of local initial deflection is more significant on load-bearing capacity of the specimens with high normalized slenderness ratio than that with low normalized slenderness ratio.

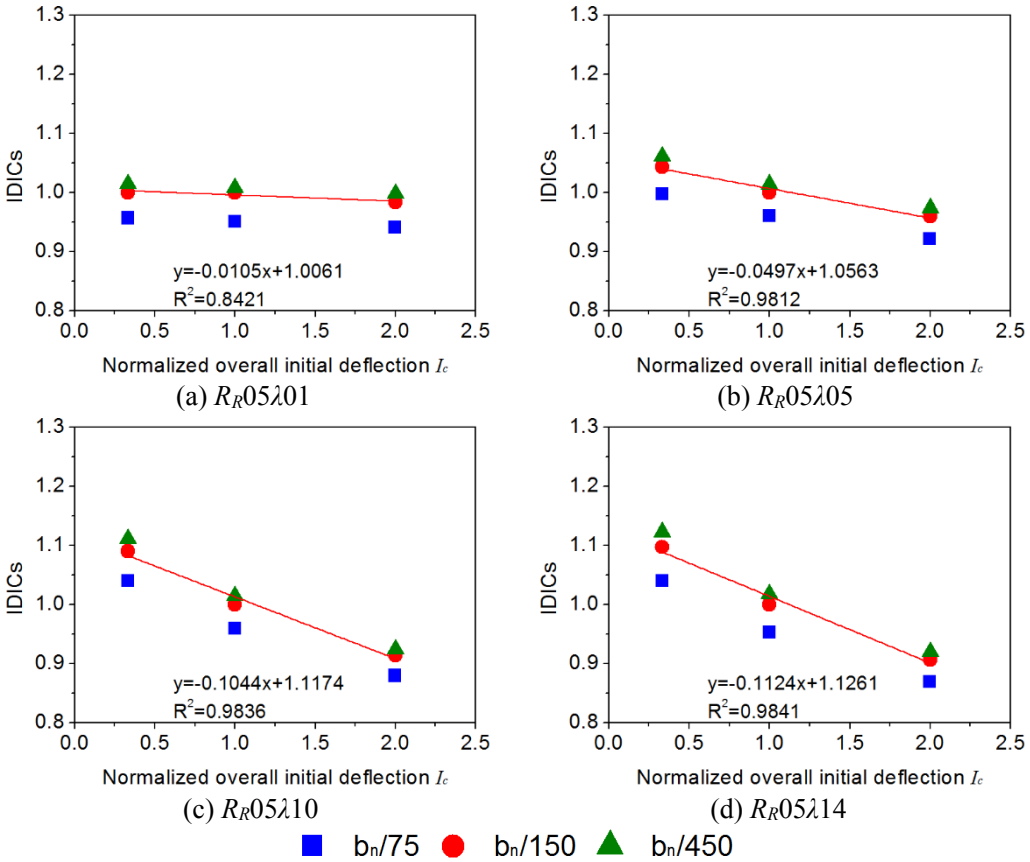

(a) $R_R05\lambda01$ (b) $R_R05\lambda05$

(c) $R_R05\lambda10$ (d) $R_R05\lambda14$

Fig. 5.10 Influence of overall initial deflection

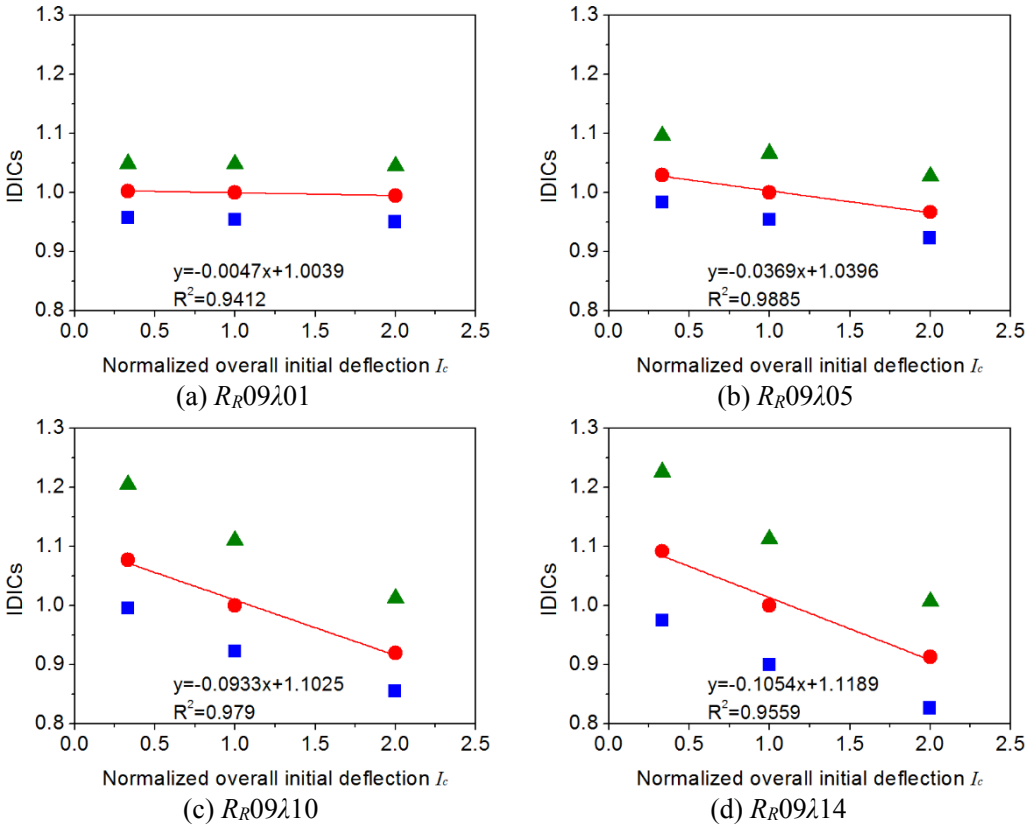

(a) $R_R09\lambda01$ (b) $R_R09\lambda05$

(c) $R_R09\lambda10$ (d) $R_R09\lambda14$

Fig. 5.11 Influence of overall initial deflection

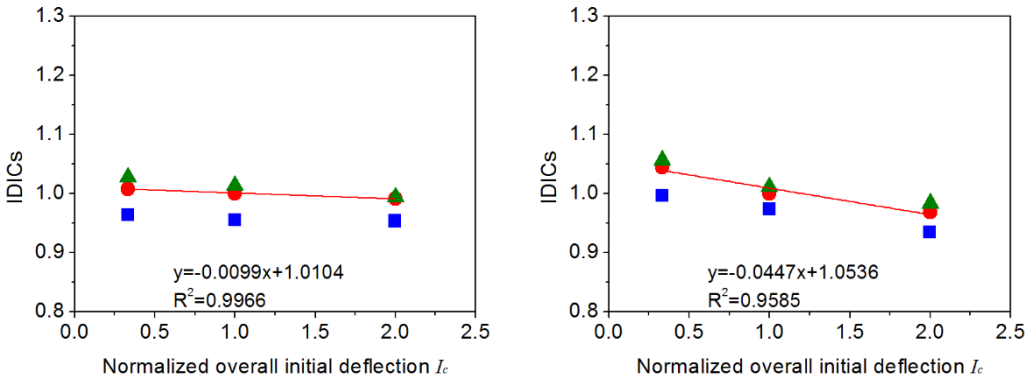

(a) $R_R12\lambda01$ (b) $R_R12\lambda05$

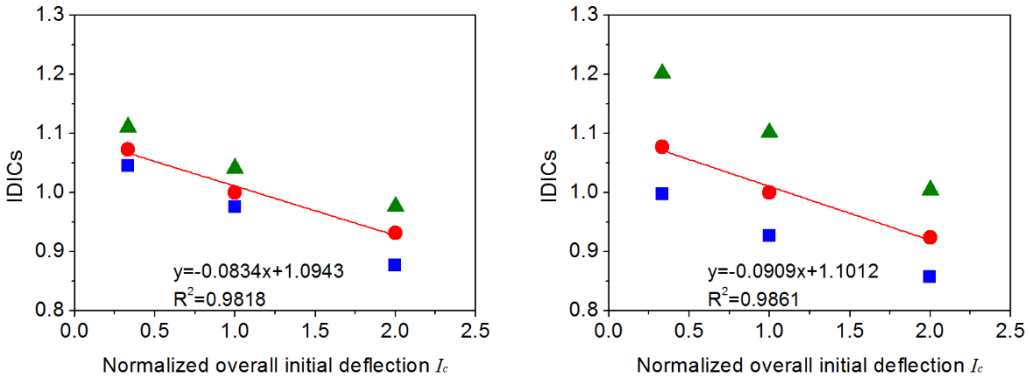

(c) $R_R12\lambda10$ (d) $R_R12\lambda14$

■ $b_n/75$ ● $b_n/150$ ▲ $b_n/450$

Fig. 5.12 Influence of overall initial deflection

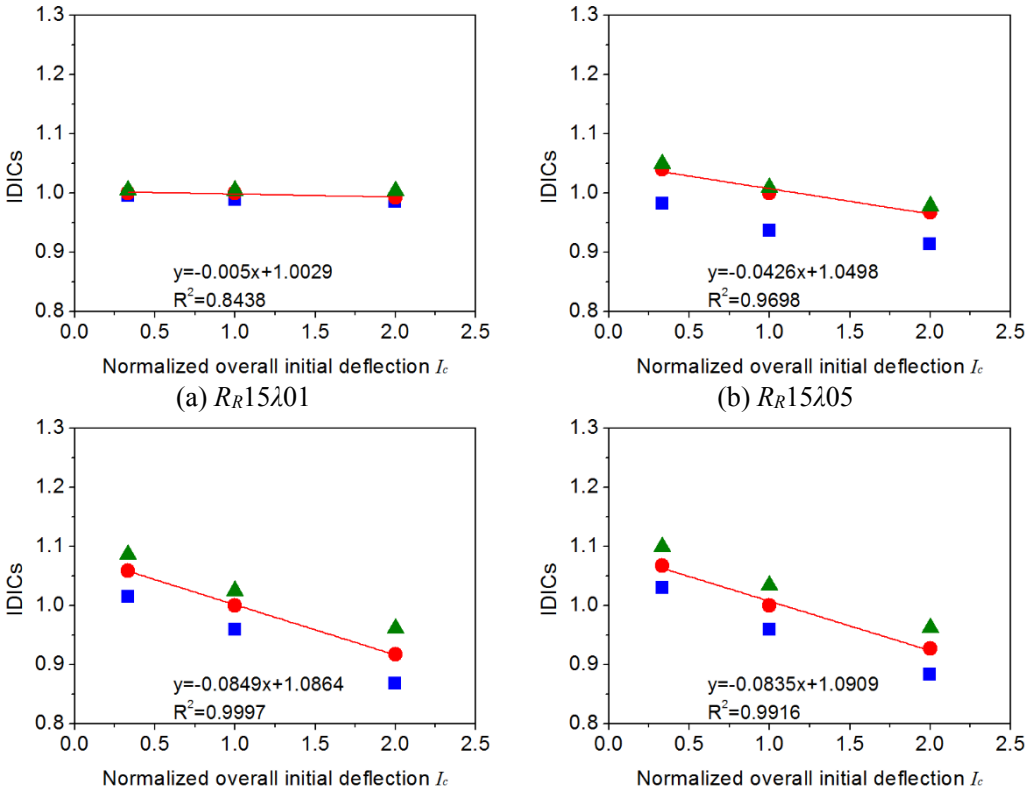

(a) $R_R15\lambda01$ (b) $R_R15\lambda05$

(c) $R_R15\lambda10$ (d) $R_R15\lambda14$

■ $b_n/75$ ● $b_n/150$ ▲ $b_n/450$

Fig. 5.13 Influence of overall initial deflection

5.4 Applicability of formulae developed for unstiffened welded box section columns

In previous research, parametrical formulae of IDICs targeting on the quantitative influence of initial deflections for unstiffened box section columns have been developed as described in Chapter 4. In this part, IDIC formulae were used to evacuate the quantitative influence of initial deflections stiffened box section columns. In order to examine their applicability to the stiffened box section columns, the IDICs were calculated according to the previous formulae and compared with the FEA results as shown in **Fig. 5.14**. The maximum and average errors between the formulae and FEA results are summarized in **Table. 5.2** and **Table. 5.3**. It can be seen that the formulae results show good agreement with FEA results in general. Most of the errors are less than 5%. Only for a part of models, the errors of formulae results are more than 5%, but less than 10%. This fact indicates that the formulae developed for unstiffened welded box section columns can also provide good prediction of the quantitative influence of initial deflections on load-bearing capacity of stiffened welded box section columns. The possible reason may be explained as follows. The stiffness of the stiffeners was set so as to satisfy the requirement by the Specifications **[10]** in all FE models. Therefore, the local buckling was thought to occur within the subpanel between every two stiffeners, which is similar to the unstiffened box section columns.

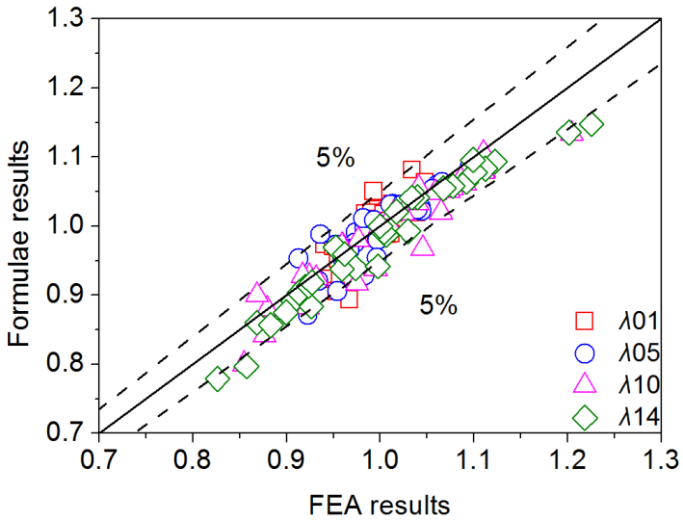

Fig. 5.14 Comparison of IDICs between formulae and FEA results

Table. 5.2 Maximum errors between formulae and FEA results

R_R	λ			
	0.1	0.5	1.0	1.4
0.5	3.39	1.82	2.78	2.58
0.9	7.65	5.64	6.41	6.35
1.2	5.71	4.31	7.43	7.03
1.5	1.82	5.49	4.22	3.58

Table. 5.3 Average errors between formulae and FEA results

R_R	λ			
	0.1	0.5	1.0	1.4
0.5	1.62	1.13	1.10	1.33
0.9	3.36	2.29	3.64	3.31
1.2	2.35	1.50	2.80	3.63
1.5	0.91	2.37	1.91	1.53

5.5 Summary

In this chapter, numerical analyses were conducted on the load-bearing capacity of stiffened box section columns. A variety of initial deflection combinations was considered to investigate their quantitative influence on load-bearing capacity. Main conclusion can be summarized as follows.

(1) The load-bearing capacity linearly decreases as the amplitude of local/overall initial deflection increases. Coupled effects between local and overall initial deflections on IDIC are not observed.

(2) With the increase of local initial deflection from $b_n/450$ to $b_n/75$, the load-bearing capacity of column with R_R=0.9 and λ=1.4 decreases linearly at most 19.2%.

(3) With the increase of overall initial deflection from $L/3000$ to $L/1000$, the load-bearing capacity of column decreases linearly at most 16.3%.

(4) The formulae previously developed to predict the quantitative influence of initial deflection on load-bearing capacity of unstiffened box section columns could be applied to stiffened box section columns within the range of parameters discussed in this study.

CHAPTER 6

Conclusions and future works

6.1 Conclusions

The objective conducted in this dissertation is to improve the stability design of steel compression members with welded unstiffened and stiffened box cross sections. Comparison on stability design among four codes, validation of the numerical analysis on simulation for experimental results, formulation of quantitative influence for unstiffened box section column and its applicability for stiffened box section columns were conducted. The main conclusions can be summarized as follows:

First of all, the provision for the stability of steel compression member in the four codes adopting the Partial Factor Design Method are investigated. The nominal strength of this structure based on the design codes is calculated and compared with each other. The design strengths and safety factors among the four codes are discussed. Further, the allowable strength is compared to investigate the difference among those codes. The main findings can be summarized as follows.

(1) In the range of $0.5 \leq R \leq 0.7$, closed nominal strengths can be obtained from AASHTO, EC3 and JRA, while JTG D64 gives a lower nominal strength due to local buckling reduction considered from $R > 0.4$.

(2) When the local buckling reduction is considered (i.e. $R \geq 0.9$), the nominal strength following AASHTO is higher than that of EC3, while the results in JRA and JTG D64 are on the conservative side of EC3. In addition, the results following EC3 correspond with the FEA results better than others.

(3) Safety factor increases along with the increase of ρ_D-value. JTG D64 I provides the highest safety factors, and then is JTG D64 II and JRA in the order, while EC3 offers lowest safety factors.

(4) In the case of ρ_D-value less than 0.25, safety factors based on AASHTO is smaller than JRA. In the range from 0.25 to 2.0, safety factor following AASHTO locates between JTG D64 II and JRA. When the ρ_D-value exceeds 2.0, AASHTO gives higher safety factors than JTG D64 II.

(5) Design strength following AASHTO is highest, and then is that of EC3 in the order, while JRA and JTG D64 offer conservative results.

(6) Allowable strength following EC3 is higher than that in AASHTO in major part due to lower safety factor considered in EC3, while high safety factor in JTG D64 results in further conservative allowable strength than other codes.

(7) Considering ρ_D of 0.3 and 1.2, it does not change the comparison tendency of allowable strength among the four codes.

Secondly, a precise FE model to replicate the load-bearing capacity of unstiffened box section columns with a wide range of normalized slenderness and width-thickness ratios into consideration was developed. Its accuracy was proved by comparing with the experimental results. The main findings can be summarized as follows.

(1) Reasonable postbuckled results can be obtained by means of arc length method.

(2) Reasonbale element type, intensive meshing size as well as inputing measured residual stress and initial deflection will results in accurate prediction on the load-bearing capacity of unstiffened box section columns.

Thirdly, 486 models were analyzed to investigate the quantitative influence of the initial deflections on the load-bearing capacity of unstiffened welded square box section columns with a variety of normalized slenderness and width-thickness ratios. The main findings can be summarized as follows.

(1) The load-bearing capacity linearly decreases as the amplitude of local/overall initial deflection increases. The decreasing slope is nearly the same for different amplitudes of overall/local initial deflection.

(2) With the normalized width-thickness and slenderness ratios equal to 1.2 and 1.8, respectively, the influence of the local initial deflection reaches the maximum with the decreasing slope of 0.1375 corresponding to the 20.7% reduction on load-bearing capacity.

(3) With the normalized width-thickness and slenderness ratio equal to 0.3 and 1.4, respectively, the influence of the overall initial deflection reaches the maximum with decreasing slope of 0.1166 corresponding to the 17.9% reduction on load-bearing capacity.

(4) Based on numerous FEA results, the formulae for the initial deflection influence coefficient (IDIC) are developed, which describe the quantitative influence caused by the initial deflections. Compared with the FEA results, the accuracy of the formulae is verified.

(5) Compared with the experimental results, it is verified that the product between the IDIC and the simplified formula can predict the load-bearing capacity with good accuracy in the case of columns with various amplitudes of the initial deflections.

(6) The residual stress has slight influence on the relationship between IDICs and local initial deflection, while it has negligible influence on the relationship between IDICs

and overall initial deflection.

Finally, numerical analyses were conducted on the load-bearing capacity of stiffened box section columns. A variety of initial deflection combinations was considered to investigate their quantitative influence on load-bearing capacity. Main conclusion can be summarized as follows.

(1) The load-bearing capacity linearly decreases as the amplitude of local/overall initial deflection increases. Coupled effects between local and overall initial deflections on IDIC are not observed.

(2) With the increase of local initial deflection from $b_n/450$ to $b_n/75$, the load-bearing capacity of column with R_R=0.9 and λ=1.4 decreases linearly at most 19.2%.

(3) With the increase of overall initial deflection from $L/3000$ to $L/1000$, the load-bearing capacity of column decreases linearly at most 16.3%.

(4) The formulae previously developed to predict the quantitative influence of initial deflection on load-bearing capacity of unstiffened box section columns could be applied to stiffened box section columns within the range of parameters discussed in this study.

6.2 Future works

The study in this dissertation has certain deficiencies and need further improvement in the future work. Some works deserve conducting for improvement are as follows:

(1) The validity of the proposed formulae has been evaluated only for the conditions examined in this research. Their applicability to different cross-sections, residual stress pattern and high strength steel columns as well as wider range of initial deflection value need to be studied in the future work.

(2) Experimental study combined with numerical analysis are worth carrying out in order to further investigate the quantitatively influence of initial deflections on load-bearing capacity for stiffened box section columns and finally modified the proposed formulae.

Reference

[1] Bleich, F. Buckling strength of metal structures. McGraw-Hill, New York, America, 1952.

[2] Timoshenko SP, Gere JM. Theory of elastic stability. McGraw-Hill, New York, America, 1961.

[3] Bazant ZP, Cedolin L. Stability of structures: Elastic, inelastic, fracture and damage theories. World Scientific, Singapore, 2010.

[4] Bushnell D. Buckling of shells-pitfall for designers. AIAA Journal, 1981, 19 (9): 1183-1226.

[5] Bulson PS. The Stability of Flat Plates. Chatto and Windus, London, UK, 1970.

[6] Budiansky B. Theory of buckling and post-buckling behavior of elastic structures. Advance in Applied Mechanics, 1974, 14: 1-65.

[7] Svensson SE, Croll JGA. Interaction between local and overall buckling. International Journal of Mechanical Sciences, 1975, 17 (4): 307-321.

[8] Van der Neut A. The interaction of local buckling and column failure of thin-walled compression members. Proceedings of the 12th International Congress on Applied Mechanics, Springer, 1969: 389-399.

[9] Becque J. Local-overall interaction buckling of inelastic columns: A numerical study of the inelastic Van der Neut column. Thin-walled structures, 2014, 81: 101-107.

[10] Wadee MA, Li B. Cellular buckling in I-section struts. Thin-Walled Structures. 2014, 81: 89-100.

[11] Shen JJ, Wadee MA, Sadowski AJ. Interactive buckling in long thin-walled rectangular hollow section struts. International Journal of Non-Linear Mechanics, 2017, 89: 43-58.

[12] Van der Neut A. The sensitivity of thin-walled compression members to column axis imperfection. International Journal of Solids Structures, 1973, 9 (8): 999–1011.

[13] Wadee, MA. Effects of periodic and localized imperfections on struts on nonlinear foundations and compression sandwich panels. International Journal of Solids Structures, 2000, 37(8): 1191–1209.

[14] Becque J, Rasmussen KJR. Experimental investigation of the interaction of local and overall buckling of stainless steel I-columns. Journal of Structural Engineering 2009,

135(11): 1340–1348.
[15] Quach WM, Teng JG, Chung KF. Effect of the manufacturing process on the behaviour of press-braked thin-walled steel columns. Engineering Structures, 2010, 32(11): 3501–3515.
[16] Li B, Wadee MA. Imperfection sensitivity of thin-walled I-section struts susceptible to cellular buckling. International Journal of Mechanical Sciences, 2015, 104: 162–173.
[17] Xia ZB, Pan YC. Structural Stability Theory. Higher Education Press, Beijing, China, 1988. (in Chinese)
[18] Beer H, Schultz G. Theoretical basis of European column curves. Construction Metallique. 1970, No.3, p.58.
[19] Sfintesco D. Experimental basis of European column curves. Construction Metallique.1970, No.3, p.5.
[20] European Committee for Standardization. EN 1993-1-1: Eurocode 3: General rules and rules for buildings, 2005.
[21] Li KX, Xiao YH. Calculation of ultimate strength of steel compression member under uniaxial in stability by the contrary calculation segment length method. Journal of Civil and Environmental Engineering, 1982, 4:26-45. (in Chinese)
[22] Li KX, Xiao YH, Nao XF, Cui J, Zhu W. Column curves for steel compression member. Journal of Chongqing Institute of Architecture and Engineering, 1985, 1:24-33. (in Chinese)
[23] Ministry of Construction People's Republic of China. GB50017-2003: Code for Design of Steel Structure. China Architecture & Building Press, Beijing, 2003. (in Chinese)
[24] Fukumoto Y, Itoh Y. Evaluation of multiple column curves from the experimental data-base approach. Journal of Constructional Research, 1983, 3 (3): 2-19.
[25] Fukumoto Y, Itoh Y. Numerical data bank for the system evaluating the ultimate strength of steel members. Japan Society of Civil Engineering, 1981, 312: 59-72. (in Japanese)
[26] Fukumoto Y, Itoh Y. Basic strength of steel columns from test data. Japan Society of Civil Engineering, 1983, 335: 59-68. (in Japanese)
[27] Japan Road Association. Specifications for Highway Bridges, Part II Steel Bridges and Members. Maruzen Publishing Co. Ltd, Tokyo, Japan, 2002. (in Japanese)

[28] Bjorhovde R. Deterministic and probabilistic approaches to the strength of steel columns. Ph.D thesis, 1972.
[29] American Institute of Steel Construction. Load and Resistance Factor Design Specification for Structural Steel Buildings. Chicago, America, 1986.
[30] Ministry of Transport of the People's Republic of China. JTG D64: Specifications for Design of Highway Steel Bridge. China Communication Press, Beijing, China, 2015. (in Chinese)
[31] Japan Road Association, Specifications for Highway Bridges, Part II Steel Bridges and Members. Maruzen Publishing Co. Ltd, Tokyo, Japan, 2017. (in Japanese)
[32] American Association of State Highway and Transportation Officials. AASHTO LRFD Bridge Design Specification. Washington, America, 2017.
[33] European Committee for Standardization. EN 1993-2: Eurocode 3: Design of steel structure – Part 2: Steel Bridges, 2006.
[34] Bryan GH. On the stability of a plane plate under thrusts in its own plane, with application to the buckling of the sides of a ship. Proceedings of the London Mathematical Society, 1890, S1-22, 1:54-67.
[35] Von Kármán T, Sechler EE, Donnell LH. The strength of thin plates in compression. Transactions, ASME, 1932, 54: 53-57.
[36] Winter G. Strength of thin steel compression flanges. Transactions, ASCE, 1947, 112: 527-576.
[37] American Association of State Highway and Transportation Officials. AASHTO LRFD Bridge Design Specification. Washington, America, 2012.
[38] Schafer BW, Pekoz T. Direct strength prediction of cold-formed steel members using numerical elastic buckling solutions. Proceedings of the 14th International Specialty Conference on Cold-formed Steel Structures, 1998: 137-144.
[39] Silvestre M, Camotim D, Dinis P. Direct strength prediction of lipped channel columns experiencing local-plate/distortional interaction. Advanced Steel Construction, 2009, 5 (1): 45-67.
[40] Yang D, Hancock GJ. Compression tests of high strength steel channel columns with interaction between local and distortional modes. Journal of Structural Engineering, ASCE, 2004, 130 (12): 1954-1963.

[41] Lecce M, Rasmussen K. Distortional buckling of cold-formed stainless steel sections; finite element modeling and design Journal of Structural Engineering, 2006, 132 (4) (2006): 505-514.

[42] American Iron and Steel Institute. North American Specification for the Design of Cold-formed Steel Structural Members. America, 2004.

[43] Kwon YB, Kim NG, Hancock GJ. Compression tests of welded section columns undergoing buckling interaction. Journal of Constructional Steel Research, 2007, 63: 1590-1602.

[44] Kwon YB, Seo EG. Prediction of the compressive strength of welded RHS columns undergoing buckling interaction. Thin-Walled Structures, 2013, 68: 141-155.

[45] Kwon YB. The development of the direct strength method for welded steel members with buckling interactions. Thin-Walled Structures, 2014, 81: 121-131.

[46] Shen HX. Local-overall interaction buckling of high strength steel welded square box columns. Engineering Mechanics. 2012, 29 (7): 221-227.

[47] Van der Neut. A: The sensitivity of thin-walled compression members to column axis imperfection, International Journal of Solids and Structures, 1973, 9 (8): 999-1011.

[48] Li. B, Wadee. MA: Imperfection sensitivity of thin-walled I-section struts susceptible to cellular buckling. International Journal of Mechanical Sciences, 2015, 104: 162-73.

[49] Kiymaz G. FE based mode interaction analysis of thin-walled steel box columns under axial compression. Thin-Walled Structures, 2005, 43 (7): 1051-1070.

[50] Becque J, Rasmussen KJR. Numerical investigation of the interaction of local and overall buckling of stainless steel I-columns. Journal of Structural Engineering, 2009, 135 (11): 1349-1356.

[51] Smith TG. The effect of initial imperfections on the strength of thin-walled box columns. International Journal of Mechanical Sciences. 1971, 13 (11): 911–925.

[52] Thompson JMT, Tulk JD, Walker AC. An experimental study of imperfection-sensitivity in the interactive buckling of stiffened plates. International Union of Theoretical and Applied Mechanics, Springer, Berlin Heidelberg, 1976: 149–159.

[53] Loughlan J. The ultimate load sensitivity of lipped channel columns to column axis imperfection. Thin-Walled Structure. 1983, 1 (1): 75–96.

[54] Gioncu V. General theory of coupled instabilities. Thin-Walled Structures, 1994, 19 (2): 81-127.

[55] Becque J, Rasmussen KJR. Numerical investigation of the interaction of local and overall buckling of stainless steel I-columns. Journal of Structural Engineering, 2009, 135 (11): 1349-1356.

[56] Shen JJ, Wadee, MA, Imperfection sensitivity of thin-walled rectangular hollow section struts susceptible to interactive buckling. International Journal of Non-Linear Mechanics, 2018, 99: 112-130.

[57] T. Usami, Y. Fukumoto, Local and overall buckling of welded box columns, Journal of the Structural Division 1982, 108 (3): 525–542.

[58] Rasmussen KJR, Hancock GJ, Tests of high strength steel columns. Journal of Constructional Steel Research, 1995, 34 (1): 27–52.

[59] Somodi B, Kövesdi B, Flexural buckling resistance of welded HSS box section members. Thin-Walled Structures 2017, 119: 266–281.

[60] Shi G, Zhou WJ, Bai Y, Lin CC, Local buckling of 460 MPa high strength steel welded section stub columns under axial compression. Journal of Constructional Steel Research 2014, 100: 60–70.

[61] European Committee for Standardization. EN 1993-1-5: Eurocode 3: Design of steel structures - Part 1-5: Plated structural elements. CEN, 2006.

[62] Ministry of Construction People's Republic of China. Code for Acceptance of Construction Quality of Steel Structures. China Planning Press, Beijing, China, 2002. (in Chinese)

[63] Degée H, Detezel A, Kuhlmann U, Interaction of global and local buckling in welded RHS compression members. Journal of Constructional Steel Research 2008, 64: 755–765.

[64] Kwon YB, Seo EG, Prediction of the compressive strength of welded RHS columns undergoing buckling interaction. Thin-Walled Structures 2013, 68: 141–155.

[65] Inose K, Hirohata M, Nakanishi Y, Kim YC. Ultimate strength of non-stiffened welded structural member assembled by using laser beam. Journal of Structural Engineering, 2008, 54A: 50–57. (in Japanese)

[66] Ban HY, Shi G, Overall buckling behavior and design of high-strength steel welded section columns. Journal of Constructional Steel Research, 2018, 143: 180–195.

[67] Coelho AMG, Simão PD, Wadee MA, Imperfection sensitivity of column instability revisited. Journal of Constructional Steel Research 2013, 90: 265-282.

[68] Kang SB, Yang B, Zhou X, Nie SD. Global buckling behaviour of welded Q460GJ

steel box columns under axial compression. Journal of Constructional Steel Research, 2018, 140: 153–162.
[69] Lu Y, Shi G, Zhao MH, Zhou WJ. Research on interactive buckling behavior of welded steel box-section columns. Thin-Walled Structures, 2017, 115: 34–47.
[70] Wang YB, Li GQ, Chen SW, Sun FF. Experimental and numerical study on the behavior of axially compressed high strength steel box-columns. Engineering Structures, 2014, 58: 79-91.
[71] Nakai H, Kitada R, Miki T: An experimental study on ultimate strength of thin-walled box stub-columns with stiffeners subjected to compression and bending. Proceedings of the Japan Society of Civil Engineering, 1985, 362 (I-4): 87-97.
[72] Usami T, Fukumoto Y, Aoki T, Matsukawa A. Experimental study on eccentrically loaded stiffened box columns. Proceedings of the Japan Society of Civil Engineering, 1984, 350 (I-2): 197-205. (in Japanese)
[73] Murakoshi J, Toyama N, Yanadori N, Sawada M, Arimura K, Maeda K, Ono K. Ultimate strength of compressive member with steel box sections. Technical Note of PWRI, No.4221, 2012.3. (in Japanese)
[74] Li GH. Stability and vibration of bridge structures. China Railway Press. Beijing, China, 2010. (in Chinese)
[75] Zhang YL, Gou MK, Li N, Liang C. Research on overall stability of axially compressed member of high strength steel. Steel Construction, 2010, 25(6): 29-34. (in Chinese)
[76] Ban HY, Shi G. Overall buckling behavior and design of high-strength steel welded section columns. Journal of Constructional Steel Research, 2018, 143: 180-195.
[77] Shen HX. Local-overall interaction buckling of high strength steel welded square box columns. Engineering Mechanics, 2012, 29(7): 221-227. (in Chinese)
[78] Winter G. Strength of thin steel compression flanges. Transaction of the American Society of Civil Engineers, 1947, 112: 527-576.
[79] Ministry of Transport of the People's Republic of China. JTG D60: General Specifications for Design of Highway Bridges and Culverts. China Communication Press, Beijing, China, 2015. (in Chinese)
[80] Hansell WC, Viest IM. Load factor design for steel highway bridges. AISC Engineering Journal, 1971, 8(4): 113-123.

[81] MSC Software Corporation. MARC user manual: volume A – volume E. 2013.
[82] Pavlovčič L, Froschmeier B, Kuhlmann U, Beg D, Finite element simulation of slender thin-walled box columns by implementing real conditions. Advances in Engineering Software 2012, 44: 63–74.
[83] Cook RD, David SM, Michael EP. Concepts and applications of finite element analysis. Wiley, New York, America, 2007.
[84] Somodi B, Kövesdi B, Residual stress measurements on welded square box sections using steel grades of S235-S960. Thin-Walled Structures 2018,123:142–154.
[85] Fukumoto Y, Itoh Y. Basic compressive strength of steel plates from test data. Proc. of JSCE 1984, 344(I-1):129-139.
[86] Chen J. Stability of Steel Structure Theory and Design, 6th Edition. Science Press, 2011.
[87] Kishi Y, Nakamura S, Ikezue K, Nogami K, Hirayama H, Mizuguchi T, Shirato M. Numerical evaluation for coupled buckling strength of steel compression members with box section. The 14th East Asia-Pacific Conference on Structural Engineering and Construction, Vietnam, 2016: 1889-1896.
[88] Li GQ, Wang YB, Chen SW, Sun FF. Parametric analysis of ultimate bearing capacity of Q460 high strength steel welded box columns under axial compression. Hournal of Building Structures. 2011, 32 (11):149-155. (in Chinese)
[89] Zhou WJ. Research on interactive buckling behavior of welded section steel members under axial compression. Master Thesis. Tsinghua University, 2014. (in Chinese)
[90] Murakoshi J, Toyama N, Yanadori N, Sawada M, Arimura K, Maeda K, Ono K. Ultimate strength of compressive member with steel box sections, Technical Note of PWRI, No.4221, 2012.3. (in Japanese)
[91] Nara S, Komatsu S, Yasumatsu T, Ikeda H. Flexural rigidity of longitudinally stiffened plates under uniaxial compression. Journal of Structural Engineering, 1988, 34A: 215-220. (in Japanese)
[92] Japan Society of Civil Engineers. Guidelines for Stability Design of Steel Structures, 2nd Edition. Maruzen Publishing Co. Ltd, Tokyo, Japan, 2005. (in Japanese)